

Rafael Kenji Nishihora

**MANUFACTURING OF POLYSILOXANE-BASED
MICROFILTRATION CERAMIC MEMBRANES BY TAPE
CASTING FOR PREMIX EMULSIFICATION PROCESS**

Doctorate thesis for the degree of
Doctor in Chemical Engineering
presented to the Graduate Program in
Chemical Engineering at Federal
University of Santa Catarina.

Advisor:

Prof. Dr. Mara Gabriela Novy Quadri

Co-advisors:

Prof. Dr. Dachamir Hotza

Dr. Michaela Wilhelm

Florianópolis

2019

Ficha de identificação da obra elaborada pelo autor,
através do Programa de Geração Automática da Biblioteca Universitária da UFSC.

Nishihora, Rafael Kenji
MANUFACTURING OF POLYSILOXANE-BASED
MICROFILTRATION CERAMIC MEMBRANES BY TAPE CASTING
FOR PREMIX EMULSIFICATION PROCESS / Rafael Kenji
Nishihora ; orientadora, Mara Gabriela Novy Quadri,
coorientador, Dachamir Hotza, coorientadora,
Michaela Wilhelm, 2019.
202 p.

Tese (doutorado) - Universidade Federal de Santa
Catarina, Centro Tecnológico, Programa de Pós
Graduação em Engenharia Química, Florianópolis, 2019.

Inclui referências.

1. Engenharia Química. 2. Tape casting. 3.
Ceramic membrane. 4. Polysiloxane. 5. Premix
membrane emulsification. I. Quadri, Mara Gabriela
Novy. II. Hotza, Dachamir. III. Wilhelm, Michaela
IV. Universidade Federal de Santa Catarina.
Programa de Pós-Graduação em Engenharia Química. V.
Título.

Rafael Kenji Nishihora

**MANUFACTURING OF POLYSILOXANE-BASED
MICROFILTRATION CERAMIC MEMBRANES BY TAPE
CASTING FOR PREMIX EMULSIFICATION PROCESS**

This thesis was considered adequate for the degree of Doctor in
Chemical Engineering and was approved in its final form by the
Graduate Program in Chemical Engineering at Federal University of
Santa Catarina.

Florianópolis, May 20th 2019.

Prof. Cíntia Soares, Dr.

Coordinator of the Graduate Program in Chemical Engineering

Examination Board:

Prof. Mara G. N. Quadri, Dr.
Advisor

Federal University of Santa Catarina

Prof. Dachamir Hotza, Dr.
Co-advisor

Federal University of Santa Catarina

Michaela Wilhelm, Dr.
Co-advisor
Universität Bremen

Prof. Marco Di Luccio, Dr.
Federal University of Santa Catarina

Prof. José Vladimir de Oliveira,
Dr.
Federal University of Santa Catarina

Prof. Samuel Bernard, Dr.
University of Limoges, France

To my beloved parents who always trusted in my decisions even when
they couldn't understand them.

To my love who evermore understand me even when I can't.

Acknowledgements

I think that perhaps the doctorate could be described as a lifestyle given its particular flow, demands, and challenges. We feel immersed in an environment of competition, crazy ideas, true friendships, failure, success, etc. It is a roller coaster of feelings packed in 4 years. Even though in the end I am the one getting the doctoral degree, I have to say that the work required to achieve this position would be impossible to be done only by myself. Therefore, I have to start acknowledging those who either directly or indirectly made this possible within this time frame.

First, I would like to thank both institutions Universidade Federal de Santa Catarina (UFSC) and Universität Bremen (UniBremen) for providing me a great work infrastructure. More important than the institutions themselves are the people who give life and motion to these places. Therefore, I extend my gratitude to my advisors Prof. Mara and Prof. Dachamir for trusting in my work and for always pushing me to new limits, and to Prof. Marco, for several fruitful discussions. From the German side, I would like to thank Prof. Rezwani for kindly receiving me in the Advanced Ceramics Group and for this great experience abroad. Still from the German side, I have to especially thank Dr. Michaela Wilhelm for accepting me as a member in the PDC group, for guiding me patiently and for providing me space to grow not only as a scientist but as a person too.

Concerning those sharing the working environment with me, I am really grateful for the awesome colleagues and friends I met during this journey. Firstly, I would like to thank Ellen Rudolph for trusting in my work as her advisor and for her hard work in face of the proposed challenges. Now, starting from the Brazilian lab, I have to thank a lot of people for all the partnership and friendship: Stéphanie, Valdir, Deise, Clara, Vivian, Marcelo, Eduardo, Vanderlei, Priscila, Carina, Andressa, and Fábio. From the German side, before mentioning all the names I need to say that although I loved Germany as a country, what I miss the most are the amazing people that I met there during one and a half year.

For instance, Daniel “Cabrón” Carmona, the crazy Spanish Dr.; Dr. Renato “was here” Almeida, the old soul in a young body; Joeri, the “party king”; Thamires, the selfie master; Reshma, the friend selective specialist; Jéssica, the step reader; Benjamin, the latest German I ever met; Helo(ísa), the party sleeper; Sarabjeet, the returned post-doc; Natália, the scientist “black swan”; Daniel “early bird” Schumacher; and Marcos, the young married Brazilian-Portuguese-German guy. I have also to acknowledge the technical staff: Tina, Christian E., Christian N., Gabriela, and Jorgen, for all the help and support. Some honorable mentions: Bernardo, Marieke, Vignesh, Gesa, Huixing, and Prabu.

Besides those from the workspace, certainly, I have to acknowledge my parents, Rosimeri and Gilson, who were guiding me way before this journey started. I have to mention in special my father, Gilson Barbosa. Although he could not see my final steps on this path, I want to say that without his efforts I could not have had the optimum conditions to succeed. Last but not least, a huge thanks to my love Gidiane, who is not only sharing her life with me but also this journey in all its fullness. It was not easy at all. Nevertheless, I am deeply happy for growing together with her as a scientist, person, partner, and in every sense that we can imagine. I also extend my gratitude towards Gidiane's family.

Finally, I am really grateful by the Brazilian funding agencies: CNPq (National Council for Scientific and Technological Development) and CAPES (Coordination for the Improvement of Higher Education Personnel) for the scholarships. The Erasmus+ program is also acknowledged in this work.

Abstract

In this work, an investigation on the manufacturing of polysiloxane-based microfiltration membranes is presented. The shaping technique employed was tape casting in conjunction with different pore forming strategies. First, polysiloxanes were used as ceramic precursor for the preparation of a symmetric microfiltration SiOC-based membrane. Porosity and surface properties were tailored by sacrificial pore forming content (azodicarbonamide) and pyrolysis temperature (600 or 1000 °C) under nitrogen atmosphere, respectively. Secondly, mullite-based powder ($3\text{Al}_2\text{O}_3 \cdot 2\text{SiO}_2$) were synthesized using polymethylsiloxane as silica precursor and aluminum diacetate as alumina precursor. High purity mullite powder (~99%) was obtained at relative low temperature and holding time (1200 °C/3 h). Additionally, the prepared powder was used to manufacture an asymmetric microfiltration mullite membrane via phase-inversion tape casting. The membranes were characterized by their morphology, macrostructure, composition, mechanical behavior, and water permeation flux. Finally, the most promising membranes produced by both aforementioned methods were applied on premix membrane emulsification process. The SiOC and mullite membranes were compared to a commercially symmetric membrane (Por5 from Robuglas). The influence of membrane characteristics on the production of a fine emulsified oil-in-water emulsion was studied.

Keywords: Tape casting, Ceramic membranes, Polysiloxane, Mullite, Membrane emulsification.

Resumo

Neste trabalho é apresentado uma investigação sobre a manufatura de membranas de microfiltração baseadas em polissiloxanos. A técnica de conformação empregada foi o *tape casting* em conjunto com diferentes estratégias para formação de poros. Primeiro, polissiloxanos foram usados como precursores cerâmicos para o preparo de membranas simétricas de microfiltração a base de SiOC. Porosidade e propriedades superficiais foram ajustadas pela variação do conteúdo de agente de sacrifício (azodicarbonamida) e temperatura de pirólise (600 ou 1000 °C) sob atmosfera de nitrogênio, respectivamente. Segundo, pó cerâmico a base de mulita ($3\text{Al}_2\text{O}_3 \cdot 2\text{SiO}_2$) foi sintetizado usando polimetilsiloxano como precursor de sílica e diacetato de alumínio como precursor de alumina. Pó de mulita de alta pureza (~99%) foi obtido a uma temperatura e tempo de forno relativamente baixos (1200 °C/3 h). Adicionalmente, o pó preparado foi usado na manufatura de membranas de microfiltração feitas de mulita e com estrutura assimétrica via inversão de fase e *tape casting*. As membranas foram caracterizados pela sua morfologia, macroestrutura, microestrutura, composição, propriedades mecânicas e permeação de água. Finalmente, as membranas mais promissoras produzidas pelos métodos mencionados foram aplicadas no processo de emulsificação de pré-mistura. As membranas SiOC e mulita foram comparadas a uma membrana simétrica comercial (Por5 da Robuglas). A influência das características da membrana na produção de emulsões finas de óleo-em-água foi estudada.

Palavras-chave: *Tape casting*, Membranas cerâmica, Polissiloxanos, Mulita, Emulsificação por membrana.

Resumo estendido

FABRICAÇÃO DE MEMBRANAS CERÂMICAS DE MICROFILTRAÇÃO À BASE DE POLISSILOXANO POR COLAGEM DE FITA PARA PROCESSO DE EMULSIFICAÇÃO POR PRÉ-MISTURA

Introdução

A busca contínua por tecnologias mais eficientes tanto do ponto de vista energético quanto ambiental, impulsiona pesquisa e desenvolvimento na área de membranas. Além do mais, há um crescente interesse no uso de membranas cerâmicas, que possuem como principal vantagem, em relação às tradicionais poliméricas, o maior tempo de vida útil e estabilidade físico-química inerentes ao material cerâmico. Embora membranas sejam amplamente difundidas no processo de separação, recentemente, tem emergido estudos no processo de emulsificação por membranas. Em particular, o processo de emulsificação por pré-mistura (*premix*), o qual geralmente produz emulsões estáveis com baixa dispersão e a vazões maiores que o processo por emulsificação direta. Todavia, um dos principais parâmetros de controle do tamanho de gota dá-se pela seleção de membranas adequadas.

Com relação às membranas cerâmicas, percebe-se na literatura que os estudos relativos à fabricação de membranas cerâmicas são substancialmente relacionados ao uso dos óxidos, como alumina (Al_2O_3) e zircônia (ZrO_2). Entretanto, há uma classe de material que tem recebido destaque ultimamente: cerâmica derivada de polímeros ou *Polymer Derived Ceramics* (PDCs). Os PDCs consistem, essencialmente, de polímeros cujo componente central é o silício (Si), o qual pode estar ligado também a outros elementos como nitrogênio (N), carbono (C) e oxigênio (O). Devido ao seu caráter polimérico, os PDCs podem ser conformados por diferentes técnicas de processamento. Em particular, a colagem de fita (*tape casting*) consiste em um método tradicional para

produzir peças planas com espessura controlada, sendo bastante atrativa na produção de membranas.

As diferentes classes de PDCs podem ser convertidas em materiais cerâmicos sob condições mais brandas de temperatura que cerâmicas tradicionais, e sua estrutura final é dependente do precursor inicial, da atmosfera de queima e temperatura final. Dentre as principais estratégias utilizadas para o desenvolvimento de PDCs porosos, tem-se o uso de agentes de sacrifício, a espumação direta, a lixiviação de componentes da matriz por ácidos ou gases de halogênios, liofilização (*freeze casting*), emulsificação, e produção de aerogéis. Adicionalmente, PDCs termicamente tratados em atmosfera oxidativa podem ser utilizados como fontes de sílica amorfa reativa. A sílica resultante pode ser combinada com outros óxidos resultando em diferentes materiais cerâmicos a temperaturas inferiores a de métodos convencionais.

Embora a literatura contemple diversos estudos recentes sobre a produção de PDCs com porosidade controlada, ainda persiste o desafio de desenvolver materiais com aplicação prática. Logo, a flexibilidade oferecida pelos PDCs em termos de controle de propriedades superficiais e estruturais é promissora para a elaboração de membranas cerâmicas porosas.

Objetivos

O principal objetivo do trabalho consiste na produção de membranas cerâmicas planas de microfiltração utilizando *tape casting* como método de conformação e polissiloxanos como principais precursores cerâmicos. Adicionalmente, tenciona-se avaliar a aplicação de tais membranas em processo de emulsificação por membrana via *premix* (pré-mistura).

Metodologia

A primeira etapa do trabalho envolveu a produção de membranas cerâmicas e híbridas (cerâmicas/poliméricas) por meio de *tape casting* de polissiloxanos comerciais (metilpolissiloxano ou MK, e fenilmetilpolissiloxano ou H44). Esses polímeros foram dissolvidos em xileno e

acrescidos de aditivos como: carga inerte de carbeto de silício (SiC) de dois tamanhos distintos ($d_{50} = 4,5 \mu\text{m}$; ou $d_{50} = 6,5 \mu\text{m}$) para auxiliar no processamento e prover estabilidade mecânica; agente formador de poros (azodicarbonamida), em diferentes quantidades (0 – 30 m.%); e um catalisador de reticulação (imidazol). Os *tapes* produzidos foram pirolizados em duas temperaturas, a 600 ou 1000 °C em atmosfera inerte (N_2). As amostras foram caracterizadas em termos de macroestrutura via microscopia eletrônica de varredura (MEV) e porosimetria por intrusão de mercúrio. A microestrutura e área superficial específica foram avaliadas por meio de adsorção de nitrogênio, enquanto que as características superficiais de hidrofiliicidade/hidrofobicidade foram acessadas por meio de adsorção de vapor de água (solvente polar) e n-heptano (solvente apolar). Por fim, as propriedades mecânicas dos *tapes* pirolizados foram analisadas por método de flexão de três pontos.

A segunda parte do projeto contemplou o preparo de membranas assimétricas de mulita ($3\text{Al}_2\text{O}_3 \cdot 2\text{SiO}_2$) utilizando diacetato de alumínio como fonte de alumina (Al_2O_3) e metilpolisiloxano (MK) como fonte de sílica (SiO_2). Inicialmente, foi preparada a mistura estequiométrica dos precursores de mulita, seguida de calcinação a 850 °C (5 h) ou 1200 °C (3 h). Os pós cerâmicos foram analisados por meio de MEV, difração de laser (tamanho de partícula), e difração de raios-X (DRX) com análise de percentual cristalino via refinamento de Rietveld. Para o preparo das membranas, utilizou-se a técnica de *tape casting* combinada com a inversão de fase para o ajuste da morfologia e obtenção da microestrutura desejada. As membranas obtidas foram avaliadas por meio de MEV, porosimetria de intrusão de mercúrio, DRX em conjunto com refinamento de Rietveld, resistência mecânica (flexão de três pontos), e permeação de água.

Por fim, foram realizados ensaios de emulsificação de pré-mistura com as melhores membranas de cada etapa citada. Foram testadas as membranas SiC6.5-A30-1000 e Diac-1200-1650, aqui referidas como SiOC e mulita, respectivamente. Adicionalmente, as membranas preparadas foram comparadas com uma membrana comercial de borossilicato (Por5, da empresa Robuglas). Dessa forma, emulsões de óleo-

em-água foram preparadas utilizando 10 m.% de óleo (MCT, triglicérides de cadeia média) e 1 m.% de surfactante (Tween80 ou polissorbito 80). A emulsão inicial (*premix*) apresentou gotas de tamanho médio de 6,30 μm e dispersão (*span*) igual a 1,05 μm . Realizou-se a passagem do *premix* por duas vezes em cada membrana a 5 bar, avaliando, assim, o tamanho de gota e fluxos resultantes. Testes a diferentes pressões (2, 3 e 4 bar) foram conduzidos para membrana de mulita devido aos melhores fluxos obtidos por essa amostra.

Resultados e Discussão

Na primeira etapa da pesquisa, foram obtidas membranas simétricas com faixa de poros na região de microfiltração (0,1 a 10 μm) e porosidade aberta máxima na região de 38%. Características superficiais foram ajustadas através da manipulação da temperatura de pirólise em atmosfera inerte de nitrogênio (N_2). Membranas hidrofílicas foram preparadas por tratamento térmico a 1000 °C enquanto que caráter hidrofóbico foi obtido através de pirólise a 600 °C. A hidrofobicidade resultante neste último caso se deve à conversão cerâmica incompleta, a qual resulta em cerâmica híbrida contendo grupos orgânicos na estrutura da matriz. O controle da microestrutura foi realizado pela seleção de cargas inertes (SiC) de diferentes tamanhos médios (4,5 ou 6,5 μm), e também pela variação da quantidade de agente formador de poro (azodicarbonamida). O aumento da porosidade e o uso de cargas maiores (6,5 μm) afetou negativamente a propriedade mecânica das amostras, enquanto que o aumento da temperatura (1000 °C) teve efeito contrário.

Durante a segunda etapa, pós a base de mulita foram obtidos quando calcinados a 1200 °C (3 h), enquanto que pós calcinados a 850 °C (5 h) resultaram em materiais amorfos (conforme DRX). A partir dos pós calcinados, membranas assimétricas foram produzidas, com porosidade aberta máxima de aproximadamente 70% e tamanho de poro na região de microfiltração (capazes de reter partículas entre 0,1 a 10 μm). Propriedades mecânicas e porosidade foram avaliadas considerando diferentes tratamentos térmicos (1600, 1650, 1700 °C). Como esperado, o aumento da temperatura acarretou no aumento da resistência

mecânica e diminuição da porosidade. A estrutura cristalina foi caracterizada por difração de raios-X e quantificada por refinamento de Rietveld, o qual demonstrou que todas as membranas foram compostas por >99% de mulita em sua constituição. A permeação de água mostrou que a membrana Diac-1200-1650 (porosidade = 68%; tamanho médio de $\text{poro}_{\text{skin-layer}} = 1,18 \pm 0,8 \mu\text{m}$) é a amostra mais promissora em termos de aplicação prática, levando em conta os altos fluxos obtidos ($133 \text{ m}^3/\text{m}^2 \cdot \text{h}$) e baixa resistência hidráulica ($1,86 \times 10^{10} \text{ m}^{-1}$).

Finalmente, as membranas foram aplicadas na produção de emulsão de óleo-em-água via emulsificação de pré-mistura. Foi possível, assim, analisar a eficiência das membranas preparadas e compará-las com a membrana comercial de borossilicato. A emulsão precursora (*premix*) apresentou tamanho médio de gotas de $6,30 \mu\text{m}$ e span de 1.05. Após passagem nas membranas, foram obtidos tamanhos de gota na faixa de $4,57$ a $2,22 \mu\text{m}$, com valores de span inferior a 1. A membrana com estrutura assimétrica (mulita, Diac-1200-1650) demonstrou o melhor desempenho, especialmente no que concerne ao fluxo de permeação.

Considerações Finais

Os resultados obtidos na primeira etapa apontam resultados promissores no preparo de membranas cerâmicas e híbridas com diferentes características superficiais, em especial, sem a necessidade de etapas adicionais de funcionalização. Já na segunda parte, observa-se a flexibilidade dos precursores empregados e da técnica de conformação adotada para o preparo de membranas cerâmicas com morfologia controlada e alto desempenho. Finalmente, os dados de aplicação sugerem que a membrana simétrica de SiOC ainda necessita de otimizações frente ao excelente desempenho da membrana cerâmica assimétrica de mulita, a qual também teve desempenho superior a Por5.

Palavras-chave: Polissiloxano. *Tape casting*. Membrana cerâmica. Emulsificação por membrana.

List of figures

Figure 2.1: General processing flowchart of tape cast products. 11

Figure 2.2: Representation of a typical tape casting setup. 12

Figure 2.3: Scheme of the sacrificial method used for manufacturing macroporous ceramics..... 14

Figure 2.4: Effect of the binder (PVB) content on the pore size (a) and pore volume (b) of porous alumina membrane produced by cast tapes fired at 1350 °C (alumina powder size: a=0.5 μm; b=0.3 μm). (Data extracted from Das and Maiti [88] with the software GetData Graph Digitalizer© version 2.26.0.20; reproduced with permission..... 15

Figure 2.5: Effect of the SPF content on the porosity of YSZ ($d_{50} = 0.47 \mu\text{m}$) cast tape membrane after sintering at 1550 °C (adapted from Boaro et al. [90]; reproduced with permission)..... 15

Figure 2.6: Effect of the mixing process on the pore morphology of YSZ membranes with starch (20 vol%, $d_{50}=19 \mu\text{m}$) as SPF produced by tape casting: (a) mixing by an impeller for 4 h, (b) milling for 2.5 h, and (c) milling for 16 h (adapted from Corbin and Apté [89]; reproduced with permission)..... 16

Figure 2.7: Effect of various SPFs on the pore morphology of YSZ membranes: (a) flake graphite, (b) spheroidal graphite, (c) PMMA, (d) sucrose and (e) polystyrene (from Sarikaya and Dogan [94]; reproduced with permission)..... 17

Figure 2.8: Phase inversion technique by immersion precipitation and main pore structures. 19

Figure 2.9: General processing steps in the phase inversion applied to tape casting..... 21

Figure 2.10: Sequential tape casting: (a) scheme; SEM images of cross section of sintered (b) 3 alumina layers membrane, and (c) 2 alumina layers with one graphite layer membrane (adapted from Gu et al. [118]; reproduced with permission)..... 21

Figure 2.11: The processing steps of freeze-cast sintered parts: (a) initial slurry, (b) solidified body, (c) green body after sublimation and (d) sintered body (adapted from Deville [123]; reproduced with permission)..... 22

Figure 2.12: Scheme of freeze tape casting apparatus. RT: Real Temperature, MT: Melting Temperature, FT: Freezing Temperature (adapted from Sofie [127]; reproduced with permission). 23

Figure 2.13: SEM images of freeze tape cast YSZ at 30 vol% solids loading: (a) cross-section, frozen at $-50\text{ }^{\circ}\text{C}$; (b) cross-section, frozen at $-25\text{ }^{\circ}\text{C}$; (c) cross-section, frozen at $-5\text{ }^{\circ}\text{C}$; and (d) surface morphology (scale bar = $25\text{ }\mu\text{m}$) (from Sofie [127]; reproduced with permission). . 24

Figure 2.14: Partial sintering and material transport phenomena during sintering. 25

Figure 2.15: Effect of particle size on the pore size of the tape cast alumina membrane. Data extracted from Das and Maiti [136] with the software GetData Graph Digitalizer© version 2.26.0.20; reproduced with permission. 26

Figure 2.16: Change of pore size (a) and porosity (b) of alumina membranes with sintering temperature (at a constant soaking time of 4 h) and soaking time (at a constant temperature of $1350\text{ }^{\circ}\text{C}$). Data extracted from Das et al. [135] with the software GetData Graph Digitalizer© version 2.26.0.20; reproduced with permission. 27

Figure 2.17: (a) Microstructures of the surface of anode-supported electrolytes depending on the sintering temperatures; (b) effect of the ratio of fine YSZ (FYT) to coarse YSZ (TZ8Y) in anode compared with YSZ electrolyte on the sintering shrinkage (adapted from Moon et al. [140]; reproduced with permission). 28

Figure 2.18: Variations of flow rate with pore size and porosity of alumina membranes and influence of sintering temperature for membranes prepared with a particle size of 0.3 μm . (adapted from Das et al. [135]; reproduced with permission). 30

Figure 2.19: Main classes of organosilicon polymers used as ceramic precursors and typical thermal events (adapted from [5]). 52

Figure 2.20: Schematic representation of the production of oil-in-water emulsion by (a) direct or cross-flow membrane emulsification (DME) and (b) premix membrane emulsification (PME). 55

Figure 3.1: Flowchart of polysiloxane-derived, cast and pyrolyzed tapes (600/1000 $^{\circ}\text{C}$). 62

Figure 3.2: SEM images from the fracture of the pyrolyzed tapes at 600 or 1000 $^{\circ}\text{C}$ and 30 wt.% pore former (azodicarbonamide): (a) SiC4.5-A30-600 $^{\circ}\text{C}$, (b) SiC4.5-A30-1000 $^{\circ}\text{C}$, (c) SiC6.5-A30-600 $^{\circ}\text{C}$, (d) SiC6.5-A30-1000 $^{\circ}\text{C}$. Horizontal length of the white and red boxes represents the sizes given therein. 66

Figure 3.3: Influence of ADA content on open porosity (a) and average pore size (b). 67

Figure 3.4: (a) Influence of ADA content and different SiC particle sizes (4.5 or 6.5 μm) on specific BET surface areas of pyrolyzed (600/1000 $^{\circ}\text{C}$) tapes, (b) Isotherms obtained for two tape compositions (SiC4.5-A0 and A30) pyrolyzed at 600 $^{\circ}\text{C}$ and 1000 $^{\circ}\text{C}$ 69

Figure 3.5: Water and n-heptane vapor adsorption at 25 °C (left axis) and ratio of maximum water and n-heptane adsorption (right axis) for samples with different SiC particle size of 4.5 μm (a) and 6.5 μm (b), varying azodicarbonamide amount and pyrolysis temperature (600 and 1000 °C)..... 70

Figure 3.6: Maximum flexural strength (σ_{max}) of the tapes produced with two silicon carbide particle sizes, pyrolyzed at 600/1000 °C and varying pore former content. (Values with the same amount of ADA followed by different numbers were significantly different at $p < 0.05$ according to Tukey's test – Columns with the same color followed by different letters were significantly different at $p < 0.05$ according to Tukey's test.)..... 72

Figure 3.7: 3D representation of the influence of azodicarbonamide amount, pyrolysis temperatures, and inert particle size on: open porosity (a); average pore size (b); specific surface area (c); and maximum flexural strength (d)..... 75

Figure 3.8: Surface roughness (Ra) for samples with different SiC particle sizes (4.5 or 6.5 μm), varying azodicarbonamide content (0 or 30 wt.%), and non-pyrolyzed samples (light blue and pink bars) and pyrolyzed at 600 °C or 1000 °C..... 81

Figure 3.9: Pore size distribution versus relative pore volume and open porosity curves obtained from mercury intrusion porosimetry of pyrolyzed sample. 82

Figure 3.10: Nitrogen adsorption-desorption isotherms for samples with different SiC particle sizes, varying azodicarbonamide content and pyrolyzed at 600 °C/1000 °C..... 83

Figure 4.1: Process scheme of the preparation of mullite-based (a) powder and (b) membrane..... 90

Figure 4.2: SEM images (left) of the prepared mullite-based powders and particle size distribution analysis by laser diffraction (right). 93

Figure 4.3: X-ray diffraction (XRD) analysis of the obtained mullite-based powders. A – α -Alumina or Corundum (ref.: PDF#04-071-1123); M – Mullite ($3\text{Al}_2\text{O}_3 \cdot 2\text{SiO}_2$) (ref.: PDF#01-079-1454). (The values in the blue box represent the crystalline phases of Diac-1200 sample quantified by Rietveld Refinement; Goodness of fit: sig = 1.5; Rwp = 13.96%; Mullite-COD ID 2310785; Corundum-COD ID 2300448; Cristobalite-COD ID 9001579.)..... 94

Figure 4.4: SEM images of the cross-sections (a, b, c), top surface (d, e, f), and bottom surface (g, h, i) of the membranes sintered at 1700 °C. Pore diameter distribution graphs are displayed for the top and bottom surface based on image analysis using ImageJ..... 97

Figure 4.5: Pore size distribution (μm) versus relative pore volume (%) and open porosity (%) curves obtained from Hg-intrusion porosimetry of the sintered mullite membranes at different temperatures: (a) 1600 °C, (b) 1650 °C and (c) 1700 °C. 98

Figure 4.6: (a) Weibull failure distribution of flexural strength of selected sintered membranes measured by three-point bending test; (b) flexural strength as a function of open porosity for tested membranes and literature comparison (She and Ohji “▲” [42], Dong et al. “▼” [43], Cao et al. “◆” [25], Hou et al. “◀” [29], and Hua et al. “▶” [44]). (Diac-X-X samples in Fig.6b followed by different letters were significantly different at $p < 0.05$ according to Tukey's test). 100

Figure 4.7: Water permeation flux ($\text{m}^3/\text{m}^2\cdot\text{h}$) as a function of the applied pressure (bar) for selected membranes in a dead-end configuration (the values inside the colored boxes represent the average pore size (top) and the open porosity (bottom). Values signed with “*” were obtained from Hg-porosimetry; values without markers were determined by image analysis from SEM pictures of the top surface).101

Figure 4.8: Scheme of the water permeability and membrane emulsification setup. 114

Figure 4.9: XRD and Rietveld Refinement of the sintered membranes (Mullite-COD ID 2310785; Corundum-COD ID 2300448; Cristobalite-COD ID 9001579.)..... 115

Figure 4.10: Viscosity curves of the prepared slurries..... 116

Figure 4.11: Pore size distribution and open porosity obtained from Hg-porosimetry of a commercial borosilicate membrane – Por5 from Robuglas (Company information: 1 – 1.6 μm by ISO 4793-80, and 0.9 – 1.4 μm by ASTM E128-99/ Available on: <https://www.robuglas.com/en/service/poresizes.html>). 116

Figure 4.12: Determination of the permeance ($\text{m}^3/\text{m}^2\cdot\text{h}\cdot\text{bar}$) of selected sintered membranes based on the pure water flux measurements as a function of the applied transmembrane pressure. 117

Figure 5.1: Schematic representation of the membrane permeation flux and emulsification setup (adapted from [20]). 123

Figure 5.2: Cross-section and top surface SEM images of the symmetric membranes (a,d) Por5 and (b,e) SiOC (the image presented in “b” was adapted from [19]), and the asymmetric Mullite membrane (c,f). 125

Figure 5.3: (a) Pore size distribution versus relative pore volume (bars) and open porosity curves (lines) measured by Hg-porosimetry (the data

referred to SiOC and mullite were adapted from [19] and [20], respectively). (b) Pore size distribution of the skin-layer of the mullite asymmetric membrane obtained from an SEM image analyzed by ImageJ software. 126

Figure 5.4: Surface hydrophilicity-hydrophobicity measured by water and n-heptane vapor adsorption analysis of the ceramic membranes at 25 °C (the data correspondent to SiOC sample was extracted from [19]). 127

Figure 5.5: Water permeation flux of the ceramic membranes at a fixed pressure of 5 bar in a dead-end configuration (the data correspondent to Por5 was extracted from [20]; values showed inside the graph correspond to average pore size (μm) and open porosity (%); value signed with “*” was determined by image analysis from SEM pictures of the top surface, and values without marker were obtained from Hg-porosimetry). 128

Figure 5.6: (a) Droplet size distribution obtained from premix emulsification of oil-in-water emulsion (Premix = MCT 10 wt.% + 1 wt.% Tween[®] 80) at 5 bar for the studied ceramic membranes (vertical lines and values within the boxes indicate the mean droplet size given by the Sauter mean diameter in μm – d_{32}). (b) Span values and characteristics sizes in terms of d_{10} , d_{50} , and d_{90} according to the membrane and number of passes at 5 bar..... 130

Figure 5.7: Premix permeation flux ($\text{m}^3/\text{m}^2\cdot\text{s}$) at 5 bar as a function of the mean droplet size ($d_{32}/\mu\text{m}$) and the number of passes for the studied membranes in a dead-end configuration. 132

Figure 5.8: (a) Droplet size distribution (μm) and span values obtained from the premix membrane emulsification experiment of oil-in-water

emulsion (MCT 10 wt.%) at different pressures (2, 3, and 4 bar) and 2 passes through the mullite asymmetric membrane. (b) Premix permeation flux ($\text{m}^3/\text{m}^2\cdot\text{s}$) as a function of the applied pressure and number of passes for the mullite membrane. 134

Figure 5.9: Linear fittings of the studied premix permeation fluxes as a function of the transmembrane pressure for the asymmetric mullite membrane..... 135

Figure 5.10: Pore size distribution versus relative pore volume (bars) and open porosity curves (lines) measured by Hg-porosimetry of commercial borosilicate glass membranes (Por 2 and Por4 from Robuglas). 142

Figure 5.11: Evaluation of the isolated effect of the porous support (Por2-Robuglas) on the premix membrane emulsification process. ... 143

List of tables

Table 2.1: Main pore former parameters studied to manufacture porous ceramics materials by tape casting. 31

Table 2.2: Authors contributions for section 2.1 of Chapter 2. 35

Table 3.1: Authors contributions for Chapter 3..... 76

Table 4.1: Slurry compositions (vol.%) for the preparation of the mullite-based membranes..... 89

Table 4.2: Crystalline phases content (wt.%) and goodness of fit determined by Rietveld refinement method of the X-ray powder diffractograms from the sintered membranes..... 95

Table 4.3: Membrane thickness (δ_m) and transport properties in terms of permeance (k_w), clean membrane resistance (R_m), and intrinsic permeability ($k_{V,inv}$) of the tested asymmetric and symmetric ceramic membranes. 103

Table 4.4: Authors contributions for Chapter 4..... 106

Table 5.1: Main characteristics and additional remarks of the membranes used in the premix emulsification experiments..... 121

Table 5.2: Premix emulsification studies of oil-in-water emulsions using different ceramic membranes in a dead-end configuration..... 136

Table 5.3: Authors contributions for Chapter 5..... 138

List of acronyms, symbols and abbreviations

<i>A</i>	Membrane cross-sectional surface area (m ²)
ADA	Azodicarbonamide
BBP	Benzyl butyl phthalate
COD	Crystallography open database
<i>d</i> ₃₂	Sauter mean diameter (μm)
<i>d</i> _m	Mean pore size (μm)
DME	Direct membrane emulsification
DMF	N,N-dimethylformamide
DOP	Diocetyl phthalate
<i>dt</i>	Differential in time (h, s)
<i>dV</i>	Differential in volume (L, m ³)
EtOH	Ethanol
FAS	1H,1H,2H,2H-perfluorooctyltriethoxysilane
H44	Polymethylphenylsiloxane
H62C	Polymethylvinylphenylhydrido siloxane
<i>J</i>	Membrane permeation flux (m ³ /m ² ·h, m ³ /m ² ·s)
<i>K</i>	Carman-Kozeny constant
<i>k</i> _{<i>v,intr</i>}	Intrinsic permeability (m ²)
<i>k</i> _w or <i>L</i> _p	Permeance (m ³ /m ² ·h·bar)
<i>m</i>	Weibull modulus
MAUD	Material analysis using diffraction
MCE	Nitrocellulose mixed ester
ME	Membrane emulsification
MEK	Methyl ethyl ketone
MK	Polymethylsiloxane
MTES	Methyltriethoxysilane
N/A	Not available
NH ₄ PAA	Ammonium polyacrylate
NMP	N-methyl-2pyrrolidone
PCP	Preceramic polymer
PDC	Polymer derived ceramics
PE	Polyethylene

PEG	Polyethylene glycol
PESf or PES	Polyethersulfone
PME	Premix membrane emulsification
PMMA	Poly(methyl methacrylate)
PS	Polystyrene
PSD	Particle size distribution
PVA	Polyvinyl alcohol
PVB	Polyvinylbutyral
PVP	Polyvinylpyrrolidone
R_m	Membrane resistance (m^{-1})
R_{wp}	Weighted profile R-factor (%)
S	Membrane specific surface area (m^2)
SEM	Scanning electron microscopy
Sig	$R_{wp}/R_{expected}$
SOFC	Solid oxide fuel cell
SPF	Sacrificial pore former
SPG	Shirasu porous glass
SR-CT	Synchrotron-radiation computer tomography
SSA	Specific surface area (m^2/g)
TBA	Tert-butyl alcohol
XRD	X-ray diffraction
YSZ	Yttria-stabilized zirconia
δ_m or Δz	Membrane thickness (μm , m)
ΔP	Transmembrane pressure (bar)
E	Membrane open porosity (%)
σ_0	Characteristic flexural strength (MPa)
σ_{max}	Maximum flexural strength (MPa)
M	Dynamic viscosity (Pa·s)
P	Specific mass or density (kg/m^3)

Table of contents

1	Introduction.....	1
1.1	Aim of the work.....	3
1.2	Structure of the thesis	3
1.3	References	4
2	Literature review	7
2.1	Manufacturing porous ceramic materials by tape casting.....	8
2.1.1	Introduction	8
2.1.2	Tape casting of porous materials.....	10
2.1.2.1	Tape casting with sacrificial pore formers	13
2.1.2.2	Phase inversion tape casting.....	18
2.1.2.3	Freeze tape casting	21
2.1.2.4	Partial sintering	24
2.1.3	Porous tape materials, microstructure and applications ...	28
2.1.3.1	Filtration.....	29
2.1.3.2	Porous supports	32
2.1.3.3	Other applications	33
2.1.4	Summary and outlook	34
2.1.5	Acknowledgements	34
2.1.6	Authors contributions	35
2.1.7	References	35

2.2	Polymer-derived ceramics	52
2.3	Membrane emulsification	54
2.4	References	55
3	Tape casting of polysiloxane-derived ceramic with controlled porosity and surface properties	59
3.1	Introduction	59
3.2	Material and methods	61
3.2.1	Precursors, solvents and additives	61
3.2.2	Preparation of the polysiloxane-based tapes	61
3.2.3	Sample notation	63
3.2.4	Characterization	63
3.3	Results	64
3.3.1	Pore morphology and macroporosity	64
3.3.2	Surface area and surface characteristics	68
3.3.3	Flexural strength of the pyrolyzed tapes	71
3.4	Discussion	73
3.5	Conclusions	75
3.6	Acknowledgements	76
3.7	Authors contributions	76
3.8	References	77
3.9	Supplementary material	81

4 Asymmetric mullite membranes manufactured by phase-inversion tape casting from polymethylsiloxane and aluminum diacetate	85
4.1 Introduction	85
4.2 Experimental.....	87
4.2.1 Materials.....	87
4.2.2 Mullite-based powder preparation.....	88
4.2.3 Membrane preparation.....	88
4.2.4 Specimen denotation	89
4.2.5 Characterization.....	90
4.3 Results	92
4.3.1 Powder size and composition	93
4.3.2 Membrane composition.....	95
4.3.3 Membrane morphology and macroporosity	96
4.3.4 Mechanical behavior of sintered membranes	99
4.3.5 Membrane performance and transport properties.....	101
4.4 Discussion.....	103
4.5 Conclusions	105
4.6 Acknowledgements	106
4.7 Authors contributions	106
4.8 References	107

4.9	Supplementary material.....	114
5	Premix membrane emulsification using flat ceramic membranes with tailored structure and composition	119
5.1	Introduction.....	119
5.2	Experimental	121
5.2.1	Chemicals and membranes.....	121
5.2.2	Premix preparation.....	122
5.2.3	Membrane permeation flux and premix emulsification tests 123	
5.2.4	Membrane and emulsion characterization.....	124
5.3	Results and discussion.....	125
5.3.1	Membrane characteristics.....	125
5.3.2	Premix emulsification using different ceramic membranes 129	
5.3.3	Premix emulsification using mullite membrane at lower pressures	132
5.4	Conclusions.....	137
5.5	Acknowledgements	137
5.6	Authors contributions.....	138
5.7	References	138
5.8	Supplementary material.....	142
6	Conclusion	145

7 Outlook	149
Appendix	151
A.1 Doctor blade project and 3D design	151
A.2 Simple 3D design of the membrane module setup for permeation and premix experiments	152
A.3 New design of the membrane module setup for permeation, separation, premix, and direct emulsification experiments	153
Curriculum vitae	159
Supervised student project	163
List of publications	165

1 Introduction

Currently there is a growing interest in the development of products and technologies that are more energy efficient and environmental friendly. A clear example that permeates the chemical engineering field is the membrane processes. Generally, a membrane is a medium that serves as a selective barrier to the passage of one or more components (permeate) of a mixture and restricts the passage of other (retained) [1]. However, the application of this technology is not limited only to separation processes, but can also be exploited in other processes, such as membrane emulsification [2].

The membrane emulsification (ME) process has received great attention because of the ease scalability and control of the droplet size by the adjustment of a few parameters, such as membrane pore size and working pressure [2]. As its name suggests, membrane emulsification involves the preparation of emulsions (oil-in-water or vice versa) using a porous membrane. It is important to note that this process can be found in two distinct configurations, direct emulsification (DE, or cross-flow) and premix membrane emulsification (PME) [3]. In the first case, one of the fluids (oil or water) is permeated through one side of the membrane and on the other side there is a mixture of the opposite fluid containing stabilizers (surfactants) [3]. In the PME process, initially an emulsion with coarse droplets is reduced by passing through a membrane. Typically, in direct emulsification, the droplet size tends to be bigger than the membrane pore. While in the PME, droplet sizes can be smaller than the pore size, which may be achieved by the multiple passage of the emulsion through the membrane [4].

Up to now, an overview of the possible membrane application has been given. Nevertheless, it is essential to emphasize the role of the membrane constitution and fabrication methods. The membrane industry began in the preparation of polymer membranes, whose cost of production and incorporation of functional groups are characterized as their market advantage [5]. However, the advances in ceramic processing allowed the entry of ceramic membranes into the market. Although the

initial cost of production and acquisition is greater than the polymer competitor, ceramics have a great advantage in terms of process longevity. This is due to the nature of the ceramic material, which has as main characteristics high chemical-thermal resistance, and structural stability due to non-plastic deformation [6].

The studies on the manufacture of ceramic membranes are substantially related to the use of oxides, such as alumina and zirconia. Nonetheless, there is a class of material that has received great attention lately, which is called by the acronym PDCs (Polymer Derived Ceramics). The PDCs consist essentially of polymers whose central component is silicon (Si) which can also be bound to other elements such as nitrogen (N), carbon (C), oxygen (O), among others. [7]. Thus, different classes of PDCs can be converted into ceramic materials under milder temperature conditions than traditional ceramics, and their final structure is dependent on the initial precursor, the burning atmosphere and final temperature [8].

The main strategies involved to produce porous PDCs are the use of sacrificial agents, direct foaming, leaching of matrix components by acid or halogen gases, freeze casting, emulsification, and aerogels production [9]. Considering the polymeric nature of PDCs, this material can undergo different shaping techniques. For instance, tape casting is a well-established processing method to prepare planar structures with controlled thickness. Additionally, a great variety of methods can be explored with tape casting to prepare porous ceramic components [10]. Planar ceramics of silicon oxycarbide (SiOC) were produced by tape casting, using different polysiloxanes and silanes as precursors, and silicon carbide (SiC) as inert filler, to avoid shrinkage problems. Porosities in the range of 1.6 to 45% and pores of 0.025 to 2.05 μm were obtained. The increase in porosity and pore size was a result of the pyrolysis temperature increase from 1200 °C to 1600 °C, because Si metal was used as a pore forming agent [11,12].

Although the literature mentions several recent studies on the production of PDCs with controlled porosity, the challenge of developing materials with practical application still persists. The flexibility of-

ferred by the PDCs (polysiloxanes in particular) in terms of control of surface and structural properties are promising.

1.1 Aim of the work

This work aims to prepare planar microfiltration ceramic membranes applied in PME process, exploring different pore forming strategies while using polysiloxanes as one of the main precursors and tape casting as shaping technique.

1.2 Structure of the thesis

This thesis is divided into several Chapters, whose key points are provided below:

In the current Chapter (1), a general contextualization is displayed alongside with the aim of this work.

Chapter 2 is intended to help the reader to visualize the big picture where this thesis might be framed. This chapter is composed of a published literature review paper (section 2.1) on porous ceramics prepared via tape casting. In this review, different strategies to prepare porous ceramics in conjunction with tape casting is discussed. Subsequently, the reader will encounter some concise information on Polymer-Derived Ceramics (PDCs), Polysiloxanes, and Membrane Emulsification (ME) process.

Chapters 3, 4, and 5 consist of the experimental results achieved during this doctorate. In Chapter 3 and 4, microfiltration ceramic membranes are produced using polysiloxane as one of the precursors and tape casting as the processing method. Furthermore, two strategies are shown to obtain a symmetric (sacrificial pore former, Chapter 3) and an asymmetric (phase-inversion, Chapter 4) microfiltration ceramic membrane. Chapter 3 is the first experimental published work, in which the preparation steps and characterizations of amorphous porous SiOC-based ceramics are described. Chapter 4 constitutes the second experi-

mental published paper; here asymmetric mullite membranes ($3\text{Al}_2\text{O}_3 \cdot 2\text{SiO}_2$) are prepared using aluminum diacetate as alumina precursor and polysiloxane as silica precursor. Finally, Chapter 5 (to be submitted to publication) reveals the possible use of the best membranes prepared (in the Chapters 3 and 4) in the premix membrane emulsification process. In addition, they are compared to a commercial borosilicate membrane.

Chapter 6 presents a summary of the main conclusions from this doctorate, putting into perspective the contributions derived from it. Moreover, the interconnection between the papers originated from this work is evidenced as well.

Chapter 7 extrapolates the horizon of possibilities for future works related to this topic, discussing some outlooks and remnant gaps in this matter.

1.3 References

- [1] R.W. Baker, *Membrane Technology and Applications*, Wiley, 2012.
- [2] S.M. Joscelyne, G. Trägårdh, Membrane emulsification — a literature review, *J. Memb. Sci.* 169 (2000) 107–117.
- [3] L. Giorno, G. De Luca, A. Figoli, E. Piacentini, E. Drioli, Membrane Emulsification: Principles and Applications, in: E. Drioli, L. Giorno (Eds.), *Membr. Oper. Innov. Sep. Transform.*, Wiley-VCH Verlag GmbH & Co. KGaA, 2009: pp. 463–497. doi:10.1002/9783527626779.ch21.
- [4] A. Nazir, K. Schroën, R. Boom, Premix emulsification: A review, *J. Memb. Sci.* 362 (2010) 1–11. doi:10.1016/j.memsci.2010.06.044.
- [5] N. Hilal, A.F. Ismail, C. Wright, *Membrane Fabrication*, CRC Press, 2015.
- [6] D. da Silva Biron, V. dos Santos, M. Zeni, *Ceramic Membranes Applied in Separation Processes*, 2018. doi:10.1007/978-3-319-58604-5.

- [7] G. Mera, E. Ionescu, Silicon-Containing Preceramic Polymers, in: *Encycl. Polym. Sci. Technol.*, John Wiley & Sons, Inc., 2002. doi:10.1002/0471440264.pst591.
- [8] P. Greil, Polymer Derived Engineering Ceramics, *Adv. Eng. Mater.* 2 (2000) 339–348. doi:10.1002/1527-2648(200006)2:6<339::AID-ADEM339>3.0.CO;2-K.
- [9] C. Vakifahmetoglu, D. Zeydanli, P. Colombo, Porous polymer derived ceramics, *Mater. Sci. Eng. R Reports.* 106 (2016) 1–30. doi:10.1016/j.mser.2016.05.001.
- [10] R.K. Nishihora, P.L. Rachadel, M.G.N. Quadri, D. Hotza, Manufacturing porous ceramic materials by tape casting-A review, *J. Eur. Ceram. Soc.* 38 (2018) 988–1001. doi:10.1016/j.jeurceramsoc.2017.11.047.
- [11] P. Cromme, M. Scheffler, P. Greil, Ceramic Tapes from Preceramic Polymers, *Adv. Eng. Mater.* 4 (2002) 873–877. doi:10.1002/1527-2648(20021105)4:11<873::AID-ADEM873>3.0.CO;2-G.
- [12] F. Scheffler, M. Scheffler, Polymer derived ceramic tapes as substrate and support for zeolites, *Adv. Appl. Ceram.* 108 (2009) 468–475. doi:10.1179/174367609X459540.

2 Literature review

The objective of this chapter is to give the reader an overview on the topic of manufacturing porous ceramic materials by tape casting, as well as polymer-derived ceramics (PDCs), and membrane emulsification. The first section of this chapter (2.1) is composed by a published review paper, which brings the description of the tape casting technique, the main strategies to achieve porous structures by this method, and some applications regarding porous ceramic tapes. The next section (2.2) a detailed information about PDCs is given, in which the main focus is on polysiloxanes. Finally, this chapter presents a section (2.3) concerning the membrane emulsification process.

2.1 Manufacturing porous ceramic materials by tape casting¹

Tape casting is a well-established technique to fabricate ceramic tapes. This technique has been usually applied to produce dense substrates for electronic applications, but recently there are increasing efforts regarding the production of porous cast tapes. The aim of this paper is to present the latest strategies and achievements to manufacture porous ceramic materials by tape casting. The pores morphology can be manipulated by adjusting particle size, sacrificial pore formers, sintering conditions, and combined techniques (phase inversion and freeze casting). Moreover, tape casting enables adjusting the thickness of the product, which is a key property in separation applications using membranes and/or support materials with tailorable structure.

2.1.1 Introduction

Ceramic materials are known for the manufacturing of structural and dense components, where the presence of pores is usually treated as a defect in the final product. However, the advances in processing technology of ceramic particles associated with industrial and scientific demand for porous materials with chemical, thermal, and structural stability has led to the increasing interest in porous ceramic materials [1]. There are a plenty of applications where porous structures are essential, such as catalyst supports [2–8], membranes for filtration processes [9–18], substrates for electrochemical system electrodes [19–25], among many others. It is worth to mention that the application is strongly related to material composition and structural parameters (e.g. pore size, shape, distribution, connectivity, tortuosity, etc.).

Concerning the production of porous ceramic materials, there are some basic strategies described in the literature to obtain the desired structure. The main routes to generate macroporous ceramics are divided into four categories including: (i) partial sintering [26–30], (ii) sacrifi-

¹ Based on a paper published in the Journal of the European Ceramic Society:
<https://doi.org/10.1016/j.jeurceramsoc.2017.11.047>

cial agents [31–36], (iii) replica templates [37–42], and (iv) direct foaming [43–48]. A background information about these routes is firmly set and well reviewed in the literature [49–54]. However, manufacturing of ceramic membranes consists of three major steps: raw material preparation, shaping, and heat treatment [55,56]. Regarding the shaping methods, the most usual ceramic membrane fabrication methods are extrusion, pressing, sol-gel, slip casting and tape casting [57].

Tape casting is a well-established technique that was developed in the mid-1940s to produce thin piezoelectric materials. Since then, this process has been improved and widely applied to fabricate dense ceramic substrates and multi-layered materials in large scale [58,59]. Nevertheless, this method, which is able to produce flat ceramic components with tailored thickness, has gained some attention in manufacturing porous ceramic materials. Furthermore, the thickness control plays an important role in the separation performance in membrane process [60].

According to the pore size, porous ceramics can be classified as: (a) microporous (<2 nm), mesoporous (2–50 nm), and macroporous (>50 nm) [61]. By the proper combination of raw materials and processing techniques, porous ceramic structures with tailorable pores size and porosity may be created [62]. Moreover, an important information on the production of porous materials concerns the transition region between open to closed porosity [63]. This region is often associated in literature by using minimum solid areas models, that are, respectively, the: (1) bond (e.g. neck) area between particles defining pores smaller than the particles, or (2) minimum web thickness between adjacent pores being more than or equal to the surrounding particles (e.g. bubbles in a foam) [64,65].

The aim of the current review is to present the state-of-the-art of porous ceramic materials manufactured by tape casting. Thus, this work presents an overview of the fundamental aspects related to the tape casting technique and reviews the strategies that have been applied to produce thin ceramic membranes with tailored porosity. These strategies include the use of sacrificial pore formers, freeze casting, phase-inversion by immersion precipitation principle, and partial sintering.

2.1.2 Tape casting of porous materials

Tape casting is a standard shaping technique used to produce flat ceramic sheets with a thickness range varying between 10 μm to 1 mm [58]. The process was originally developed by Glenn Howatt during 1940s to manufacture capacitor dielectrics, which remains one of the most important applications of tape casting [66]. The general fabrication process of ceramic thin materials by tape casting can be summarized in the flowchart in Figure 2.1.

This method consists of a wet-shaping process based on casting of a tape from a suspension with pseudoplastic nature, also known as slurry or slip. The slurry is composed of an inorganic powder dispersed in a liquid (water or organic), which acts as a solvent for organic additives (dispersants, plasticizers, and binders) and as a dispersion medium for the ceramic particles [67]. Carter and Norton [56] provide a concise description of the function of the principal slurry components:

- The liquid (also referred to as solvent in the literature) controls the viscosity of the slurry allowing it to be spread on the carrier film (usually a polymer), and provides a vehicle to homogeneously distribute the additives and disperse the ceramic powder.
- Dispersants (also known as deflocculants) avoid settling of the powder particles.
- Binders hold the ceramic particles together after shaping until the tape is sintered and must be removed by heat treatment.
- Plasticizers increase the flexibility of the green tape.

A tape casting slurry must be adjusted in order to yield tapes that satisfy some quality criteria, such as (i) no defects during drying; (ii) cohesion to allow the manipulation of dried sheets; (iii) microstructural homogeneity; (iv) good thermopressing (lamination) ability; (iv) easy pyrolysis (debinding); and (v) high mechanical strength after sintering [68]. This requires careful selection of the slurry additives together with accurate control of many processing parameters, which makes the preparation of the slurry a critical step.

As stated by Gutiérrez and Moreno [69], the preparation of a slurry for tape casting strongly depends on solids concentration, order of addition of the additives, binder amount and characteristics, among other process parameters. All these parameters may affect the final properties of the ceramic tapes like density, thickness, porosity, surface quality, and mechanical behavior. In order to produce a slurry with well-dispersed powder, the preparation process is usually performed in two steps. In the first step, the powder is dispersed into the liquid using a proper dispersant. Second, the additives – such as binder, plasticizer, and defoamer – are added to the slurry. A pseudoplastic behavior of the slurry is desired to ensure the production of homogeneous tapes [70]. In this case, during casting, the viscosity is decreased due to shear forces between the blade and the carrier. Right after casting, the viscosity increases rapidly to suppress uncontrolled flow and to prevent sedimentation of the ceramic particles [70].

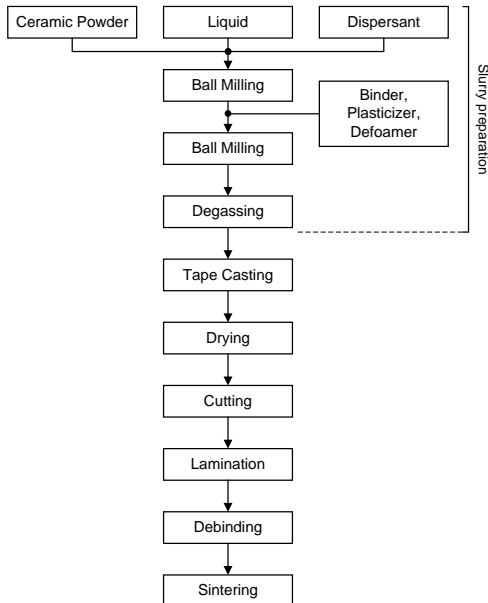


Figure 2.1: General processing flowchart of tape cast products.

The prepared slurry is poured into a container and after casting, the tape is formed onto a moving polymer tape, where a leveling blade, commonly named “doctor blade”, controls the thickness of the green tape (Figure 2.2). The green tape is dried and cut into parts, which can be subsequently laminated to obtain thicker parts to ensure mechanical stability. The laminates are then sintered to remove organics and promote the desired densification [55,71].

During the drying step, the slurry is converted into a semirigid, flexible tape upon removal of the solvent. This can be accomplished by drying at room temperature or using an auxiliary dryer and heat source to provide a temperature below the boiling point of the solvent, which increases the drying rate [72]. The drying process has to be carefully controlled to avoid the generation of cracks in the green tape due to stress development and heterogeneous shrinkage [73,74]. Depending on the slurry composition, the thickness of the dried green tape can decrease around 50% of the originally defined gap in the doctor blade.

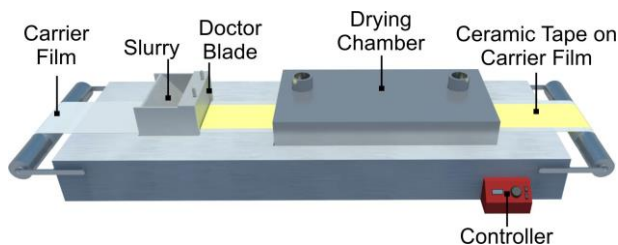


Figure 2.2: Representation of a typical tape casting setup.

As previously mentioned, the lamination is proceeded with the dried tape to increase thickness and structural stability. A multilayer green body is produced by applying pressure to the stacked tapes (10–30 MPa) at a temperature above the softening temperature of the binder and plasticizer system [75]. The thermopressing process induces the interpenetration of the adjacent particles, hence increasing green density [76]. The tapes can be thermopressed in many ways, for example: multilayers by folding a single big tape (multi-folding lamination process) [77]; unidirectional or multidirectional laminating process [78]; or simp-

ly by changing the tape side (face-to-face or back-to-face). However, it is also possible to perform the lamination under room temperature and low pressure (2.5–5.0 MPa) by using double-sided adhesive tapes, overcoming some former problems of deformation during thermopressing [79–81]. Alternatively to lamination, tape overcasting (also known as sequential tape casting) can be adopted, in which slurries are cast on the top of a slightly dried green tape [82,83].

The final step includes firing the shaped green body. In a first step, the organic additives (dispersant, plasticizer, defoamer, binder) are burned out by heating the tapes or laminates. This is carried out in the air for oxide ceramic, and it is necessary to pay close attention to the complex processes occurring, which include vaporization, decomposition, depolymerization, and oxidation [84]. Therefore, the organic additives must be slowly removed from the tapes to avoid deterioration, such as delamination of laminates [75]. Afterward, the sintering process takes place consolidating the powder compacts via the application of thermal energy. In this case, the thermodynamic driving force is the reduction in the total interfacial energy of the system [85].

2.1.2.1 Tape casting with sacrificial pore formers

Sacrificial pore formers (SPFs) are incorporated into the slurry to act as a place holder, which will be later removed through evaporation and/or burning leaving empty pores behind (Figure 2.3) [54]. Usually employed SPFs include synthetic organics (polymer beads, organic fibers, etc.), natural organic substances (starch, cellulose, cotton, etc.), as well as metallic and inorganic elements (nickel, carbon, graphite, etc.) and liquids (water, gel, emulsions, etc.) [52]. **Erro! Fonte de referência não encontrada.** synthesizes the main sacrificial pore formers used in tape casting. Although a solvent (e.g. water) can be considered a SPF, its use will be discussed in more detail in a separate topic (freeze casting) owing to its unique features.

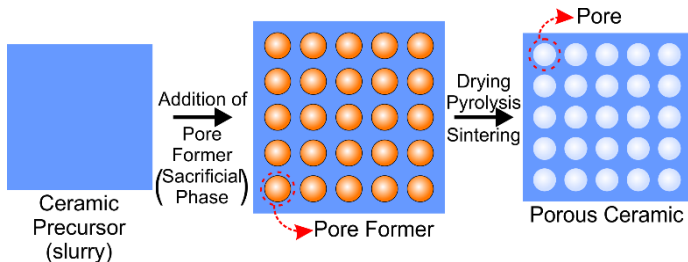


Figure 2.3: Scheme of the sacrificial method used for manufacturing macroporous ceramics.

The approach of the sacrificial method is widely used primarily because of the easiness and possibility to produce tailored porosity, pore size distribution, and pore morphology of the final ceramic component through the proper selection of the sacrificial pore former [50]. Considering that after heat treatment, the ceramic powder is the only component that remains in the material, basically, all of the organic slurry components can be treated as potential pore formers. However, to produce a tape it is necessary to optimize the slurry composition; for this reason, some slurry components cannot exceed a limit value in order to maintain processability.

Polyvinylbutyral (PVB) is a common organic substance that can be used as a binder or dispersant in tape casting, so that PVB is only employed in organic solvent-based systems [86,87]. Das and Maiti [88] produced porous alumina membranes by tape casting and evaluated the effect of the binder content (PVB) on the pores formation. According to Figure 2.4, it is possible to conclude that the increase in binder content, beyond a specific amount (18–20 wt%), can lead to a broader range of porous radii (Figure 2.4a), and to an increment in closed porosity accompanied by the reduction of open porosity (Figure 2.4b). These peculiar responses are justified by the tendency of particles agglomeration in the green tape due to the large amount of binder, favoring the particles compaction and close pore formation during sintering [88]. However, previous reports showed that the average pore size is mainly dictated by the initial ceramic powder size when pore formers are not employed.

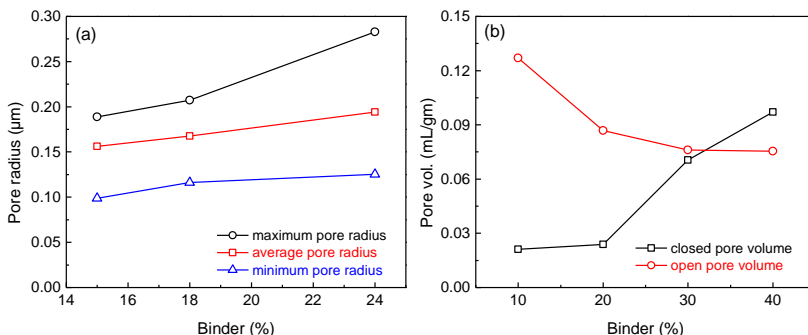


Figure 2.4: Effect of the binder (PVB) content on the pore size (a) and pore volume (b) of porous alumina membrane produced by cast tapes fired at 1350 °C (alumina powder size: a=0.5 μm; b=0.3 μm). (Data extracted from Das and Maiti [88] with the software GetData Graph Digitalizer© version 2.26.0.20; reproduced with permission).

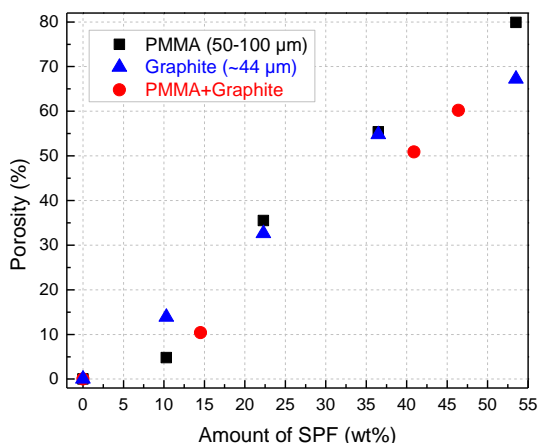


Figure 2.5: Effect of the SPF content on the porosity of YSZ ($d_{50} = 0.47 \mu\text{m}$) cast tape membrane after sintering at 1550 °C (adapted from Boaro et al. [90]; reproduced with permission).

For the generation of tailored pores, it is generally preferred to employ components designed with the purpose to act only as pore formers in the slurry. The use of those materials allows producing a very broad and controllable range of porosity, depending on the amount,

shape, distribution and size of the pore formers. The range can vary from almost zero to around 80% (values observed for membranes produced by tape casting) [89,90]. Figure 2.5 depicts a positive linear relationship between total porosity and the amount of SPF of some tape casted membranes. This behavior is quite expected since the increasing of the SPF content leads to an increment in the percolation network among particles [91].

On the other hand, the mixing step of pore formers into the slurry also has a substantial influence on the pores formation [92,93]. Figure 2.6 shows that the mixing method and the milling time generate different porosities in the sintered ceramic membrane [89]. It is noticed that high milling time (16 h) introduces a narrow pore size distribution in the structure, probably owing to the uniform introduction of the SPF in the slurry. Meanwhile, paddle mixing (4 h) and jar milling (2.5 h) maintain a certain degree of agglomeration in the pore-forming particles, causing more heterogeneity in the ceramic structure. Nevertheless, a noticeable difference is observed between both techniques in Figure 2.6a. Impeller mixing seems to be less effective than milling, as seen in Figure 2.6b–c.

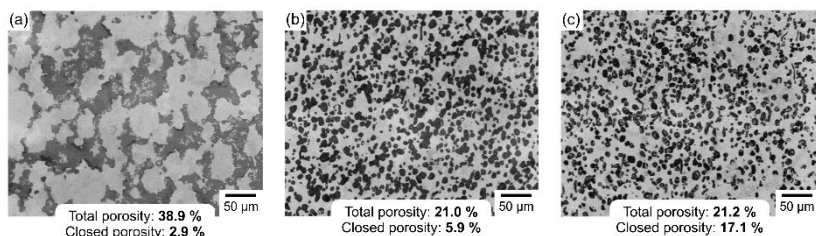


Figure 2.6: Effect of the mixing process on the pore morphology of YSZ membranes with starch (20 vol%, $d_{50}=19\ \mu\text{m}$) as SPF produced by tape casting: (a) mixing by an impeller for 4 h, (b) milling for 2.5 h, and (c) milling for 16 h (adapted from Corbin and Apté [89]; reproduced with permission).

PMMA is one of the most frequent synthetic polymers used to produce high controllable and spherical pores by the sacrificial method. The size of PMMA microspheres can vary from a few micrometers (8.39 μm [94]; 10 μm [95,96]) to values around 100 μm [90] depending

on the polymerization degree, that is, the average molecular weight of the polymer. On the other hand, starch appears as the most employed natural pore-forming alternative, exhibiting different particles sizes conforming to the starch source: rice (4–6 μm) [97,98], corn (10–15 μm) [97,99], or potato (5–40 μm) [98,100]. In addition, graphite is the inorganic option most applied as SPF, showing a wide range of size (3–82 μm) for either spheres or platelets shapes [89,90,94–6,98,99,101,102].

Figure 2.7 shows the internal morphologies of some porous ceramics produced by tape casting with various pore formers. Even though many types of sacrificial pore formers have been used in tape casting of ceramic porous membranes (Table 2.1), it seems that the central role of the chemical nature of the SPF (in the pores formation) resides in its thermal behavior. Thus, the pore structure is governed inherently by thermal and morphological properties of the SPFs [94].

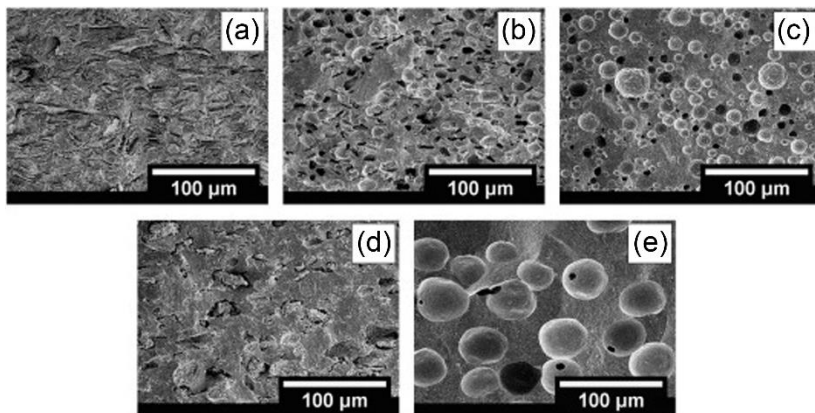


Figure 2.7: Effect of various SPFs on the pore morphology of YSZ membranes: (a) flake graphite, (b) spheroidal graphite, (c) PMMA, (d) sucrose and (e) polystyrene (from Sarikaya and Dogan [94]; reproduced with permission).

The use of NiO as SPF consists in a different strategy to create pores in ceramics. NiO is not removed during sintering like the pyrolyzable pore formers. Thus, for NiO to act as a SPF, it has to be initially

reduced to Ni (in H₂ atmosphere) and after reduction, Ni is removed by acid leaching, producing pores in this final step [90].

Polymer derived ceramic (PDC) tapes were produced using a mixture of silane and polysiloxanes that act as a binder at cast temperature and produce ceramic components after thermal treatment. In this case, silicon carbide (SiC) as inert filler helps to reduce shrinkage related problems, and elemental silicon (Si) as reactive filler controls the porosity of the tapes [103]. Si is removed from the tape during pyrolysis at high temperature (>1400 °C) in different atmospheres (N₂ or Ar) owing to the formation of SiO gaseous phase, which is accelerated at temperatures above 1400 °C. Basically, the gaseous SiO is generated via two mechanisms: (i) Si_(s) reacts with SiO_{2(s)} generating 2SiO_(g); (ii) C_(s) interacts with SiO_{2(s)} resulting in the formation of CO_(g) and SiO_(g) [104]. Tapes with the same composition exhibited higher porosity when treated in argon atmosphere, which can be explained by the formation of silicon oxynitride in the samples pyrolyzed under N₂. A composition with 30 vol% Si and 10 vol% treated at 1600 °C in Ar and N₂ resulted in porosity around 45% (d₅₀–2.05 μm) and 25% (d₅₀–0.07 μm), respectively. The flexural strength of the PDC tapes varied in the range of 67–115 MPa, being later on applied as support or substrate for zeolites [105].

2.1.2.2 Phase inversion tape casting

Phase inversion is one of the most common techniques for preparing polymeric membranes [106]. In this method, a polymer is dissolved in an appropriate solvent and shaped into a desired form (thin film, tube, hollow fiber). A precipitant or nonsolvent (e.g. water) is added to this polymer solution, causing separation of the homogeneous phase into a solid polymer and a liquid solvent phase. The precipitated polymer forms a porous structure containing a network of more or less uniform pores [107]. It is worth to mention that the concept of phase inversion covers a range of different techniques such as solvent evaporation, precipitation by controlled evaporation, thermal precipitation, pre-

precipitation from the vapor phase and mostly immersion precipitation [108].

During the phase inversion by immersion precipitation, the homogeneous solution becomes thermodynamically unstable. The solution can decrease its free energy from mixing by dividing into two liquid phases of different composition: polymer poor phase and polymer rich phase [109]. The polymer poor phase corresponds to the pore structure, which is surrounded by the polymer-rich phase. Asymmetric membranes result from this process, normally, present a thin top layer (skin layer) supported by porous sublayer that often contains large void spaces or macrovoids. These macrovoids may exhibit different morphologies, for instance, finger-like or sponge-like pores, depending on the phase inversion kinetics and thermodynamics (see Figure 2.8) [110].

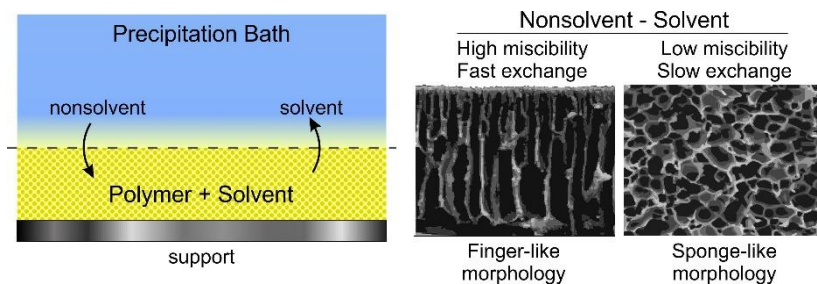


Figure 2.8: Phase inversion technique by immersion precipitation and main pore structures.

Porous ceramic membranes have been manufactured by coupling phase inversion technique with typical ceramic processing methods (extrusion, spinning and tape casting). Several studies have been carried out to produce hollow fiber structures, many of them including the use of ceramic powders like alumina [111–113] or YSZ [21,114,115]. Nevertheless, here the membranes obtained by tape casting with phase inversion will be reviewed. Figure 2.9 depicts the general steps of the process in the phase-inversion applied to tape casting. The most employed compounds to prepare the solution for phase inversion are Polyethersulfone (PESf – polymer) and Polyvinylpyrrolidone (PVP – addi-

tive); as solvents N-methyl-2-pyrrolidone (NMP) or N,N-dimethylformamide (DMF) stand out; finally, water appears as the coagulant.

Fang et al. [116] produced asymmetric alumina membranes by phase-inversion tape casting, characterizing the morphology through synchrotron-radiation computer tomography (SR-CT). This technique generates 3D images of the structure, but it is only capable to show the macroporosity due to its limited spatial resolution of $\sim 4 \mu\text{m}$. Thus, the porosity measured by SR-CT was $\sim 30\%$ and by Archimedes was 59% (total porosity). As expected, finger-like structures (oriented pores) were formed in the middle and sponge layers at the bottom, which can interfere negatively on the permeability. To overcome this issue, Huang et al. [117] and Gu et al. [118] showed that the sponge layer could be effectively removed by using graphite sacrificing agent as observed in Figure 2.10.

Asymmetric membranes constituted of YSZ with LSM [119] or LSCrF [120–122] have been prepared to separate oxygen molecules, where the porous layer acts as a support to the separation dense layer. The total porosity of the YSZ-LSM and YSZ-LSCrF membranes was 35% and 50%, respectively. The higher porosity of the YSZ-LSCrF membrane is mainly because of the addition of graphite as sacrificial pore forming in the support slurry. However, both works concluded that the orientation of the pores in the support (owing to the finger-like structure) optimized O_2 permeability. This allowed fast gas phase transport through the membrane when compared to membranes produced by sequential two-step tape casting with pyrolyzable substances (graphite) as pore former. Another great advantage of the phase inversion technique by immersion precipitation is the simplicity because it is possible to produce the green porous support and dense layer in a single step. Most methods require at least two separate forming steps.

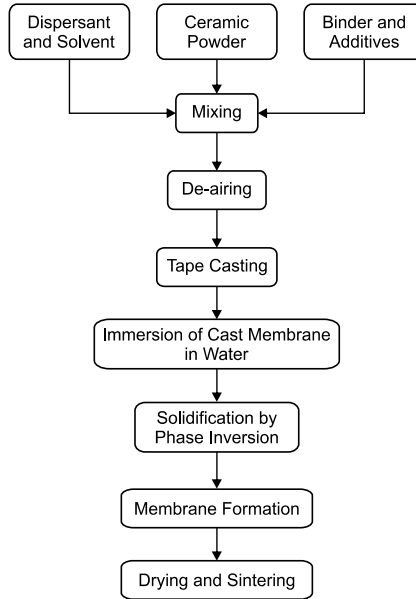


Figure 2.9: General processing steps in the phase inversion applied to tape casting.

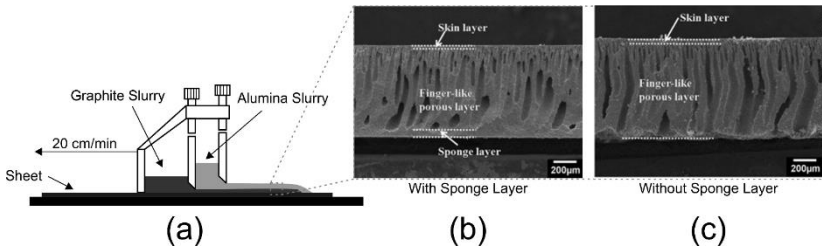


Figure 2.10: Sequential tape casting: (a) scheme; SEM images of cross section of sintered (b) 3 alumina layers membrane, and (c) 2 alumina layers with one graphite layer membrane (adapted from Gu et al. [118]; reproduced with permission).

2.1.2.3 Freeze tape casting

The freeze casting technique consists of freezing a liquid colloidal suspension (aqueous or organic systems), followed by sublimation

of the solidified phase, and subsequent sintering to consolidate and densify the walls. Unidirectional channels can form from the resultant porous structure when unidirectional freezing is employed, considering that pores are a replica of the solvent crystals (see Figure 2.11) [123].

Since the porosity of the sintered porous ceramics is a replica of the solidified solvent structure, the final pore morphology can be tuned by varying fabrication parameters such as the solid particle size and content in the slurry, the freezing conditions (pressure, temperature, time and rate), and type of solvent and additives [124].

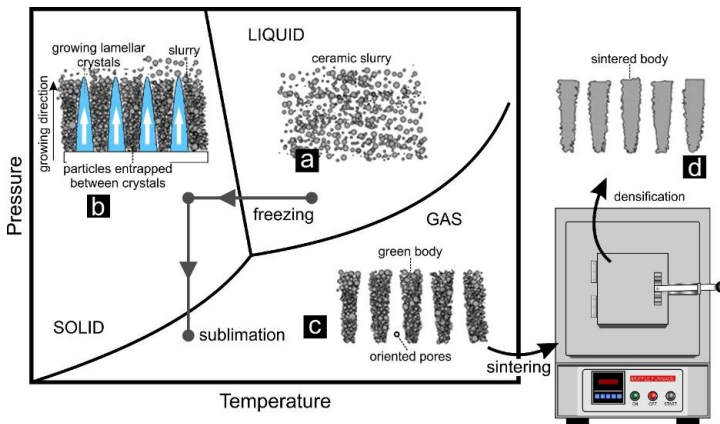


Figure 2.11: The processing steps of freeze-cast sintered parts: (a) initial slurry, (b) solidified body, (c) green body after sublimation and (d) sintered body (adapted from Deville [123]; reproduced with permission).

Freeze tape casting is the combination of the tape casting method with freeze casting principles. According to Li et al. [125], this technique produces vertical graded porous structures for large area tape samples. Firstly, a suspension is cast onto a casting bed through a doctor blade assembly. Then, the casting bed is moved into a freezing zone to perform directional freeze casting, generating a controlled morphology by adjusting the freeze conditions and the bed temperature (Figure 2.12).

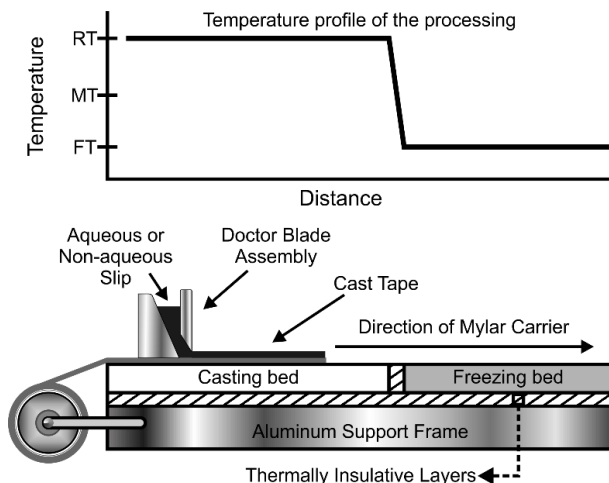


Figure 2.12: Scheme of freeze tape casting apparatus. RT: Real Temperature, MT: Melting Temperature, FT: Freezing Temperature (adapted from Sofie [127]; reproduced with permission).

Freeze tape casting has been employed to manufacture porous ceramics from TiO_2 [126,128] in aqueous system and YSZ [127] in aqueous and non-aqueous (TBA: tert-butyl alcohol) systems. The studies showed that the porosities decrease with the incorporation of solid loadings. For both components, the solid loading was varied in the aqueous medium from 2.6 to 19.5 vol% TiO_2 and 10–50 vol% for YSZ, in which the porosity range was, respectively, 88%–74% for TiO_2 , and 86%–40% for YSZ.

Sofie [127] stated that for the aqueous casting of YSZ, the solid content plays a more relevant role than the freezing temperature for the pores formation. The critical solid loading to generate continuous pores channels is 35 vol%. Higher values introduce heterogeneous nucleation and/or incomplete ceramic particle rejection, resulting in graded, but non-continuous, pore morphologies. Figure 2.13 shows the tailoring of microstructure by altering the freezing temperature of freeze tape cast YSZ at 30 vol% solid loading. Very low temperatures ($-50\text{ }^\circ\text{C}$) induces fast freezing rates, resulting in little to no deviation of columnar growth of the ice during the solidification (Figure 2.13a). When the freezing

temperature is raised ($-25\text{ }^{\circ}\text{C}$), the dendritic growth of the ice crystals became evident (Figure 2.13b). As the freezing temperature ($-5\text{ }^{\circ}\text{C}$) reached values close to the water freezing point (Figure 2.13c), irregular patterns are formed that deviate strongly from columnar. Figure 2.13d illustrates the influence of the casting direction and reveals the acicular nature of the pores on the upper surface of the tape.

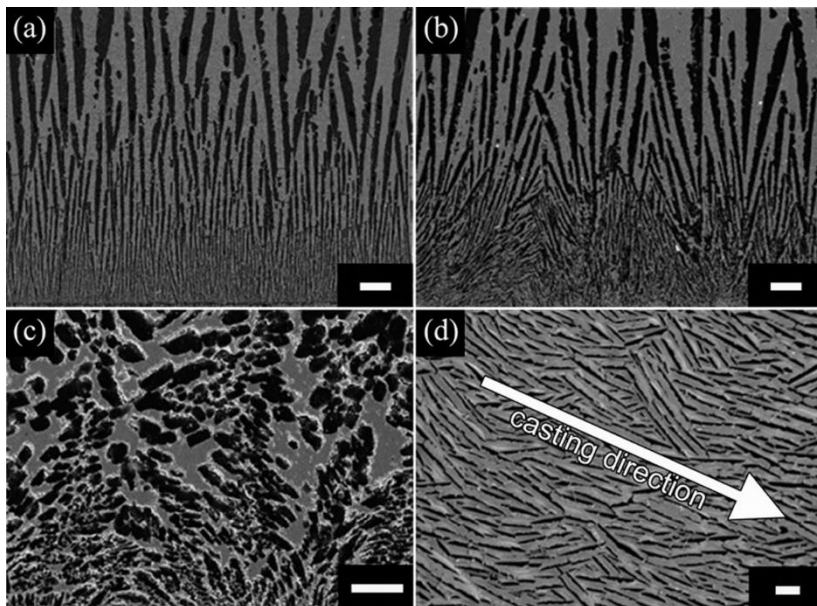


Figure 2.13: SEM images of freeze tape cast YSZ at 30 vol% solids loading: (a) cross-section, frozen at $-50\text{ }^{\circ}\text{C}$; (b) cross-section, frozen at $-25\text{ }^{\circ}\text{C}$; (c) cross-section, frozen at $-5\text{ }^{\circ}\text{C}$; and (d) surface morphology (scale bar = $25\text{ }\mu\text{m}$) (from Sofie [127]; reproduced with permission).

2.1.2.4 Partial sintering

Sintering is often referred to as the densification step, because of the combination of time-temperature that leads to the porosity decreasing in the ceramic body. Normally, the temperature applied during sintering corresponds to values around 60% to 80% of the material melting

temperature. For example, Al_2O_3 presents a melting temperature of $2073\text{ }^\circ\text{C}$, and the sintering temperature is commonly $1400\text{--}1650\text{ }^\circ\text{C}$ [129]. Hence, when the full densification is undesired, a common approach to fabricate porous ceramics materials with small grain sizes and low density is through partial sintering [130]. Figure 2.14 illustrates the partial sintering process, where some sintering phenomena related to material transport are limited by controlling time- temperature. The connection between particles is mainly achieved by the neck formation owing to surface diffusion [131,132]. Since complete densification is avoided, a porous structure can be produced. However, this causes some degradation of mechanical properties characterized by a decrease in both elastic modulus and fracture strength [133].

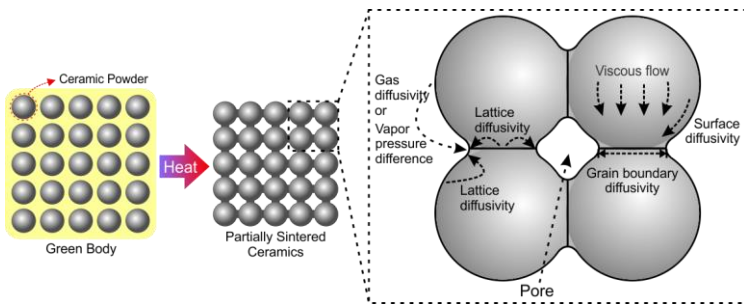


Figure 2.14: Partial sintering and material transport phenomena during sintering.

Partial sintering provides a good control degree of the porosity whilst the pore size is also regulated by the size of starting powders. Porosity increases with decreased forming pressure, sintering temperature and time. The porosities of porous materials obtained by partial sintering are usually below 50% [134]. Studies conducted with alumina powder have indicated that the major parameter controlling the pore size is the initial particle size of the alumina used to prepare the membrane [135,136]. Das et al. varied the mean particle size (d_{50}) in a broad range ($0.2\text{--}1.5\text{ }\mu\text{m}$) whilst maintaining a high solid content in the slurry formulation (71–83 wt.%), resulting in a pore size range between $0.1\text{--}0.7\text{ }\mu\text{m}$ and porosity of 25% to 55%. The microstructure analysis exhib-

ited a linear correlation between the pore size and d_{50} , wherein the finer particle sizes generate smaller pore sizes (Figure 2.15). As stated by Das and Maiti [136], this response provides a simple and effective manner to tailor the mean pore size of the tape cast membrane at a desired value.

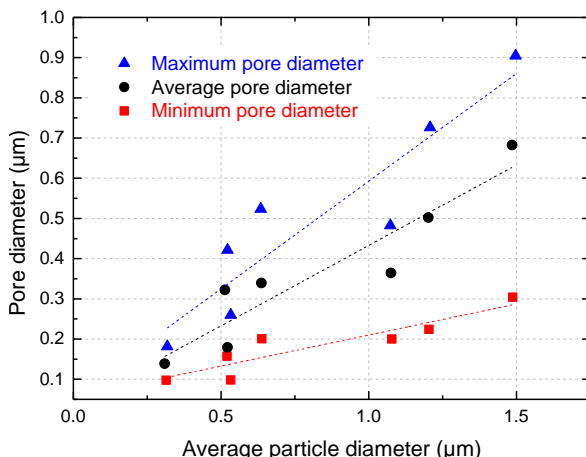


Figure 2.15: Effect of particle size on the pore size of the tape cast alumina membrane. Data extracted from Das and Maiti [136] with the software GetData Graph Digitalizer© version 2.26.0.20; reproduced with permission.

As expected, not only the initial particle size but also the particle size distribution (PSD) has an influence on the pore size. Nevertheless, the use of an initial broad range of particle sizes can decrease porosity due to the increment in densification as a result of higher packing capability of the particles [137,138].

Porous alumina membrane has been prepared by varying sintering temperatures and soaking times. Analyzing Figure 2.16a, it is reasonable to assume that the sintering temperature and time have only a small effect on the mean pore size. Notwithstanding, Figure 2.16b establishes that porosity is strongly affected by the sintering conditions. In view that an increase in sintering temperature and time resulted in linear decreasing of porosity in the final body. This is the direct consequence of the sintering phenomena in which neck growth followed by pore

closure takes place to a greater extent as the sintering temperature or soaking time is increased [135]. In a further work, Das and Maiti observed that a relatively insignificant sintering takes place at or below 1350 °C, and a reduction in pore volume occurs as result of enhanced sintering, especially, at temperatures above 1350 °C [31]. Vasconcelos and et al. [139] have reported similar behavior for the preparation of diatomite membranes. Increasing sintering temperatures (1000–1300 °C) and soaking times (1–8 h) resulted in a reduction in porosity, whereas the average pore size increased.

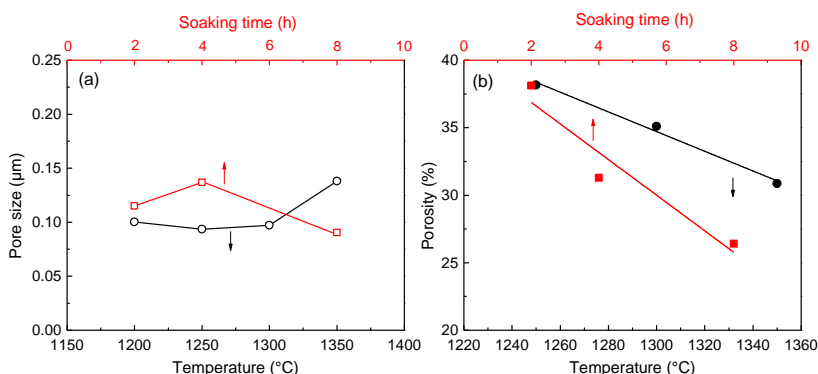


Figure 2.16: Change of pore size (a) and porosity (b) of alumina membranes with sintering temperature (at a constant soaking time of 4 h) and soaking time (at a constant temperature of 1350 °C). Data extracted from Das et al. [135] with the software GetData Graph Digitalizer© version 2.26.0.20; reproduced with permission.

Moon et al. [140] developed solid oxide fuel cells (SOFC) composed of NiO-YSZ (56:44 wt ratio), producing anode-supported thin electrolytes via tape casting and co-firing. In Figure 2.17a, the authors also showed the same behavior of reducing porosity due to increasing sintering temperature (1200–1400 °C for 3 h). The growth in grain size clearly seems a result of high temperature (energy) in the system which induces the mass transport between the particles. It is also interesting to observe the relationship between sintering temperature and shrinkage (Figure 2.17b). For all samples, it is evident that an increment in tem-

perature results in higher shrinkage. However, when the content of coarse YSZ powder is increased, the final shrinkage is less pronounced and vice versa. This is an expected response since the driving force of sintering is the reduction in the surface free energy of the particles [55]. Thus, small particles possess larger surface areas leading typically to higher shrinkage when compared to coarse particles [141].

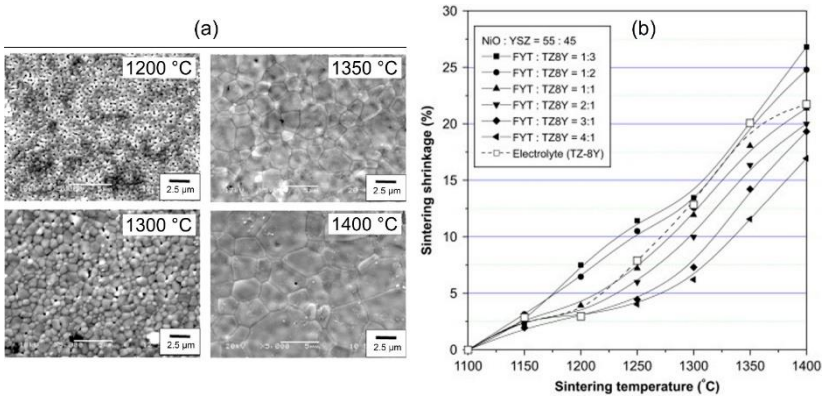


Figure 2.17: (a) Microstructures of the surface of anode-supported electrolytes depending on the sintering temperatures; (b) effect of the ratio of fine YSZ (FYT) to coarse YSZ (TZ8Y) in anode compared with YSZ electrolyte on the sintering shrinkage (adapted from Moon et al. [140]; reproduced with permission).

2.1.3 Porous tape materials, microstructure and applications

Table 2.1 summarizes the strategies to produce porous ceramic tapes, including materials and applications listed in the works reviewed. The following discussion connects the influence of the processing parameters with the microstructure, performance, and application of the porous materials.

2.1.3.1 Filtration

Porous ceramics for filtration applications may require mechanical strength, material and environmental compatibility, thermal and chemical stability, selectivity, and high flow-rate and permeability constitute important parameters to evaluate the efficiency of a filter [124]. According to Table 2.1, the main strategies used to fabricate these porous ceramics tapes for filtration are based on the use of sacrificial pore formers, control of sintering conditions and powder size.

Flat alumina membranes have been manufactured for applications in microfiltration [135] and as support and an intermediate layer for ultrafiltration [97]. Microfiltration membranes (with a thickness around 0.5 mm) presented a mean pore size varying from 0.12 to 0.68 μm , and porosity in a range of 31% to 53%. The deviation observed in the porosity of the sample A6 is probably due to the broader particle size distribution of this sample. Thus, this implies that the presence of coarse particles reduces the green and sintered density of the ceramic tape. In other words, an increment of the overall porosity is observed [145]. As displayed in Figure 2.18, the permeate flux is highly influenced by the pore size (more than by the porosity), which is directly related to the particle size as discussed previously. Water permeability (under suction conditions of 0.01 mbar) varied from 110 to 908 $\text{L}\cdot\text{m}^{-2}\cdot\text{h}^{-1}$, when the pore size increased from 0.12 to 0.68 μm . Taking a closer look at the table at the bottom right in Figure 2.18, it is noticeable that porosity is reduced by increasing both sintering temperature and time, resulting in a reduction of water flux. Most of the membranes (with a pore size smaller than 0.5 μm) are suitable for complete removal of bacteria from water and are also reusable after cleaning by acid or heat sterilization.

The pores in the support for ultrafiltration were generated using starch (from corn and rice) as a sacrificial pore former (see Table 2.1) [97]. The alumina supports presented the following characteristics: pores with a size range of 0.8–5 μm , 5.6–13.4 mD of N_2 permeability (200–1000 mbar) and 2.3–5.5 mD of distilled water permeability, and a flux of 108.1–405.9 $\text{L}\cdot\text{m}^{-2}\cdot\text{h}^{-1}\cdot\text{bar}^{-1}$. Nevertheless, confirming the ex-

pectations, the permeability decreases, to 3.1–4.2 mD for the gas and 0.5 mD for the liquid, when intermediate and top layers (ultrafiltration structure) were employed. Hence, the permeability started to be dominated by the small pores in the top layer.

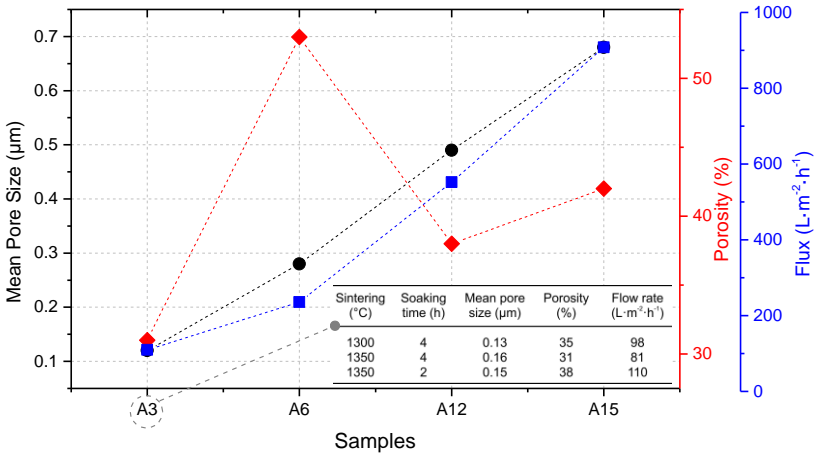


Figure 2.18: Variations of flow rate with pore size and porosity of alumina membranes and influence of sintering temperature for membranes prepared with a particle size of 0.3 µm. (adapted from Das et al. [135]; reproduced with permission).

Vasconcelos et al. [139] showed that the permeability of diatomite membranes ($3.8\text{--}12.8\text{ cm}^2\cdot 10^{-11}$) increases as a function of the increment in pore size. Furthermore, it is worth mentioning that they established a relationship between sintering conditions (time and temperature) and pore size and porosity, as described in Section 2.1.2.4. Thus, the pore size range (0.27–0.78 µm) suggests a feasible application in microfiltration systems. Moreover, the membrane thickness, in this case, lays between 0.5 and 1.5 mm. The first value (0.5 mm) concerns to the minimal mechanically reliable thickness and the last one (1.5 mm) refers to the maximum thickness to obtain a feasible flux for the separation.

Table 2.1: Main pore former parameters studied to manufacture porous ceramics materials by tape casting.

Main Pore Former Strategy	Ceramic Powder	Particle Size (µm)	Solvent/ Dispersant	Binder/ ¹ Plasticizer/ ² SPF ³	Sintering Temperature (°C)	Pore Size (µm)	Total Porosity (%)	Application	Ref.
Pore Forming Agent	Al ₂ O ₃	0.4	Water/ Displex A 40	Mowilit DM 765S; Hoechst Perstorp AB/ Starch ¹	1100 – 1300	0.07 – 1.1	28 – 57	Support for ultrafiltration	[97]
	Al ₂ O ₃	0.31 – 0.51	MEK:EtOH/ Emphos 2A	PVB/ ¹ PEG:BBP ²	800 – 1600	0.06 – 0.25	N/A	Microfiltration	[88]
	YSZ	0.3	Toluene: EtOH/ fish oil Defloc Z3	Burvar B79/ Sanitizer 1607/ Starch ¹ , PE ² , Graphite ³	1475	30	20 – 80	N/A	[89]
	YSZ-NiO	0.26 – 1.2	Water/ Duramax 3005	HA12 ¹ :B1000/ ¹ PMMA ³ , PE ³ , Graphite ³ , NiO ³	1550	~1	0 – 83.4	SOFC	[90]
	YSZ-NiO	0.3 and 1.0	MEK:EtOH/ GTO Fluka	PVB/ ¹ PEG:BBP ² /Starch ³ , Carbon Black ³ , Graphite ³	1200	0.27 – 0.45	26.8 – 48.3	Supporting anode for SOFC	[98]
	YSZ	N/A	Toluene:EtOH/ KD-1	PVB/ ¹ DOP/ ¹ PS ² , Graphite ³ , PMMA ³ , Sucrose ³	1350	2 – 200	2.69 – 35.27	SOFC	[94]
	C ₆₀ ,Gd ₂ O ₃ , ₉₅	~0.35	MEK:EtOH/ PVP	PVB/ ¹ Graphite ³ , PMMA ³	1250	~1	35 – 44	Electrochemical fuel gas purification cell	[95,96]
	SiC	2.0	-----	Silanes ¹ -Polysiloxanes/ ¹ Crosslinking catalysts ² / Si ³	1000 – 1600 (N ₂ or Ar)	0.025 – 2.05	1.6 – 53.4	Substrate and support for zeolites	[103,105]
	Al ₂ O ₃	~0.7	NMP	PESt ¹ +PVP	1500	0 – 80	~33	N/A	[116]
	YSZ-LSM	N/A	NMP	PESt ¹ +PVP/ Graphite ³	1320	~10	~20	O ₂ separation	[119]
Phase Inversion	YSZ-NiO	N/A	NMP	PESt ¹ +PVP/ Graphite ³	1350	N/A	N/A	SOFC	[117]
	Al ₂ O ₃	~1.21	NMP	PESt ¹ +PVP/ Graphite ³	1500	0.02 – 2	N/A	Membrane distillation (water purification)	[118]
Freeze Casting	YSZ-LSiGF	N/A	NMP	PESt ¹ +PVP/ Graphite ³	1450	N/A	N/A	O ₂ separation and partial oxidation of methane	[120]
	TiO ₂	0.1 – 0.2	Water/ NHPAA	PVA/ ¹ PEG ² / Water ³	1000	1.4 – 14.3	75 – 88	N/A	[126]
	YSZ	0.55	Water or TBA/ Darvan C-N – Fish oil Z-3	Duramax ¹ or PVB/ ¹ Water ³	1400	<5 – 100	~4 – 86	Supporting anode for SOFC	[127]
	TiO ₂ -NiO	0.1 – 0.2	Water/ NHPAA	PVA/ ¹ PEG ² / Water ³	1000	0.3627 – 10.75	~61	Photocatalysis	[128]
	Al ₂ O ₃	0.22 – 1.5	MEK:EtOH/ Emphos 2A	PVB/ ¹ PEG:BBP ²	800 – 1600	0.1 – 0.7	25 – 55	Microfiltration (e.g. bacterial removal from water)	[135,136,142]
Partial Sintering	Diatomite	28	Water/ Dolapix CE 64	Mowilit DM 60P ¹	1000 – 1300	0.27 – 0.78	~44	Filtration (e.g. air)	[139,143]
	YSZ-NiO	~2.2	Water	PVA/ ¹ Glycerol ²	1450	N/A	~20	SOFC	[144]
	YSZ-NiO	0.2 – 1.3	Toluene:EtOH/ M1201	B74001 ¹ / Carbon black ³	1200 – 1400	N/A	38 – 60	SOFC	[140]

BBP: benzyl butyl phthalate; DOP: dioctyl phthalate; EtOH: ethanol; KD-1: polyester polyamine copolymer (Mw ~ 10,000 g·mol⁻¹); LSCF: La_{0.8}Sm_{0.2}Fe_{0.8}O_{3-δ}; LSM: La_{0.8}Sr_{0.2}MnO_{3-δ}; MEK: methyl ethyl ketone; N/A: not available; NHPAA: ammonium polyacrylate; NMP: N-methyl-2-pyrrolidone; PE: polyethylene; PEG: polyethylene glycol; PESt: polyethersulfone; PVB: polyvinylbutyral; PVP: polyvinylpyrrolidone; SOFC: solid oxide fuel cell; TBA: tertiary butyl alcohol; YSZ: yttria-stabilized zirconia

¹Silanes: Methyltriethoxysilane (MTES) as a viscosity modifier.

²Polysiloxanes: Polymethylsiloxane (MK) and Polydimethylsilylphenylhydrido siloxane (HG2C).

³Crosslinking catalysts: Oleic acid and Aluminum acetylacetonate.

2.1.3.2 Porous supports

Tape casting consists of a flexible technique to obtain large and flat ceramic tapes, plates and laminated structures. Thus, it has been explored for the fabrication of porous anode substrate in anode-supported planar SOFC to provide a path to incoming and outgoing gases [146]. The literature points out a plenty of approaches employed for manufacturing porous structures for SOFC by tape casting (see Table 2.1). For instance, the use of sacrificial pore formers, manipulation of sintering conditions, and combined techniques (e.g. tape casting with phase inversion or freeze casting).

The most commonly applied anode and substrate material is the composite of YSZ-Ni or YSZ-NiO [147]. Nickel serves as a catalyst dispersed around YSZ particles so that the zirconia skeleton actuates to stabilize the porous structure [148]. Many studies have shown the reliability of PFA to develop tailored pore structures in YSZ and YSZ-NiO substrates [89,90,94,98]. Starches are highlighted as inexpensive pore formers, delivering high porous materials proportionally to the employed added amount. Sanson et al. [98] found out that the use of rice starch and carbon black is recommended for the production of anode supports for SOFCs because they lead to channel porosity, which is favorable in this application.

Tape casting associated with phase inversion [117,119,120] and freeze casting [126–128] have been reported as promising alternatives to achieve unidirectional pores in ceramic materials. The pore morphology facilitates the flux through the support structure until the membrane, since the unidirectional path imposes less resistance to the flux. He et al. [119] used phase inversion tape casting in a very simple and effective way for the preparation of supported planar oxygen separation membranes composed of YSZ-LSM. The authors showed that the pore morphology obtained with phase inversion enhanced O₂ flux, approximately, 5.74 times ($1.90 \cdot 10^{-3} \text{ mol} \cdot \text{m}^{-2} \cdot \text{s}^{-1} \text{ O}_2$) in comparison with the traditional two-step tape casting with pyrolyzable pore former ($3.31 \cdot 10^{-4} \text{ mol} \cdot \text{m}^{-2} \cdot \text{s}^{-1}$).

The studies involving PDCs have been increasing recently, and one of the main attempts to use these materials in tape casting processing was made for the production of a substrate and support for zeolites. The layer with a higher amount of Si (30 wt%) undergoes to hydrothermal crystallization, resulting in the formation of the MFI type zeolite layers (silicalite I). The zeolization was more effective in temperatures in the range of 1200–1350 °C, where an increment in the specific surface area was observed by raising the hydrothermal crystallization time [105].

2.1.3.3 *Other applications*

Ren et al. have prepared porous TiO₂ [126] and NiO-loaded TiO₂ [128] sheets by freeze tape casting for photocatalysis purpose. Thus, ceramic sheets with high porosity (61.43%) and a specific surface area of 1.095 m²·g⁻¹ have been manufactured, in which photocatalytic activity was greatly improved by adding NiO (0.1 M) via chemical solution deposition. For application purposes, freeze tape casting was used to generate the gradient pore structure in the sheets, which is a direct result of the phase separation process during freezing.

Recently, a work reported the suitability of phase-inversion tape casting to produce porous alumina membrane coated with 1H,1H,2H,2H-perfluorooctyltriethoxysilane (FAS) for application in membrane distillation of saline solution (4 wt% NaCl) [118]. Membrane distillation is a thermally-driven separation process, in which only vapor molecules transfer through a microporous hydrophobic membrane [149]. Therefore, Gu et al. [118] confirmed that the removal of the sponge-like structure (see Figure 2.10) increased by two times the flux of water vapor through the membrane, achieving a permeate flux of 21 L·m⁻²·h⁻¹ at 90 °C operating in sweep gas (N₂) mode.

2.1.4 Summary and outlook

In this paper, the tape casting technique and its variations in manufacturing porous ceramic membranes were discussed. The main strategies to produce tailored porous structures are detailed and the applications are reviewed. The pore morphology can be manipulated by adjusting process parameters such as size and shape of the initial ceramic particles, sintering conditions, amount of sacrificial pore formers, and combination with other techniques.

Phase inversion and freeze casting are easily combined with tape casting for generating porous ceramics with unidirectional pores. Depending on the ceramic powder and pore size distribution of the resultant material, some applications of the final parts include filtration (microfiltration, ultrafiltration, and nanofiltration), support for gas separation, support for catalysis, and membrane distillation.

Tape casting constitutes a consolidated method to manufacture planar ceramic materials, which has been extensively applied in both scientific research and industrial field. Even though the literature reports several studies on the preparation of porous ceramic membranes from cast tapes, a lack of studies is still noticeable in this area. For instance, lack of quantitative models for porosity adjustment, strategies for graded porosity without warping, and the majority of the studies reported are based on the use of organic solvents, rather than water-based systems. Since tape casting enables adjusting the thickness of the product, which plays a crucial role in separation applications, this technique in combination with other approaches offers a great potential for manufacturing membranes and/or support materials with tailorable structure.

2.1.5 Acknowledgements

The authors acknowledge the Brazilian agencies National Council for Scientific and Technological Development (CNPq) and Coordination for the Improvement of Higher Education Personnel (CAPES) for financial support.

2.1.6 Authors contributions

The article within this section (2.1) is mainly based on the work of the first author and author of this thesis Rafael Kenji Nishihora. The precise contributions of each author are listed below.

Table 2.2: Authors contributions for section 2.1 of Chapter 2.

Author	Contribution
Nishihora, R. K.	Conceptualized the work, performed the literature research and analyzed the papers, wrote the manuscript
Rachadel, P. L.	Gave conceptual and scientific advices, helped in the scientific evaluation and editing of the manuscript
Quadri, M. G. N.	Gave conceptual and scientific advices, helped in the scientific evaluation and editing of the manuscript
Hotza, D.	Gave conceptual and scientific advices, helped in the scientific evaluation and editing of the manuscript

2.1.7 References

- [1] M. Scheffler, P. Colombo, eds., *Cellular Ceramics: Structure, Manufacturing, Properties and Applications*, John Wiley & Sons, 2006.
- [2] J. Coronas, J. Santamaría, Catalytic reactors based on porous ceramic membranes, *Catal. Today*. 51 (1999) 377–389. doi:10.1016/S0920-5861(99)00090-5.
- [3] J.T. Richardson, Y. Peng, D. Remue, Properties of ceramic foam catalyst supports: Pressure drop, *Appl. Catal. A Gen.* 204 (2000) 19–32. doi:10.1016/S0926-860X(00)00508-1.
- [4] M. Trueba, S.P. Trasatti, γ -Alumina as a support for catalysts: A review of fundamental aspects, *Eur. J. Inorg. Chem.* (2005) 3393–3403. doi:10.1002/ejic.200500348.
- [5] E.C. Bucharsky, G. Schell, R. Oberacker, M.J. Hoffmann, Anatase-rutile transformation in TiO₂-V₂O₅ catalyst coatings for ce-

- ramic foams, *J. Eur. Ceram. Soc.* 29 (2009) 1955–1961.
doi:10.1016/j.jeurceramsoc.2008.12.007.
- [6] R. Faure, F. Rossignol, T. Chartier, C. Bonhomme, A. Maître, G. Etchegoyen, P. Del Gallo, D. Gary, Alumina foam catalyst supports for industrial steam reforming processes, *J. Eur. Ceram. Soc.* 31 (2011) 303–312.
doi:10.1016/j.jeurceramsoc.2010.10.009.
- [7] H.Q. Trinh, Y.S. Mok, Plasma-catalytic oxidation of acetone in annular porous monolithic ceramic-supported catalysts, *Chem. Eng. J.* 251 (2014) 199–206. doi:10.1016/j.cej.2014.04.071.
- [8] K. Yuan, X. Jin, Z. Yu, X. Gan, X. Wang, G. Zhang, L. Zhu, D. Xu, Electrospun mesoporous zirconia ceramic fibers for catalyst supporting applications, *Ceram. Int.* 44 (2017) 282–289.
doi:10.1016/j.ceramint.2017.09.171.
- [9] C. Yang, G. Zhang, N. Xu, J. Shi, Preparation and application in oil–water separation of ZrO₂/α-Al₂O₃ MF membrane, *J. Memb. Sci.* 142 (1998) 235–243. doi:http://dx.doi.org/10.1016/S0376-7388(97)00336-0.
- [10] S. Benfer, P. Árki, G. Tomandl, Ceramic Membranes for Filtration Applications — Preparation and Characterization, *Adv. Eng. Mater.* 6 (2004) 495–500. doi:10.1002/adem.200400577.
- [11] T. Tsuru, *Inorganic Porous Membranes for Liquid Phase Separation*, 2007. doi:10.1081/SPM-100108159.
- [12] S. Luque, D. Gómez, J.R. Álvarez, Industrial Applications of Porous Ceramic Membranes (Pressure-Driven Processes), *Membr. Sci. Technol.* 13 (2008) 177–216. doi:10.1016/S0927-5193(07)13006-0.
- [13] B.K. Nandi, R. Uppaluri, M.K. Purkait, Preparation and characterization of low cost ceramic membranes for micro-filtration applications, *Appl. Clay Sci.* 42 (2008) 102–110.
doi:10.1016/j.clay.2007.12.001.
- [14] M. Abbasi, M. Mirfendereski, M. Nikbakht, M. Golshenas, T. Mohammadi, Performance study of mullite and mullite–alumina ceramic MF membranes for oily wastewaters treatment, *Desalina-*

- tion. 259 (2010) 169–178.
doi:<http://dx.doi.org/10.1016/j.desal.2010.04.013>.
- [15] C. Su, Y. Xu, W. Zhang, Y. Liu, J. Li, Porous ceramic membrane with superhydrophobic and superoleophilic surface for reclaiming oil from oily water, *Appl. Surf. Sci.* 258 (2012) 2319–2323.
doi:<http://dx.doi.org/10.1016/j.apsusc.2011.10.005>.
- [16] J. Werner, B. Besser, C. Brandes, S. Kroll, K. Rezwani, Production of ceramic membranes with different pore sizes for virus retention, *J. Water Process Eng.* 4 (2014) 201–211.
doi:<http://dx.doi.org/10.1016/j.jwpe.2014.10.007>.
- [17] B. Das, B. Chakrabarty, P. Barkakati, Preparation and characterization of novel ceramic membranes for micro-filtration applications, *Ceram. Int.* 42 (2016) 14326–14333.
doi:10.1016/j.ceramint.2016.06.125.
- [18] M.C. Fraga, S. Sanches, V.J. Pereira, J.G. Crespo, L. Yuan, J. Marcher, M. V Martínez, D. Yuso, E. Rodríguez-castellón, J. Benavente, Morphological, chemical surface and filtration characterization of a new silicon carbide membrane, *J. Eur. Ceram. Soc.* 37 (2017) 899–905. doi:10.1016/j.jeurceramsoc.2016.10.007.
- [19] B.S.P.S. Badwal, F.T. Ciacchi, Ceramic membranes for oxygen separation, *Membr. Technol.* 2001 (2001) 16.
doi:10.1016/S0958-2118(01)80295-0.
- [20] J. Sunarso, S. Baumann, J.M. Serra, W.A. Meulenbergh, S. Liu, Y.S. Lin, J.C. Diniz da Costa, Mixed ionic-electronic conducting (MIEC) ceramic-based membranes for oxygen separation, *J. Memb. Sci.* 320 (2008) 13–41.
doi:10.1016/j.memsci.2008.03.074.
- [21] N. Yang, X. Tan, Z. Ma, A phase inversion/sintering process to fabricate nickel/yttria-stabilized zirconia hollow fibers as the anode support for micro-tubular solid oxide fuel cells, *J. Power Sources.* 183 (2008) 14–19.
doi:<http://dx.doi.org/10.1016/j.jpowsour.2008.05.006>.

- [22] S.M. Hashim, A.R. Mohamed, S. Bhatia, Current status of ceramic-based membranes for oxygen separation from air, *Adv. Colloid Interface Sci.* 160 (2010) 88–100. doi:10.1016/j.cis.2010.07.007.
- [23] M. Liu, C. Chen, M. Liu, L. Yang, Anode-supported micro-tubular SOFCs fabricated by a phase-inversion and dip-coating process, *Int. J. Hydrogen Energy.* 36 (2011) 5604–5610. doi:10.1016/j.ijhydene.2011.02.016.
- [24] Z. Han, Y. Wang, Z. Yang, M. Han, Electrochemical Properties of Tubular SOFC Based on a Porous Ceramic Support Fabricated by Phase-Inversion Method, *J. Mater. Sci. Technol.* 32 (2016) 681–686. doi:10.1016/j.jmst.2016.03.002.
- [25] D.M. Amaya, D. Estrada, D. Hotza, J.B. Rodrigues Neto, J.A. Escobar, Porous Cu/YSZ anodes processed by aqueous tape casting for IT-SOFC, *J. Eur. Ceram. Soc.* 37 (2017) 5233–5237. doi:10.1016/j.jeurceramsoc.2017.05.002.
- [26] J. Wang, L.J. Vandeperre, W.J. Clegg, Effect of grain size on the fracture behaviour of porous alumina made by partial sintering of powder compacts, *Ceram. Eng. Sci. Proc.* 22 (2001) 233–241.
- [27] Z.-Y. Deng, J.-F. Yang, Y. Beppu, M. Ando, T. Ohji, Effect of Agglomeration on Mechanical Properties of Porous Zirconia Fabricated by Partial Sintering, *J. Am. Ceram. Soc.* 85 (2002) 1961–1965. doi:10.1111/j.1151-2916.2002.tb00388.x.
- [28] W. Pabst, E. Gregorová, I. Sedlářová, M. Černý, Preparation and characterization of porous alumina–zirconia composite ceramics, *J. Eur. Ceram. Soc.* 31 (2011) 2721–2731. doi:http://dx.doi.org/10.1016/j.jeurceramsoc.2011.01.011.
- [29] G. Jean, V. Sciamanna, M. Demuynck, F. Cambier, M. Gonon, Macroporous ceramics: Novel route using partial sintering of alumina-powder agglomerates obtained by spray-drying, *Ceram. Int.* 40 (2014) 10197–10203. doi:http://dx.doi.org/10.1016/j.ceramint.2014.02.089.
- [30] Q. Guo, H. Xiang, X. Sun, X. Wang, Y. Zhou, Preparation of porous YB4 ceramics using a combination of in-situ borothermal reaction and high temperature partial sintering, *J. Eur. Ceram.*

- Soc. 35 (2015) 3411–3418.
doi:10.1016/j.jeurceramsoc.2015.05.023.
- [31] A. Díaz, S. Hampshire, Characterisation of porous silicon nitride materials produced with starch, *J. Eur. Ceram. Soc.* 24 (2004) 413–419. doi:10.1016/S0955-2219(03)00212-7.
- [32] S. Vaucher, J. Kuebler, O. Beffort, L. Biasetto, F. Zordan, P. Colombo, Ceramic foam-reinforced Al-based micro-composites, *Compos. Sci. Technol.* 68 (2008) 3202–3207.
doi:10.1016/j.compscitech.2008.08.004.
- [33] C. Vakifahmetoglu, I. Menapace, A. Hirsch, L. Biasetto, R. Hauser, R. Riedel, P. Colombo, Highly porous macro- and micro-cellular ceramics from a polysilazane precursor, *Ceram. Int.* 35 (2009) 3281–3290. doi:10.1016/j.ceramint.2009.05.022.
- [34] Y.W. Kim, Y.J. Jin, J.H. Eom, I.H. Song, H.D. Kim, Engineering porosity in silicon carbide ceramics, *J. Mater. Sci.* 45 (2010) 2808–2815. doi:10.1007/s10853-010-4270-5.
- [35] T. Prenzel, K. Döge, R.P.O. Motta, M. Wilhelm, K. Rezwan, Controlled hierarchical porosity of hybrid ceramics by leaching water soluble templates and pyrolysis, *J. Eur. Ceram. Soc.* 34 (2014) 1501–1509. doi:10.1016/j.jeurceramsoc.2013.11.033.
- [36] T. Konegger, R. Patidar, R.K. Bordia, A novel processing approach for free-standing porous non-oxide ceramic supports from polycarbosilane and polysilazane precursors, *J. Eur. Ceram. Soc.* 35 (2015) 2679–2683. doi:10.1016/j.jeurceramsoc.2015.03.009.
- [37] S.J. Powell, J.R.G. Evans, The structure of ceramic foams prepared from polyurethane-ceramic suspensions, *Mater. Manuf. Process.* 10 (1995) 757–771. doi:10.1080/10426919508935063.
- [38] W.M. Carty, P.W. Lednor, Monolithic ceramics and heterogeneous catalysts: Honeycombs and foams, *Curr. Opin. Solid State Mater. Sci.* 1 (1996) 88–95. doi:10.1016/S1359-0286(96)80015-5.
- [39] L. Montanaro, Y. Jorand, G. Fantozzi, A. Negro, Ceramic foams by powder processing, *J. Eur. Ceram. Soc.* 18 (1998) 1339–1350. doi:10.1016/S0955-2219(98)00063-6.

- [40] H.R. Ramay, M. Zhang, Preparation of porous hydroxyapatite scaffolds by combination of the gel-casting and polymer sponge methods, *Biomaterials*. 24 (2003) 3293–3302.
doi:10.1016/S0142-9612(03)00171-6.
- [41] M.A.A. Muhamad Nor, L.C. Hong, Z. Arifin Ahmad, H. Md Akil, Preparation and characterization of ceramic foam produced via polymeric foam replication method, *J. Mater. Process. Technol.* 207 (2008) 235–239. doi:10.1016/j.jmatprotec.2007.12.099.
- [42] C.R. Bowen, T. Thomas, Macro-porous Ti2AlC MAX-phase ceramics by the foam replication method, *Ceram. Int.* 41 (2015) 12178–12185. doi:10.1016/j.ceramint.2015.06.038.
- [43] P. Colombo, J.R. Hellmann, Ceramic foams from preceramic polymers, *Mater. Res. Innov.* 6 (2002) 260–272.
doi:10.1007/s10019-002-0209-z.
- [44] S. Dhara, P. Bhargava, A simple direct casting route to ceramic foams, *J. Am. Ceram. Soc.* 50 (2003) 1645–1650.
doi:10.1111/j.1151-2916.2003.tb03534.x.
- [45] U.T. Gonzenbach, A.R. Studart, E. Tervoort, L.J. Gauckler, Tailoring the microstructure of particle-stabilized wet foams, *Langmuir*. 23 (2007) 1025–1032. doi:10.1021/la0624844.
- [46] S. Barg, C. Soltmann, M. Andrade, D. Koch, G. Grathwohl, Cellular ceramics by direct foaming of emulsified ceramic powder suspensions, *J. Am. Ceram. Soc.* 91 (2008) 2823–2829.
doi:10.1111/j.1551-2916.2008.02553.x.
- [47] L. yuan Zhang, D. li Zhou, Y. Chen, B. Liang, J. bei Zhou, Preparation of high open porosity ceramic foams via direct foaming molded and dried at room temperature, *J. Eur. Ceram. Soc.* 34 (2014) 2443–2452. doi:10.1016/j.jeurceramsoc.2014.02.001.
- [48] E. Gregorová, W. Pabst, T. Uhlířová, V. Nečina, M. Veselý, I. Sedlářová, Processing, microstructure and elastic properties of mullite-based ceramic foams prepared by direct foaming with wheat flour, *J. Eur. Ceram. Soc.* 36 (2016) 109–120.
doi:10.1016/j.jeurceramsoc.2015.09.028.

- [49] P. Colombo, Conventional and novel processing methods for cellular ceramics, *Philos. Trans. R. Soc. London A Math. Phys. Eng. Sci.* 364 (2006) 109–124. doi:10.1098/rsta.2005.1683.
- [50] A.R. Studart, U.T. Gonzenbach, E. Tervoort, L.J. Gauckler, Processing Routes to Macroporous Ceramics: A Review, *J. Am. Ceram. Soc.* 89 (2006) 1771–1789. doi:10.1111/j.1551-2916.2006.01044.x.
- [51] P. Colombo, C. Vakifahmetoglu, S. Costacurta, Fabrication of ceramic components with hierarchical porosity, *J. Mater. Sci.* 45 (2010) 5425–5455. doi:10.1007/s10853-010-4708-9.
- [52] T. Ohji, M. Fukushima, Macro-porous ceramics: processing and properties, *Int. Mater. Rev.* 57 (2012) 115–131. doi:10.1179/1743280411Y.0000000006.
- [53] J.-H. Eom, Y.-W. Kim, S. Raju, Processing and properties of macroporous silicon carbide ceramics: A review, *Integr. Med. Res.* 1 (2013) 220–242. doi:10.1016/j.jascr.2013.07.003.
- [54] E.C. Hammel, O.L.R. Ighodaro, O.I. Okoli, Processing and properties of advanced porous ceramics: An application based review, *Ceram. Int.* 40 (2014) 15351–15370. doi:http://dx.doi.org/10.1016/j.ceramint.2014.06.095.
- [55] M.N. Rahaman, *Ceramic Processing and Sintering*, Taylor & Francis, 2003.
- [56] C.B. Carter, M.G. Norton, *Ceramic Materials: Science and Engineering*, Springer New York, 2007.
- [57] E. Drioli, L. Giorno, *Comprehensive Membrane Science and Engineering*, Elsevier Science, 2010.
- [58] R.E. Mistler, The principles of tape casting and tape casting applications, in: R.A. Terpstra, P.P.A.C. Pex, A.H. de Vries (Eds.), *Ceram. Process.*, Springer Netherlands, Dordrecht, 1995: pp. 147–173. doi:10.1007/978-94-011-0531-6_5.
- [59] D. Hotza, Artigo revisão: colagem de folhas cerâmicas, *Cerâmica.* 43 (1997) 159–166. http://www.scielo.br/scielo.php?script=sci_arttext&pid=S0366-69131997000400002&nrm=iso.

- [60] J.G.A. Bitter, *Transport Mechanisms in Membrane Separation Processes*, 3Island Press, 1991.
- [61] J. Rouquerol, D. Avnir, C.W. Fairbridge, D.H. Everett, J.H. Haynes, N. Pernicone, J.D.F. Ramsay, K.S.W. Sing, K.K. Unger, Recommendations for the characterization of porous solids (Technical Report), *Pure Appl. Chem.* 66 (1994) 1739–1758.
- [62] P.S. Liu, G.F. Chen, Chapter One - General Introduction to Porous Materials, in: *Porous Mater.*, Butterworth-Heinemann, Boston, 2014: pp. 1–20. doi:10.1016/B978-0-12-407788-1.00001-0.
- [63] Roy W. Rice, *Porosity of Ceramics: Properties and Applications*, CRC Press, 1998.
- [64] R.W. Rice, Evaluation and extension of physical property-porosity models based on minimum solid area, *J. Mater. Sci.* 31 (1996) 102–118. doi:10.1007/BF00355133.
- [65] R.W. Rice, Use of normalized porosity in models for the porosity dependence of mechanical properties, *J. Mater. Sci.* 40 (2005) 983–989. doi:10.1007/s10853-005-6517-0.
- [66] R.E. Mistler, E.R. Twiname, *Tape Casting: Theory and Practice*, Wiley, 2000.
- [67] A.J. Burggraaf, L. Cot, *Fundamentals of Inorganic Membrane Science and Technology*, Elsevier Science, 1996.
- [68] D. Hotza, P. Greil, Review: aqueous tape casting of ceramic powders, *Mater. Sci. Eng. A.* 202 (1995) 206–217. doi:http://dx.doi.org/10.1016/0921-5093(95)09785-6.
- [69] C.A. Gutiérrez, R. Moreno, Influence of slip preparation and casting conditions on aqueous tape casting of Al₂O₃, *Mater. Res. Bull.* 36 (2001) 2059–2072. doi:10.1016/S0025-5408(01)00683-3.
- [70] B. Bitterlich, C. Lutz, A. Roosen, Rheological characterization of water-based slurries for the tape casting process, *Ceram. Int.* 28 (2002) 675–683. doi:10.1016/S0272-8842(02)00027-5.
- [71] K.P. Plucknett, C.H. Cáceres, D.S. Willinson, *Tape Casting of Fine Alumina/Zirconia Powders for Composite Fabrication*, J.

- Am. Ceram. Soc. 77 (1994) 2137–2144. doi:10.1111/j.1151-2916.1994.tb07109.x.
- [72] J.C. Williams, Doctor-Blade Process, in: F.F.Y. Wang (Ed.), *Ceram. Fabr. Process. Treatise Mater. Sci. Technol.*, Academic Press, 1976: pp. 173–198. doi:10.1016/B978-0-12-341809-8.50016-4.
- [73] G.W. Scherer, Theory of Drying, *J. Am. Ceram. Soc.* 73 (1990) 3–14. doi:10.1111/j.1151-2916.1990.tb05082.x.
- [74] J. Kiennemann, T. Chartier, C. Pagnoux, J.F. Baumard, M. Huger, J.M. Lamérand, Drying mechanisms and stress development in aqueous alumina tape casting, *J. Eur. Ceram. Soc.* 25 (2005) 1551–1564. doi:10.1016/j.jeurceramsoc.2004.05.028.
- [75] A. Roosen, Tape Casting, in: *Ceram. Sci. Technol.*, Wiley-VCH Verlag GmbH & Co. KGaA, 2012: pp. 39–62. doi:10.1002/9783527631957.ch2.
- [76] A. Kristoffersson, E. Carlstrom, Tape casting of alumina in water with an acrylic latex binder, *J. Eur. Ceram. Soc.* 17 (1997) 289–297. doi:10.1016/S0955-2219(96)00143-4.
- [77] X.G. Capdevila, J. Folch, A. Calleja, J. Llorens, M. Segarra, F. Espiell, J.R. Morante, High-density YSZ tapes fabricated via the multi-folding lamination process, *Ceram. Int.* 35 (2009) 1219–1226. doi:10.1016/j.ceramint.2008.06.018.
- [78] H.-G. Park, H. Moon, S.-C. Park, J.-J. Lee, D. Yoon, S.-H. Hyun, D.-H. Kim, Performance improvement of anode-supported electrolytes for planar solid oxide fuel cells via a tape-casting/lamination/co-firing technique, *J. Power Sources.* 195 (2010) 2463–2469. doi:http://dx.doi.org/10.1016/j.jpowsour.2009.11.086.
- [79] M.A. Piwonski, A. Roosen, Low pressure lamination of ceramic green tapes by gluing at room temperature, *J. Eur. Ceram. Soc.* 19 (1999) 263–270. doi:10.1016/S0955-2219(98)00196-4.
- [80] A. Roosen, New lamination technique to join ceramic green tapes for the manufacturing of multilayer devices, *J. Eur. Ceram. Soc.*

- 21 (2001) 1993–1996. doi:[http://dx.doi.org/10.1016/S0955-2219\(01\)00158-3](http://dx.doi.org/10.1016/S0955-2219(01)00158-3).
- [81] K. Schindler, A. Roosen, Manufacture of 3D structures by cold low pressure lamination of ceramic green tapes, *J. Eur. Ceram. Soc.* 29 (2009) 899–904.
doi:[10.1016/j.jeurceramsoc.2008.07.041](http://dx.doi.org/10.1016/j.jeurceramsoc.2008.07.041).
- [82] J. Van Tassel, C.A. Randall, Potential for integration of electro-phoretic deposition into electronic device manufacture; demonstrations using silver/palladium, *J. Mater. Sci.* 39 (2004) 867–879. doi:[10.1023/B:JMSC.0000012916.92366.48](http://dx.doi.org/10.1023/B:JMSC.0000012916.92366.48).
- [83] C. Compson, M. Liu, Fabrication and characterization of hermetic solid oxide fuel cells without sealant, *Solid State Ionics.* 177 (2006) 367–375. doi:[10.1016/j.ssi.2005.10.017](http://dx.doi.org/10.1016/j.ssi.2005.10.017).
- [84] D. Schulze, W.A. Schiller, Burnout of Organic Components of Glass Ceramic Composite Tapes: Thermoanalytical investigations, *Therm. Anal. Calorim.* 52 (1998) 211–219.
doi:[10.1023/A:1010186912460](http://dx.doi.org/10.1023/A:1010186912460).
- [85] S.-J.L. Kang, Sintering, in: *Ceram. Sci. Technol.*, Wiley-VCH Verlag GmbH & Co. KGaA, 2012: pp. 141–169.
doi:[10.1002/9783527631957.ch6](http://dx.doi.org/10.1002/9783527631957.ch6).
- [86] D.-H. Yoon, B.I. Lee, Processing of barium titanate tapes with different binders for MLCC applications—Part II: Comparison of the properties, *J. Eur. Ceram. Soc.* 24 (2004) 753–761.
doi:[http://dx.doi.org/10.1016/S0955-2219\(03\)00334-0](http://dx.doi.org/10.1016/S0955-2219(03)00334-0).
- [87] R.A. Cutler, B. Kleinlein, Effect of the hydroxyl content and molecular weight of polyvinyl butyral on tape properties, *J. Eur. Ceram. Soc.* 29 (2009) 3211–3218.
doi:<http://dx.doi.org/10.1016/j.jeurceramsoc.2009.06.020>.
- [88] N. Das, H.S. Maiti, Formation of pore structure in tape-cast alumina membranes – effects of binder content and firing temperature, *J. Memb. Sci.* 140 (1998) 205–212.
doi:[http://dx.doi.org/10.1016/S0376-7388\(97\)00282-2](http://dx.doi.org/10.1016/S0376-7388(97)00282-2).
- [89] S.F. Corbin, P.S. Apté, Engineered Porosity via Tape Casting, Lamination and the Percolation of Pyrolyzable Particulates, *J.*

- Am. Ceram. Soc. 82 (1999) 1693–1701. doi:10.1111/j.1151-2916.1999.tb01988.x.
- [90] M. Boaro, J.M. Vohs, R.J. Gorte, Synthesis of Highly Porous Yttria-Stabilized Zirconia by Tape-Casting Methods, *J. Am. Ceram. Soc.* 86 (2003) 395–400. doi:10.1111/j.1151-2916.2003.tb03311.x.
- [91] E. Gregorová, Z. Živcová, W. Pabst, Porosity and pore space characteristics of starch-processed porous ceramics, *J. Mater. Sci.* 41 (2006) 6119–6122. doi:10.1007/s10853-006-0475-z.
- [92] A. Kritikaki, A. Tsetsekou, Fabrication of porous alumina ceramics from powder mixtures with sol–gel derived nanometer alumina: Effect of mixing method, *J. Eur. Ceram. Soc.* 29 (2009) 1603–1611.
doi:http://dx.doi.org/10.1016/j.jeurceramsoc.2008.10.011.
- [93] Y. Feng, K. Wang, J. Yao, P.A. Webley, S. Smart, H. Wang, Effect of the addition of polyvinylpyrrolidone as a pore-former on microstructure and mechanical strength of porous alumina ceramics, *Ceram. Int.* 39 (2013) 7551–7556.
doi:http://dx.doi.org/10.1016/j.ceramint.2013.03.007.
- [94] A. Sarikaya, F. Dogan, Effect of various pore formers on the microstructural development of tape-cast porous ceramics, *Ceram. Int.* 39 (2013) 403–413.
doi:http://dx.doi.org/10.1016/j.ceramint.2012.06.041.
- [95] B. Charlas, C. Grings Schmidt, H. Lund Frandsen, K. Bøhm Andersen, D. Boccaccini, K. Kammer Hansen, A. Roosen, A. Kaiser, Influence of pore former on porosity and mechanical properties of Ce_{0.9}Gd_{0.1}O_{1.95} electrolytes for flue gas purification, *Ceram. Int.* 42 (2016) 4546–4555.
doi:http://dx.doi.org/10.1016/j.ceramint.2015.11.147.
- [96] C. Grings Schmidt, K.K. Hansen, K.B. Andersen, Z. Fu, A. Roosen, A. Kaiser, Effect of pore formers on properties of tape cast porous sheets for electrochemical flue gas purification, *J. Eur. Ceram. Soc.* 36 (2016) 645–653.
doi:http://dx.doi.org/10.1016/j.jeurceramsoc.2015.09.030.

- [97] K. Lindqvist, E. Lidén, Preparation of alumina membranes by tape casting and dip coating, *J. Eur. Ceram. Soc.* 17 (1997) 359–366. doi:[http://dx.doi.org/10.1016/S0955-2219\(96\)00107-0](http://dx.doi.org/10.1016/S0955-2219(96)00107-0).
- [98] A. Sanson, P. Pinasco, E. Roncari, Influence of pore formers on slurry composition and microstructure of tape cast supporting anodes for SOFCs, *J. Eur. Ceram. Soc.* 28 (2008) 1221–1226. doi:<http://dx.doi.org/10.1016/j.jeurceramsoc.2007.10.001>.
- [99] C. Reynaud, F. Thévenot, T. Chartier, J.L. Besson, Mechanical properties and mechanical behaviour of SiC dense-porous laminates, *J. Eur. Ceram. Soc.* 25 (2005) 589–597. doi:10.1016/j.jeurceramsoc.2004.02.009.
- [100] J. Zhou, Q. Liu, L. Zhang, Z. Pan, S.H. Chan, Influence of pore former on electrochemical performance of fuel-electrode supported SOFCs manufactured by aqueous-based tape-casting, *Energy*. 115 (2016) 149–154. doi:10.1016/j.energy.2016.08.093.
- [101] R.M.C. Clemmer, S.F. Corbin, Influence of porous composite microstructure on the processing and properties of solid oxide fuel cell anodes, *Solid State Ionics*. 166 (2004) 251–259. doi:10.1016/j.ssi.2003.12.009.
- [102] S.F. Corbin, J. Lee, X. Qiao, Influence of Green Formulation and Pyrolyzable Particulates on the Porous Microstructure and Sintering Characteristics of Tape Cast Ceramics, *J. Am. Ceram. Soc.* 84 (2001) 41–47. doi:10.1111/j.1151-2916.2001.tb00605.x.
- [103] P. Cromme, M. Scheffler, P. Greil, Ceramic Tapes from Pre-ceramic Polymers, *Adv. Eng. Mater.* 4 (2002) 873–877. doi:10.1002/1527-2648(20021105)4:11<873::AID-ADEM873>3.0.CO;2-G.
- [104] Q. Wei, E. Pippel, J. Woltersdorf, M. Scheffler, P. Greil, Interfacial SiC formation in polysiloxane-derived Si-O-C ceramics, *Mater. Chem. Phys.* 73 (2002) 281–289. doi:10.1016/S0254-0584(01)00395-9.
- [105] F. Scheffler, M. Scheffler, Polymer derived ceramic tapes as substrate and support for zeolites, *Adv. Appl. Ceram.* 108 (2009) 468–475. doi:10.1179/174367609X459540.

- [106] N. Hilal, A.F. Ismail, C. Wright, Membrane Fabrication, CRC Press, 2015.
- [107] M.C. Porter, Handbook of Industrial Membrane Technology, Noyes Publications, 1990.
<https://books.google.com.br/books?id=W3pmhoD7tSAC>.
- [108] M. Mulder, Basic Principles of Membrane Technology, Springer, 1996.
- [109] T.H. Young, L.W. Chen, Pore formation mechanism of membranes from phase inversion process, Desalination. 103 (1995) 233–247. doi:10.1016/0011-9164(95)00076-3.
- [110] G.R. Guillen, Y. Pan, M. Li, E.M. V Hoek, Preparation and characterization of membranes formed by nonsolvent induced phase separation: A review, Ind. Eng. Chem. Res. 50 (2011) 3798–3817. doi:10.1021/ie101928r.
- [111] S. Liu, K. Li, Preparation TiO₂/Al₂O₃ composite hollow fibre membranes, J. Memb. Sci. 218 (2003) 269–277.
doi:[http://dx.doi.org/10.1016/S0376-7388\(03\)00184-4](http://dx.doi.org/10.1016/S0376-7388(03)00184-4).
- [112] S. Liu, K. Li, R. Hughes, Preparation of porous aluminium oxide (Al₂O₃) hollow fibre membranes by a combined phase-inversion and sintering method, Ceram. Int. 29 (2003) 875–881.
doi:[http://dx.doi.org/10.1016/S0272-8842\(03\)00030-0](http://dx.doi.org/10.1016/S0272-8842(03)00030-0).
- [113] L. Jiansheng, W. Lianjun, H. Yanxia, L. Xiaodong, S. Xiuyun, Preparation and characterization of Al₂O₃ hollow fiber membranes, J. Memb. Sci. 256 (2005) 1–6.
doi:<http://dx.doi.org/10.1016/j.memsci.2004.07.014>.
- [114] C. Jin, J. Liu, L. Li, Y. Bai, Electrochemical properties analysis of tubular NiO–YSZ anode-supported SOFCs fabricated by the phase-inversion method, J. Memb. Sci. 341 (2009) 233–237.
doi:<http://dx.doi.org/10.1016/j.memsci.2009.06.012>.
- [115] X. Zhang, S. Suo, Y. Jiang, Q. Chang, G. Ji, X. Liu, Microstructure evolution and properties of YSZ hollow fiber microfiltration membranes prepared at different suspension solid content for water treatment, Desalin. Water Treat. (2015) 1–13.
doi:10.1080/19443994.2015.1119751.

- [116] H. Fang, C. Ren, Y. Liu, D. Lu, L. Winnubst, C. Chen, Phase-inversion tape casting and synchrotron-radiation computed tomography analysis of porous alumina, *J. Eur. Ceram. Soc.* 33 (2013) 2049–2051.
doi:<http://dx.doi.org/10.1016/j.jeurceramsoc.2013.02.032>.
- [117] H. Huang, J. Lin, Y. Wang, S. Wang, C. Xia, C. Chen, Facile one-step forming of NiO and yttrium-stabilized zirconia composite anodes with straight open pores for planar solid oxide fuel cell using phase-inversion tape casting method, *J. Power Sources.* 274 (2015) 1114–1117.
doi:<http://dx.doi.org/10.1016/j.jpowsour.2014.10.190>.
- [118] J. Gu, C. Ren, X. Zong, C. Chen, L. Winnubst, Preparation of alumina membranes comprising a thin separation layer and a support with straight open pores for water desalination, *Ceram. Int.* 42 (2016) 12427–12434.
doi:<http://dx.doi.org/10.1016/j.ceramint.2016.04.183>.
- [119] W. He, H. Huang, J. Gao, L. Winnubst, C. Chen, Phase-inversion tape casting and oxygen permeation properties of supported ceramic membranes, *J. Memb. Sci.* 452 (2014) 294–299.
doi:<http://dx.doi.org/10.1016/j.memsci.2013.09.063>.
- [120] Y. Zhang, R. Yuan, Z. He, J. Gao, C. Chen, Phase inversion tape casting and oxygen permeation properties of supported planar $Zr_{0.84}Y_{0.16}O_{1.92}-La_{0.8}Sr_{0.2}Cr_{0.5}Fe_{0.5}O_{3-\delta}$ composite membrane, *Solid State Ionics.* 288 (2016) 342–346.
doi:<http://dx.doi.org/10.1016/j.ssi.2015.12.024>.
- [121] R. hua Yuan, W. He, Y. Zhang, J.F. Gao, C. sheng Chen, Preparation and characterization of supported planar $Zr_{0.84}Y_{0.16}O_{1.92}-La_{0.8}Sr_{0.2}Cr_{0.5}Fe_{0.5}O_{3-\delta}$ composite membrane, *J. Memb. Sci.* 499 (2016) 335–342.
doi:[10.1016/j.memsci.2015.10.066](http://dx.doi.org/10.1016/j.memsci.2015.10.066).
- [122] Y. Meng, W. He, X. Li, J. Gao, Z. Zhan, J. Yi, C. Chen, H.J.M. Bouwmeester, Asymmetric $La_{0.6}Sr_{0.4}Co_{0.2}Fe_{0.8}O_{3-\delta}$ membrane with reduced concentration polarization prepared by

- phase-inversion tape casting and warm pressing, *J. Memb. Sci.* 533 (2017) 11–18. doi:10.1016/j.memsci.2017.03.025.
- [123] S. Deville, Freeze-Casting of Porous Ceramics: A Review of Current Achievements and Issues, *Adv. Eng. Mater.* 10 (2008) 155–169. doi:10.1002/adem.200700270.
- [124] R. Liu, T. Xu, C. Wang, A review of fabrication strategies and applications of porous ceramics prepared by freeze-casting method, *Ceram. Int.* 42 (2016) 2907–2925. doi:http://dx.doi.org/10.1016/j.ceramint.2015.10.148.
- [125] W.L. Li, K. Lu, J.Y. Walz, Freeze casting of porous materials: review of critical factors in microstructure evolution, *Int. Mater. Rev.* 57 (2012) 37–60. doi:10.1179/1743280411Y.0000000011.
- [126] L. Ren, Y.-P. Zeng, D. Jiang, Fabrication of Gradient Pore TiO₂ Sheets by a Novel Freeze–Tape-Casting Process, *J. Am. Ceram. Soc.* 90 (2007) 3001–3004. doi:10.1111/j.1551-2916.2007.01833.x.
- [127] S.W. Sofie, Fabrication of Functionally Graded and Aligned Porosity in Thin Ceramic Substrates With the Novel Freeze–Tape-Casting Process, *J. Am. Ceram. Soc.* 90 (2007) 2024–2031. doi:10.1111/j.1551-2916.2007.01720.x.
- [128] L. Ren, Y.-P. Zeng, D. Jiang, The improved photocatalytic properties of P-type NiO loaded porous TiO₂ sheets prepared via freeze tape-casting, *Solid State Sci.* 12 (2010) 138–143. doi:http://dx.doi.org/10.1016/j.solidstatesciences.2009.09.021.
- [129] R.W. Rice, *Ceramic Fabrication Technology*, CRC Press, 2002.
- [130] R. Castro, K. van Benthem, *Sintering: Mechanisms of Conventional Nanodensification and Field Assisted Processes*, Springer Berlin Heidelberg, 2012.
- [131] S.C. Nanjangud, R. Brezny, D.J. Green, Strength and Young’s Modulus Behavior of a Partially Sintered Porous Alumina, *J. Am. Ceram. Soc.* 78 (1995) 266–268. doi:10.1111/j.1151-2916.1995.tb08401.x.

- [132] D. Hardy, D.J. Green, Mechanical properties of a partially sintered alumina, *J. Eur. Ceram. Soc.* 15 (1995) 769–775. doi:10.1016/0955-2219(95)00045-V.
- [133] X. Liu, C.L. Martin, G. Delette, D. Bouvard, Elasticity and strength of partially sintered ceramics, *J. Mech. Phys. Solids.* 58 (2010) 829–842. doi:10.1016/j.jmps.2010.04.007.
- [134] S. Somiya, *Handbook of Advanced Ceramics: Materials, Applications, Processing, and Properties*, Elsevier Science, 2013.
- [135] N. Das, S. Bandyopadhyay, D. Chattopadhyay, H.S. Maiti, Tape-cast ceramic membranes for microfiltration application, *J. Mater. Sci.* 31 (1996) 5221–5225. doi:10.1007/bf00355928.
- [136] N. Das, H.S. Maiti, Ceramic membrane by tape casting and sol-gel coating for microfiltration and ultrafiltration application, *J. Phys. Chem. Solids.* 70 (2009) 1395–1400. doi:http://dx.doi.org/10.1016/j.jpcs.2009.08.016.
- [137] M. Subbanna, P.C. Kapur, Pradip, Role of powder size, packing, solid loading and dispersion in colloidal processing of ceramics, *Ceram. Int.* 28 (2002) 401–405. doi:http://dx.doi.org/10.1016/S0272-8842(01)00108-0.
- [138] A.G. King, *Ceramic Technology and Processing: A Practical Working Guide*, Elsevier Science, 2001.
- [139] P. V Vasconcelos, J.A. Labrincha, J.M.F. Ferreira, Porosity development of diatomite layers processed by tape casting, *Ceram. Int.* 24 (1998) 447–454. doi:http://dx.doi.org/10.1016/S0272-8842(97)00034-5.
- [140] H. Moon, S.D. Kim, S.H. Hyun, H.S. Kim, Development of IT-SOFC unit cells with anode-supported thin electrolytes via tape casting and co-firing, *Int. J. Hydrogen Energy.* 33 (2008) 1758–1768. doi:http://dx.doi.org/10.1016/j.ijhydene.2007.12.062.
- [141] G. Tari, J.M.F. Ferreira, A.T. Fonseca, Influence of particle size and particle size distribution on drying-shrinkage behaviour of alumina slip cast bodies, *Ceram. Int.* 25 (1999) 577–580. doi:http://dx.doi.org/10.1016/S0272-8842(98)00068-6.

- [142] N. Das, H.S. Maiti, Effect of Size Distribution of the Starting Powder on the Pore Size and its Distribution of Tape Cast Alumina Microporous Membranes, *J. Eur. Ceram. Soc.* 19 (1999) 341–345. doi:[http://dx.doi.org/10.1016/S0955-2219\(98\)00205-2](http://dx.doi.org/10.1016/S0955-2219(98)00205-2).
- [143] P. V Vasconcelos, J.A. Labrincha, J.M.F. Ferreira, Processing of diatomite from colloidal suspensions: Tape casting, *Br. Ceram. Trans.* 97 (1998) 214–221.
<https://www.scopus.com/inward/record.uri?eid=2-s2.0-0032288222&partnerID=40&md5=cd41406b2a1d920ad0fb2d3db832d594>.
- [144] S. Ramanathan, K.P. Krishnakumar, P.K. De, S. Banerjee, Powder dispersion and aqueous tape casting of YSZ-NiO composite, *J. Mater. Sci.* 39 (2004) 3339–3344.
doi:10.1023/b:jmsc.0000026934.88520.67.
- [145] D.M. Liu, Influence of solid loading and particle size distribution on the porosity development of green alumina ceramic mouldings, *Ceram. Int.* 23 (1997) 513–520.
- [146] B. Shri Prakash, S. Senthil Kumar, S.T. Aruna, Properties and development of Ni/YSZ as an anode material in solid oxide fuel cell: A review, *Renew. Sustain. Energy Rev.* 36 (2014) 149–179.
doi:<http://dx.doi.org/10.1016/j.rser.2014.04.043>.
- [147] S.P. Jiang, S.H. Chan, A review of anode materials development in solid oxide fuel cells, *J. Mater. Sci.* 39 (2004) 4405–4439.
doi:10.1023/B:JMISC.0000034135.52164.6b.
- [148] N.H. Menzler, F. Tietz, S. Uhlenbruck, H.P. Buchkremer, D. Stöver, Materials and manufacturing technologies for solid oxide fuel cells, *J. Mater. Sci.* 45 (2010) 3109–3135.
doi:10.1007/s10853-010-4279-9.
- [149] A. Alkhubiri, N. Darwish, N. Hilal, Membrane distillation: A comprehensive review, *Desalination.* 287 (2012) 2–18.
doi:<http://dx.doi.org/10.1016/j.desal.2011.08.027>.

2.2 Polymer-derived ceramics

Polymer-Derived Ceramics (PDCs) are components to produce materials with tailored surface properties in a few steps [1]. PDCs are made from pre-ceramic polymers (PCPs) in which the central component is silicon (Si). Those silicon-based polymers are provided in a large variety of functional groups (Figure 2.19) and may be converted into ceramic materials (SiC, SiCN, SiOC, etc.) by heat treatment in an inert atmosphere [2–4]. They present flexibility in terms of tailoring surface properties, which can be favorable in selective separation/permeation.

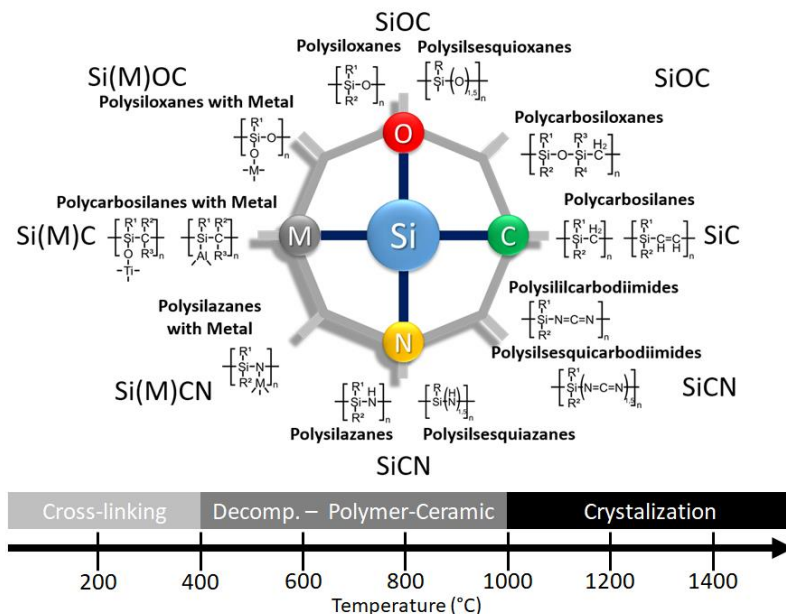


Figure 2.19: Main classes of organosilicon polymers used as ceramic precursors and typical thermal events (adapted from [5]).

As a result of its polymeric nature, PCPs can be processed by various techniques [2]. The casting methods (tape casting, slip casting, gel casting, etc.) are very promising techniques to shape this type of material. In addition to shaping and thermal treatment, the microstruc-

ture can be tailored by some processing strategies such as sacrificial templating, freeze casting, foaming, replica, phase separation, and reaction technique [6,7]. Therefore, macro/meso/microporosity of PDCs are manipulated by the proper selection of the raw materials, processing strategies, and thermal parameters [8].

Polysiloxanes belong to one of the most used and commercially available classes of PCPs. The main reason of its industrial and research interest concerns the chemical stability, availability/price, applicability, and flexibility in tailoring the chemical structure [6]. As shown in Figure 2.19, polysiloxanes are composed by a polymeric structure with alternated bonds of Si-O-C. Depending on their pyrolysis temperature and atmosphere (e.g. N₂ and/or Ar, Air, etc), miscellaneous products can be obtained. For instance, using inert atmospheres (N₂ or Ar) and temperatures in the range of 400–600 °C hybrid silicon oxycarbide (SiOC + organic moieties) is formed [1]. At higher temperatures (800–1200 °C), all the organic moieties are degraded resulting only in amorphous SiOC (this concept will be further explored in Chapter 3). When even higher temperatures are applied (> 1200 °C), crystalline silicon carbide (SiC) or silicon carbonitride (SiCN, if the atmosphere contains N₂) can be prepared [9]. On the other hand, oxidative atmospheres lead to the generation of reactive amorphous silica (SiO₂). This feature could be advantageous in the synthesis of some oxide ceramics, such as mullite (3Al₂O₃·2SiO₂) [10].

Mullite has been receiving great attention in the preparation of advanced ceramics due to its superior resistance to thermal shock compared to traditional ceramics (alumina and zirconia), considerable mechanical properties (~200 MPa), and lower density (~3.2 g/cm³; which may be beneficial to reduce the overall weight loading in big structures) [11]. However, this material is rarely available in nature, thus it must be synthesized by the combination of alumina and silica. Traditional synthesis methods uses α -alumina and silica powders, which are mixed in a stoichiometric proportion and calcined under high temperatures (> 1587 °C) and holding times (\geq 4 h) [12,13]. In order to reduce the energy consumption, there are many efforts involving the use of nanopow-

ders, γ -alumina, and/or alumina and silica precursors. With this goal in mind, several efforts concerning the use of polysiloxanes as reactive amorphous silica precursor are reported in the literature [10,14–16]. Chapter 4 will describe the production of mullite membranes using polysiloxane and an alumina precursor, contextualizing the current gaps in literature.

2.3 Membrane emulsification

Membrane emulsification (ME) technology has attracted great attention to several fields, such as pharmaceutical, chemical, cosmetic, and food industries. This innovative emulsification technology presents some major advantages over conventional methods (e.g. colloid mills, dispersing machines, ultrasound homogenizers, rotor/stator systems, high-pressure homogenizers, etc.) [17,18]. The primary features of ME process include: operational flexibility, easy scale-up, production of uniform droplets (reduced dispersity), low shear stress, and energy requirement reduction (ME = $10^4 - 10^6 \text{ J}\cdot\text{m}^{-3}$; mechanical methods = $10^6 - 10^8 \text{ J}\cdot\text{m}^{-3}$) [19]. Nevertheless, the distinguishing feature is that the final droplet size is particularly related to the membrane characteristics instead of the generation of turbulent droplet break-up [20]. In addition, oil-in-water, water-in-oil and water-in-oil-in-water emulsions have been prepared by ME process.

There are two major configurations in ME process, as shown in Figure 2.20. In the direct membrane emulsification (DME) or cross-flow, the disperse phase is pressed through a microporous membrane and the droplets are formed at the pore on the surface of the opposing side of the membrane, which is in contact with the continuous phase (water + surfactant in Figure 2.20a) [21]. In the case of DME, the droplets that reach a critical dimension can detach the membrane surface either by spontaneous deformation or via shear forces from the continuous phase flowing parallel to the surface [21]. The key advantages of DME are low shear stresses, low energy requirement, uniform droplet size (which reduces the amount of surfactant needed), and ease of design

and scale-up [22]. The premix membrane emulsification (PME, Figure 2.20b) process is characterized by the permeation of a preliminary coarse emulsion (premix) through a porous membrane, resulting in smaller droplet sizes and narrower droplet size distribution than the original premix [18]. Here, the droplet disruption within the membrane pores is the predominant mechanism responsible for the droplet size reduction [21]. The energy costs for PME can be one order of magnitude lower than DME for highly concentrated products [22]. The droplet size and distribution can be controlled by the number of passes (permeations) through the membrane, which incorporates an additional layer of flexibility to this method. Chapter 5 will approach this matter in more details.

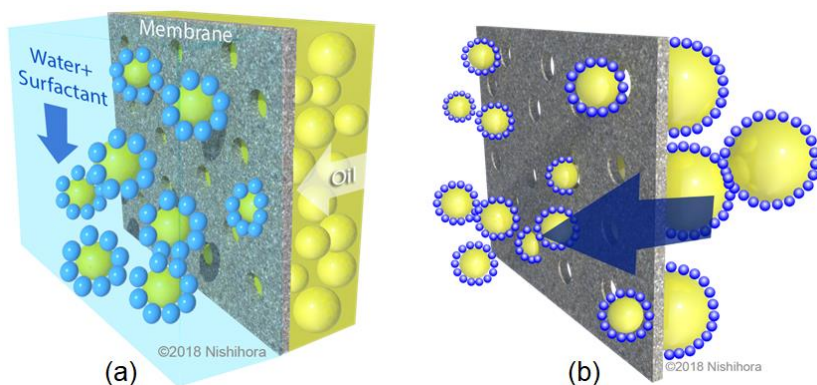


Figure 2.20: Schematic representation of the production of oil-in-water emulsion by (a) direct or cross-flow membrane emulsification (DME) and (b) premix membrane emulsification (PME).

2.4 References

- [1] T. Prenzel, M. Wilhelm, K. Rezwan, Pyrolyzed polysiloxane membranes with tailorable hydrophobicity, porosity and high specific surface area, *Microporous Mesoporous Mater.* 169 (2013) 160–167.
doi:<http://dx.doi.org/10.1016/j.micromeso.2012.10.014>.

- [2] P. Greil, Polymer Derived Engineering Ceramics, *Adv. Eng. Mater.* 2 (2000) 339–348. doi:10.1002/1527-2648(200006)2:6<339::AID-ADEM339>3.0.CO;2-K.
- [3] G. Mera, E. Ionescu, Silicon-Containing Preceramic Polymers, in: *Encycl. Polym. Sci. Technol.*, John Wiley & Sons, Inc., 2002. doi:10.1002/0471440264.pst591.
- [4] P. Colombo, G. Mera, R. Riedel, G.D. Sorarù, Polymer-Derived Ceramics: 40 Years of Research and Innovation in Advanced Ceramics, *J. Am. Ceram. Soc.* 93 (2010) 1805–1837. doi:10.1111/j.1551-2916.2010.03876.x.
- [5] G. Mera, M. Gallei, S. Bernard, E. Ionescu, Ceramic Nanocomposites from Tailor-Made Preceramic Polymers, *Nanomaterials*. 5 (2015) 468. <http://www.mdpi.com/2079-4991/5/2/468>.
- [6] B. V Manoj Kumar, Y.-W. Kim, Processing of polysiloxane-derived porous ceramics: a review, *Sci. Technol. Adv. Mater.* 11 (2010) 44303. doi:10.1088/1468-6996/11/4/044303.
- [7] P. Colombo, C. Vakifahmetoglu, S. Costacurta, Fabrication of ceramic components with hierarchical porosity, *J. Mater. Sci.* 45 (2010) 5425–5455. doi:10.1007/s10853-010-4708-9.
- [8] A. Lale, M. Schmidt, M.D. Mallmann, A.V.A. Bezerra, E.D. Acosta, R.A.F. Machado, U.B. Demirci, S. Bernard, Polymer-Derived Ceramics with engineered mesoporosity: From design to application in catalysis, *Surf. Coatings Technol.* 350 (2018) 569–586. doi:10.1016/j.surfcoat.2018.07.061.
- [9] P. Cromme, M. Scheffler, P. Greil, Ceramic Tapes from Pre-ceramic Polymers, *Adv. Eng. Mater.* 4 (2002) 873–877. doi:10.1002/1527-2648(20021105)4:11<873::AID-ADEM873>3.0.CO;2-G.
- [10] D. Suttor, H.-J. Kleebe, G. Ziegler, Formation of Mullite from Filled Siloxanes, *J. Am. Ceram. Soc.* 80 (1997) 2541–2548. doi:10.1111/j.1151-2916.1997.tb03156.x.
- [11] H. Schneider, J. Schreuer, B. Hildmann, Structure and properties of mullite-A review, *J. Eur. Ceram. Soc.* 28 (2008) 329–344. doi:10.1016/j.jeurceramsoc.2007.03.017.

- [12] D.J. Duval, S.H. Risbud, J.F. Shackelford, Mullite, in: D.R.H. Shackelford J.F. (Ed.), *Ceram. Glas. Mater.*, Springer, Boston, MA, 2008: pp. 27–39. doi:https://doi.org/10.1007/978-0-387-73362-3_2.
- [13] D. Pereira, G.R.S. Biasibetti, R. V. Camerini, A.S. Pereira, Sintering of mullite by different methods, *Mater. Manuf. Process.* 29 (2014) 391–396. doi:10.1080/10426914.2013.864400.
- [14] I. Jaymes, A. Douy, D. Massiot, J. -P Busnel, Synthesis of a Mullite Precursor from Aluminum Nitrate and Tetraethoxysilane via Aqueous Homogeneous Precipitation: An ²⁷Al and ²⁹Si Liquid- and Solid-State NMR Spectroscopic Study, *J. Am. Ceram. Soc.* 78 (1995) 2648–2654. doi:10.1111/j.1151-2916.1995.tb08035.x.
- [15] J. Anggono, B. Derby, Mullite formation from the pyrolysis of aluminium-loaded polymethylsiloxanes: The influence of aluminium powder characteristics, *J. Eur. Ceram. Soc.* 26 (2006) 1107–1119. doi:10.1016/j.jeurceramsoc.2005.01.052.
- [16] E. Bernardo, P. Colombo, E. Pippel, J. Woltersdorf, Novel mullite synthesis based on alumina nanoparticles and a preceramic polymer, *J. Am. Ceram. Soc.* 89 (2006) 1577–1583. doi:10.1111/j.1551-2916.2006.00963.x.
- [17] A.J. Gijsbertsen-Abrahamse, A. Van Der Padt, R.M. Boom, Status of cross-flow membrane emulsification and outlook for industrial application, *J. Memb. Sci.* 230 (2004) 149–159. doi:10.1016/j.memsci.2003.11.006.
- [18] H.S. Ribeiro, J.J.M. Janssen, I. Kobayashi, M. Nakajima, Membrane Emulsification for Food Applications, in: Klaus-Viktor Peinemann, S.P. Nunes, L. Giorno (Eds.), *Membr. Technol.* 3 Membr. Food Appl., Wiley-VCH Verlag GmbH & Co. KGaA, 2010: pp. 129–166. doi:10.1002/9783527631384.ch7.
- [19] E. Piacentini, E. Drioli, L. Giorno, Membrane emulsification technology: Twenty-five years of inventions and research through patent survey, in: *J. Memb. Sci.*, 2014: pp. 410–422. doi:10.1016/j.memsci.2014.05.059.

- [20] C. Charcosset, I. Limayem, H. Fessi, The membrane emulsification process - A review, *J. Chem. Technol. Biotechnol.* 79 (2004) 209–218. doi:10.1002/jctb.969.
- [21] L. Giorno, G. De Luca, A. Figoli, E. Piacentini, E. Drioli, Membrane Emulsification: Principles and Applications, in: E. Drioli, L. Giorno (Eds.), *Membr. Oper. Innov. Sep. Transform.*, Wiley-VCH Verlag GmbH & Co. KGaA, 2009: pp. 463–497. doi:10.1002/9783527626779.ch21.
- [22] A. Nazir, K. Schroën, R. Boom, Premix emulsification: A review, *J. Memb. Sci.* 362 (2010) 1–11. doi:10.1016/j.memsci.2010.06.044.

3 Tape casting of polysiloxane-derived ceramic with controlled porosity and surface properties²

Tape casting has been applied to produce porous hybrid and SiOC ceramic tapes using ceramic precursors and commercially available polysiloxanes as polymeric binders. SiC particles of two different mean sizes (4.5 or 6.5 μm) were used as inert fillers to prevent shrinkage and increase mechanical stability. Macroporosity was adjusted by varying the azodicarbonamide (ADA) content from 0 to 30 wt.%. Decomposition of the polysiloxanes at 600 °C resulted in the generation of micropores with high specific surface area (187–267 $\text{m}^2\cdot\text{g}^{-1}$) and a predominant hydrophobic behavior. At 1000 °C mainly meso/macroporosity were observed (SSA: 32–162 $\text{m}^2\cdot\text{g}^{-1}$) accompanied by increased hydrophilicity. The influence of ADA content, SiC size, and pyrolysis temperature on open porosity (2.5–37%), average pore size (<0.01–1.76 μm), surface characteristics, and flexural strength (10.5–121 MPa) were investigated. The porous tapes with different surface characteristics and controlled structure are highly promising for applications involving membrane processes, particularly microfiltration systems (0.1–10 μm).

3.1 Introduction

Tape casting is a well-established wet shaping process at industrial and laboratory scales. Conventionally, a tape casting slurry is composed of a solvent, organic polymers as binders and plasticizers, surfactants, and ceramic particles which are left after burning out the organic compounds [1,2]. This technique is traditionally applied to produce planar thin ceramic tapes (10 – 1000 μm) for electronic components such as dense multilayered substrates [3].

The advances in ceramic processing and the increasing interest in developing porous ceramic materials allowed the fabrication of thin ceramic tapes for a wide range of applications, such as: solid oxide fuel cells [4–6], photocatalysis [7], supports/substrates [8–10], and microfil-

² Based on a paper published in the Journal of the European Ceramic Society:
<https://doi.org/10.1016/j.jeurceramsoc.2018.07.016>

tration [11,12]. There are plenty of strategies to produce macroporous ceramic tapes which include sacrificial pore formers, freeze casting, phase-inversion, and partial sintering [13].

However, depending on the application, a hierarchical structure with micro-meso-macropores may be required. Macropores (> 50 nm) are responsible for providing mechanical stability and improved mass transport, while micro (< 2 nm) and mesopores (2 – 50 nm) have a major influence on the functional properties and specific surface area (SSA) [14]. To this end, the incorporation of micro-mesopores and functional properties is feasible by using preceramic polymers (PCPs) such as polysiloxanes. PCPs are capable of undergoing different shaping processing routes due to their polymeric nature [15–17]. Furthermore, these precursors can be converted into hybrid ceramics (at 500 – 700 °C) [18], when part of the polymers remains unreacted. When ceramic materials (SiC, SiOC, SiCN) are formed from silicon-based polymers by heat treatment (≥ 1000 °C) under inert atmospheres [19], those products are described as polymer-derived ceramics (PDCs).

Sacrificial templating, direct foaming, freeze casting, emulsion based or etching methods have been applied to shape porous polymer-derived ceramics [20,21]. Most of those studies are mainly focused on the production of bulk systems like monolithic or foam structures. Therefore, there are only a few mentions in the literature regarding the use of polysiloxanes as polymeric binder for the tape casting process [10,22,23]. Ceramic tapes from silanes/polysiloxanes have been fabricated using PCPs as binders and ceramic precursors, eventually including SiC as inert filler to avoid shrinkage, and Si as active filler to generate pores [10,22]. After pyrolysis at high temperatures (1200 – 1600 °C) under inert atmosphere (Ar or N₂), a Si-O-C-(N) ceramic system was obtained. Nevertheless, to the best of our knowledge, the capability of producing tape cast hybrid ceramic was not investigated.

Polysiloxanes may result in hybrid ceramics with high specific surface area, due to the formation of micropores, when pyrolyzed below 700 °C [18], keeping the hydrophobic character of the polymers. On the other hand, pyrolysis at higher temperatures (≥ 1000 °C) leads to a col-

lapse of micropores and a hydrophilic behavior is developed due to the decomposition and ceramization process [24]. Macroporosity can be produced by adding sacrificial pore formers like azodicarbonamide (ADA) [25,26].

Therefore, the present study focuses on the processability of polysiloxanes to produce PCP-based tapes with adjustable porosity and surface properties in terms of hydrophilicity or hydrophobicity.

3.2 Material and methods

3.2.1 Precursors, solvents and additives

All experiments were performed using commercially available chemicals with no additional purification step. Powders of methylphenyl polysiloxane (Silres[®] H44, Wacker Chemie) and methyl polysiloxane (Silres[®] MK, Wacker Chemie) were used as binders and ceramic precursors. Silicon carbide powders (SiC F800, $d_{50} = 6.5 \mu\text{m}$; and SiC F1000, $d_{50} = 4.5 \mu\text{m}$; EKS) were used as inert fillers to increase processability, reduce cracking due to shrinkage, and provide mechanical stability after pyrolysis. Azodicarbonamide (ADA, 97%, CAS 123-77-3, Sigma-Aldrich) was used as pore former. Imidazole (99%, A10221, CAS 288-32-4, Alfa Aesar) was applied as a cross-linking catalyst for the polysiloxanes. Xylene (98.5%, CAS 1330-20-7, Sigma-Aldrich) was the solvent for the polysiloxanes and the liquid medium to disperse the other components.

3.2.2 Preparation of the polysiloxane-based tapes

The preparation procedure of the polysiloxane-based tapes is shown in Figure 3.1. The first step comprises the slurry preparation, which was conducted at room temperature (r.t.) using magnetic stirrer. Firstly, MK (20 wt.%) and H44 (20 wt.%) powders were dissolved in xylene to get a clear solution. SiC (59 wt.%; $d_{50} = 4.5$ or $6.5 \mu\text{m}$) was then added into the obtained solution and stirred for 60 min to produce a

homogeneous slurry. Finally, the cross-linking catalyst, imidazole (1 wt.%) was added and stirred for further 60 min. In order to understand the effect of ADA, this pore former agent was added in various amounts. It was added in the obtained clear solution of MK and H44 before the addition of SiC. The calculation of the ADA (0, 10, 20, and 30 wt.%) was based on the total weight of the other solid components in the composition (MK+H44+SiC+imidazole = 100 wt.%). The slurry was cast over a polyethylene terephthalate carrier film (Mylar, G10JRM, Richard E. Mistler, Inc.) using a doctor blade (see APPENDIX A.1 for a 3D representation of the Doctor Blade) with the gap set at 1.5 mm. The tape was dried at room temperature in a fume hood for 24 h prior to cutting. Afterwards, the cut pieces were dried for at least more 24 h before pyrolysis. The tapes were pyrolyzed at 600 and 1000 °C in an atmosphere of nitrogen. The heating rate was 120 °C·h⁻¹ to 100 °C below the final temperature and 30 °C·h⁻¹ to the final temperature with a dwelling time of 4 h. The overall appearance of the pyrolyzed tapes at 600 and 1000 °C is shown in Figure 3.1.

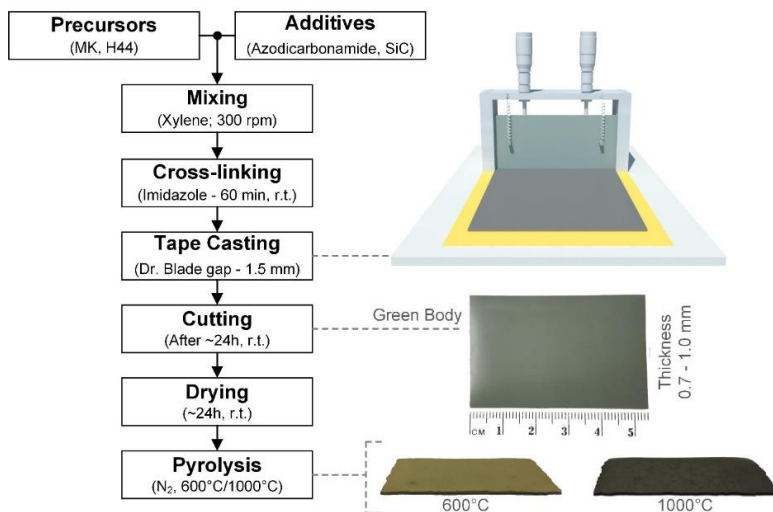


Figure 3.1: Flowchart of polysiloxane-derived, cast and pyrolyzed tapes (600/1000 °C).

3.2.3 Sample notation

Tapes were composed by varying the particle size of SiC and the weight percentage of ADA regarding the total amount of the other solids in the slurry. Sample notation was based on the following construction: SiCX –AY–Z, where X means the silicon carbide average particle size in μm ; A stands for ADA; Y refers to the ADA weight percentage (wt.%); and Z is the pyrolysis temperature in $^{\circ}\text{C}$.

3.2.4 Characterization

The macrostructure was analyzed by Scanning Electron Microscopy (SEM, 20 kV; Series 2, Obducat CamScan). For this purpose, the samples were sputtered with gold (K550, Emitech, Judges Scientific). The surface roughness (Ra) was determined in triplicate with an optical profilometer (Pll2300, Sensofar). Porosity and mean pore size of the tapes were determined using mercury intrusion porosimetry (Pascal 140/440, Porotec). Specific BET surface area (SSA) was determined by nitrogen adsorption and desorption isotherms measured at 77 K (Bel-sorp-Mini, Bel Japan). The samples were degassed at 120 $^{\circ}\text{C}$ for 3 h. Before degassing, the pyrolyzed tapes were ground and sieved with a 300 μm mesh sieve in order to diminish the limitation of nitrogen diffusion within the timeframe of the experiment. Hydrophilicity and hydrophobicity were studied by water and n-heptane vapor adsorption measurements and were carried out by placing vessels with ~ 0.4 g of sample powder (particle sizes ≤ 300 μm) inside closed Erlenmeyer flasks filled with the solvent at equilibrium with its vapor phase at room temperature (~ 22 $^{\circ}\text{C}$). Samples were weighted at the start and end of a 24 h measurement period in order to determine the vapor uptake of the material. Later, the uptake was recalculated into $\text{g}\cdot\text{m}^{-2}$ using the specific surface area of the materials.

The maximum flexural strength (σ_{max}) of the pyrolyzed tapes was obtained by three-point bending tests (Roell Z005, Zwick – DIN EN 843-1 [27]). These measurements were performed using a 5 kN load cell

(piezoelectric force sensor). The samples were cut in a rectangular shape (16 mm length, ~2 mm width, and 0.7–1.0 mm thickness) and placed in the center of a sample holder with 10 mm distance between the support rollers (diameter of 1.5 mm). The crosshead speed and pre-load were fixed at $0.1 \text{ mm}\cdot\text{min}^{-1}$ and 0.25 N, respectively. Ten samples for each composition and temperature were tested and statistically evaluated by analysis of variance (ANOVA) with Tukey's test at a significance level of $p < 0.05$.

3.3 Results

Preparation of hybrid ceramic and ceramic tapes was performed by using polysiloxanes as precursors, which feature methyl and/or phenyl groups. The green bodies were stable and easy to handle. To prevent excessive bending of the tapes during pyrolysis, porous ceramic weights were placed on the samples. The final pyrolyzed tapes show different colors owing to the pyrolysis temperature (see Figure 3.1). At 600 °C, hybrid ceramic (brownish sample) is produced whilst at 1000 °C (black sample) the methyl and phenyl groups are decomposed resulting in the amorphous SiOC ceramic [28]. All pyrolyzed samples possessed sufficient handling stability. The pore forming agent content and SiC particle size were varied to investigate their influence on pore structure and mechanical properties.

3.3.1 Pore morphology and macroporosity

The pore morphology originated by adding ADA was investigated by SEM. Considering that the resultant structures for all samples with ADA are quite similar, one composition was selected to be shown in this work. The pyrolyzed tapes (600 and 1000 °C) produced with 30 wt.% ADA and the SiC with two mean particle sizes ($d_{50} = 4.5$ or $6.5 \mu\text{m}$) is shown in Figure 3.2. Most of the pores exhibit an irregular spheroidal shape that seems to be homogeneously distributed in the matrix. The macroporous structures depicted by SEM evidence pores slightly small-

er than 1 μm up to around 7 μm . Regarding the surface roughness (R_a , Figure 3.8, section 3.9), it was observed a slight increment of R_a by increasing SiC size and pyrolysis temperature for samples without ADA. Samples containing ADA presented a stiff increase of R_a compared to samples without ADA. This could be related to the higher viscosity observed in the slurry due to the addition of ADA, which possibly causes the enlargement of the surface roughness during casting. However, after pyrolysis at both temperatures (600 $^{\circ}\text{C}$ /1000 $^{\circ}\text{C}$), ADA did not show any positive correlation on surface roughness. On the contrary, samples with 30 wt.% of ADA exhibited a slight decrease in R_a after pyrolysis. This response is probably a result of the facilitated gas releasing from the polysiloxane matrix due to the pores originated from ADA decomposition, which prevents further alteration of the surface.

It is worth mentioning that ADA is normally used as a physical blowing agent in non-cross-linked PCPs, which results in foam structures with large macropores (0.1 to 1.5 mm) [25,29]. In this work, ADA was entrapped by the cross-linked polysiloxanes, so that the typical foaming process could not take place. From the images no distinguishable differences in morphology concerning pyrolysis temperatures and inert filler sizes is observable. In addition, SiC particles seem to be embedded by the pre-ceramic polymer. Nevertheless, samples produced with larger SiC particles appear to have some inner defects that resemble cracks (highlighted by the dashed yellow circles in Figure 3.2c-d), which can affect the mechanical performance of the tapes.

Figure 3.3 presents the results obtained by mercury intrusion porosimetry for all the pyrolyzed tapes. The open porosity varies in the range of 2.5–37% according to the amount of ADA (see Figure 3.3a). As expected, an increment on pore former amount leads to increasing open porosity, in this case showing a positive linear relationship. The main factor controlling the open porosity is the ADA content, especially for ADA \geq 20 wt.%. Despite the fact that adding ADA amounts between 20 and 30 wt.% lead to the highest value of open porosity, the influence of this 10 wt.% increment on the mean pore size is negligible for most samples.

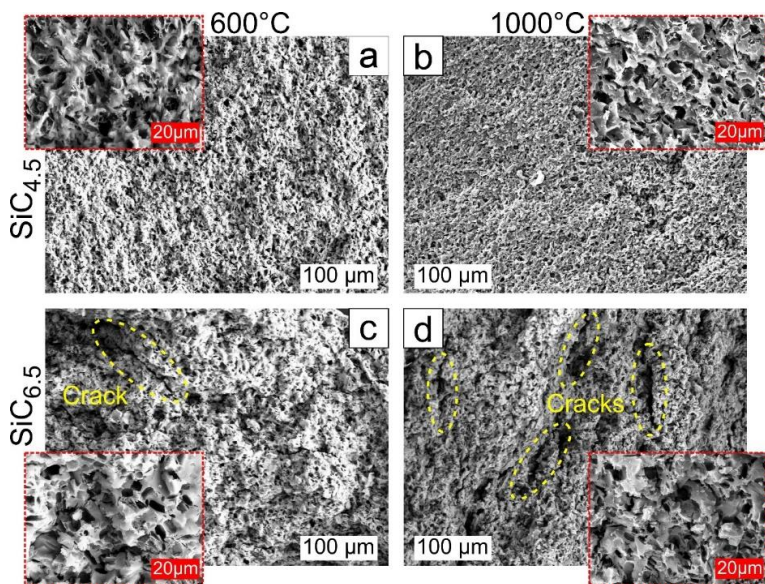


Figure 3.2: SEM images from the fracture of the pyrolyzed tapes at 600 or 1000 °C and 30 wt.% pore former (azodicarbonamide): (a) SiC_{4.5}-A30-600 °C, (b) SiC_{4.5}-A30-1000 °C, (c) SiC_{6.5}-A30-600 °C, (d) SiC_{6.5}-A30-1000 °C. Horizontal length of the white and red boxes represents the sizes given therein.

The mean pore diameter (Figure 3.3b) can be tailored primarily by altering the inert filler size and pyrolysis temperature. This diameter determined by Hg intrusion represents the interparticle pores in the matrix, which is also called pore window size. The sizes measured are comprehended between 0.01 to 1.76 μm. SiC_{4.5} samples exhibit a minor increase in the pore diameter due to the rising temperature. However, SiC_{6.5} samples are greatly affected by pyrolysis temperature. The increment of the average pore size for the SiC_{6.5}-1000 °C samples (0.89 – 1.76 μm) was around 3 times the value detected for SiC_{6.5}-600 °C samples (< 0.01 – 0.63 μm). The SiC_{4.5}-A30 samples presented a bimodal pore size distribution (see Figure 3.9, section 3.9), which can indicate the collapse of a small volume of the small pores. For all other pyrolyzed tapes, a monomodal distribution was observed, although the

pore window size distribution was broadened for the sample SiC6.5-A30-1000 °C.

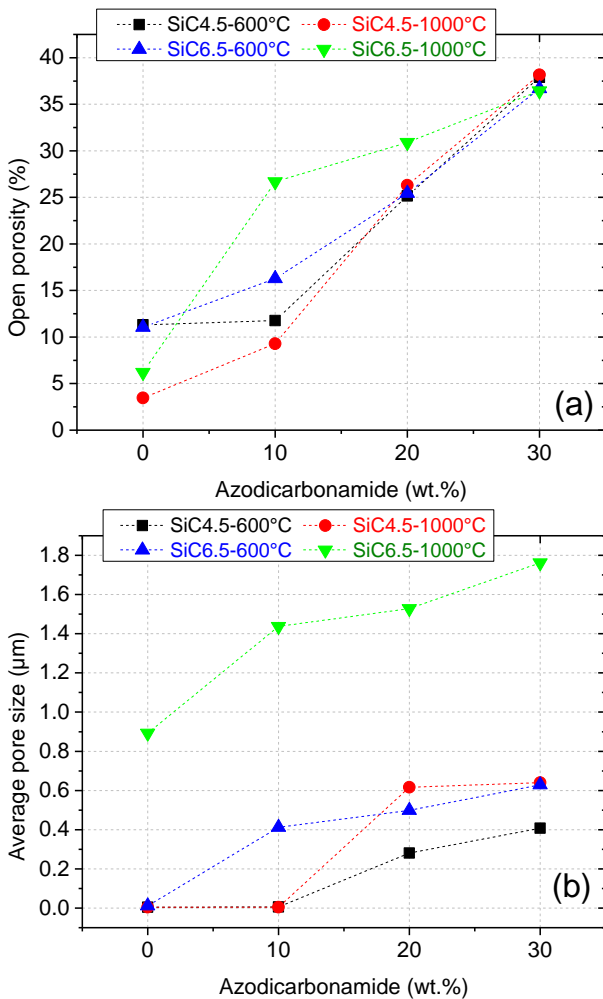


Figure 3.3: Influence of ADA content on open porosity (a) and average pore size (b).

3.3.2 Surface area and surface characteristics

The N₂ adsorption-desorption isotherms and specific surface areas (SSA) of the pyrolyzed tapes were investigated in order to determine the influence that pyrolysis temperature and tape composition (ADA amount and SiC size) may play on the microstructure. Figure 3.4a displays the specific surface area obtained from the nitrogen adsorption isotherms (see Figure 3.10, section 3.9). Specific surface areas up to 267 m²·g⁻¹ were obtained for tapes pyrolyzed at 600 °C without azodicarbonamide, which are reduced to around 187 m²·g⁻¹ (SiC4.5-A30-600 °C) due to the addition of 30 wt.% pore former. The reduction of the specific surface area is more noticeable by increasing the temperature rather than the pore former content. The increment of azodicarbonamide resulted in a slight linear decrease of SSA, which is expected due to the introduction of macroporosity in the structure. Inert filler size does not show any significant effect on the specific surface area of samples pyrolyzed at 600 °C.

On the other hand, for the samples pyrolyzed at 1000 °C, the particle size showed some considerable impact on SSA. Samples with smaller particle size (4.5 μm) result in a higher SSA at 1000 °C. For the SiC4.5-1000 °C specimens with pore former amount of 0 to 30 wt.%, SSA decrease from 162 to 77 m²·g⁻¹, respectively. Conversely, samples with 6.5 μm SiC particles (SiC6.5-1000 °C) varied in the range of 76 m²·g⁻¹ (SiC6.5-A0-1000 °C) to 32 m²·g⁻¹ (SiC6.5-A30-1000 °C). Comparable values were reported in the literature for monoliths produced via aqueous freeze casting using pyrolyzed H44 (600 °C) as filler [30].

The nitrogen sorption isotherms of the samples pyrolyzed at 600 °C can be classified as a type I isotherm (Figure 3.4b or all the isotherms see Figure 3.10, section 3.9). This is typical for microporous solids (< 2 nm) where the limiting uptake is governed by the accessible micropore volume rather than by the internal surface area [31]. The shape of isotherms for samples pyrolyzed at 1000 °C, especially those with 4.5 μm SiC particles, are associated with type IV isotherm, which

is common for mesoporous (2 – 50 nm) materials, where capillary condensation takes place. A very small hysteresis loop is shown in these isotherms, which corresponds to a hysteresis loop type H4. This type of loop is often associated with narrow slit-like pores [31].

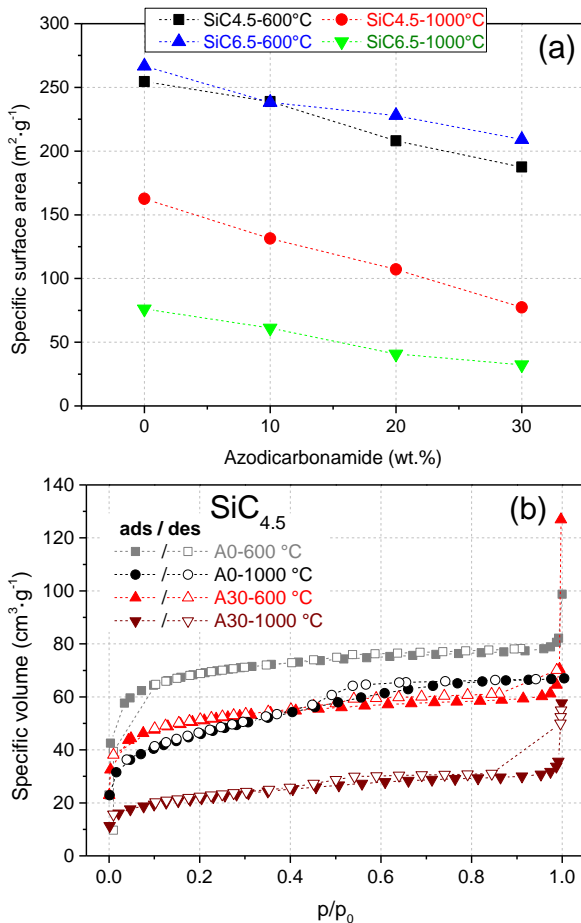


Figure 3.4: (a) Influence of ADA content and different SiC particle sizes (4.5 or 6.5 μm) on specific BET surface areas of pyrolyzed (600/1000 $^{\circ}\text{C}$) tapes, (b) Isotherms obtained for two tape compositions (SiC4.5-A0 and A30) pyrolyzed at 600 $^{\circ}\text{C}$ and 1000 $^{\circ}\text{C}$.

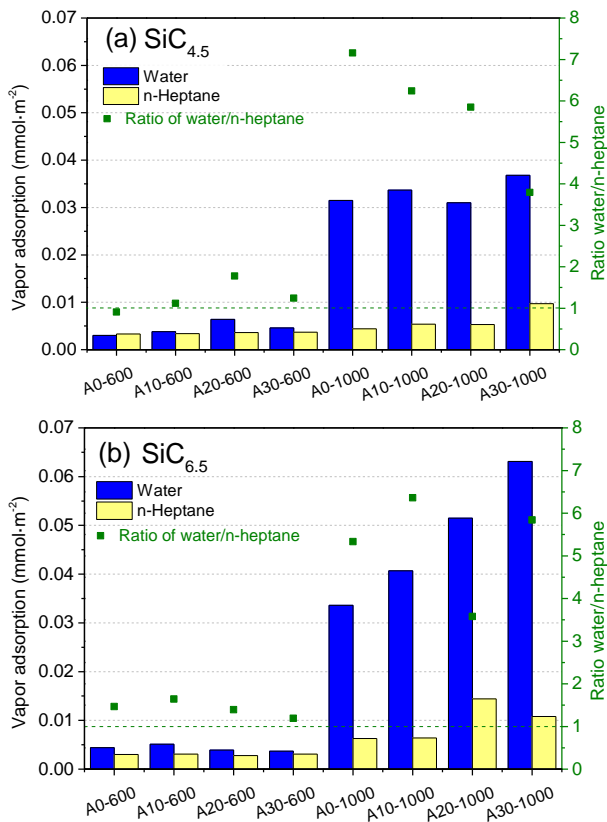


Figure 3.5: Water and n-heptane vapor adsorption at 25 °C (left axis) and ratio of maximum water and n-heptane adsorption (right axis) for samples with different SiC particle size of 4.5 μm (a) and 6.5 μm (b), varying azodicarbonamide amount and pyrolysis temperature (600 and 1000 °C).

Considering that water contact angle method is quite sensitive to surface heterogeneity and presence of porosity, the vapor adsorption of polar (water) and non-polar (n-heptane) solvents was adopted to describe the surface behavior. Hydrophilicity and hydrophobicity characteristics of the pyrolyzed tapes are displayed in Figure 3.5. Apparently, there is no influence of SiC size and ADA amount on the vapor adsorp-

tion because this property is a particular feature of the pyrolyzed polysiloxanes. Hence, the surface characteristic is dictated by the pyrolysis temperature. Beyond 600 °C, most of the remaining hydrophobic methyl groups of the preceramic polymer are decomposed, resulting in higher hydrophilicity [28,32]. Despite the fact that most of the samples present hydrophilic nature in terms of water-to-heptane ratio (> 1), tapes pyrolyzed at 600 °C clearly tend to be more hydrophobic ($1 \leq \text{ratio} \leq 2$) than those pyrolyzed at 1000 °C ($3.5 < \text{ratio} < 7.5$). For instance, the average amount of water vapor adsorbed by tapes produced at 600 °C increased from $0.0044 \pm 0.0010 \text{ mmol}\cdot\text{m}^{-2}$ to $0.0402 \pm 0.0114 \text{ mmol}\cdot\text{m}^{-2}$ after pyrolysis at 1000 °C, which represents an increment of 9.2 times. In contrast, the increase of the adsorption of n-heptane is only about 2.4 times, from $0.0033 \pm 0.0003 \text{ mmol}\cdot\text{m}^{-2}$ to $0.0078 \pm 0.0035 \text{ mmol}\cdot\text{m}^{-2}$.

3.3.3 Flexural strength of the pyrolyzed tapes

The maximum flexural strength (σ_{max}) of the pyrolyzed tapes was measured using three-point bending test. Figure 3.6 depicts the σ_{max} (MPa) for all tape compositions as a function of the azodicarbonamide amount. The highest strength could be achieved at 1000 °C when using smaller inert filler without pore former addition ($121 \pm 15 \text{ MPa}$). However, increasing the amount of ADA leads to a lowering of the mechanical strength since mechanical stability is compromised by the introduction of pores/porosity [33]. Apparently, the decrease of σ_{max} according to the increment of ADA exhibited an exponential pattern. The lowest values observed for σ_{max} were $18.9 \pm 2.8 \text{ MPa}$ (SiC4.5-A30-600 °C), $15.9 \pm 3.1 \text{ MPa}$ (SiC6.5-A20-600 °C), $10.5 \pm 3.6 \text{ MPa}$ (SiC6.5-A30-600 °C).

In order to evaluate the statistical differences in the flexural strength data, two sets of analysis were performed using ANOVA with Tukey's test at a significance level of $p < 0.05$ (Figure 3.6). Figure 3.6 describes the difference due to ADA addition at a fixed SiC size and temperature by analyzing the columns (same color), where the samples statistically different are indicated by letters with their respective color.

Because of the exponential decay trend is possible to see that most of the samples were statistically different when low ADA content was used (0 – 10 wt.%). In this regard, the average flexural strength was very similar for higher amount of ADA (≥ 20 wt.%), where just the samples SiC4.5-A20-1000 °C – SiC4.5-A30-1000 °C and SiC6.5-A20-600 °C – SiC6.5-A30-600 °C seems to be statistically different. In those samples (SiC6.5-600 °C) a linear decay can be implied.

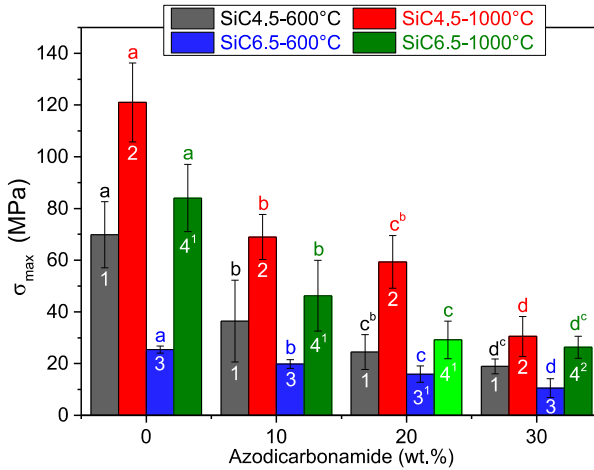


Figure 3.6: Maximum flexural strength (σ_{\max}) of the tapes produced with two silicon carbide particle sizes, pyrolyzed at 600/1000 °C and varying pore former content. (Values with the same amount of ADA followed by different numbers were significantly different at $p < 0.05$ according to Tukey's test – Columns with the same color followed by different letters were significantly different at $p < 0.05$ according to Tukey's test.).

Analyzing Figure 3.6 by looking at the numbers placed inside the columns it is possible to see the difference due to the SiC particle size and temperature at a fixed ADA content. Most of the samples differ statistically from each other, and the strongest tapes are obtained at 1000 °C using an inert filler with 4.5 μm and 6.5 μm , respectively. Interestingly, the specimens SiC4.5-600 °C (column 1) and SiC6.5-1000 °C (column 4) between 0 and 20 wt.% ADA content are

not statistically different. This indicates the great influence of the inert filler size on the mechanical stability of porous materials. Meanwhile, at the highest ADA content (30 wt.%) only the samples pyrolyzed at 1000 °C do not differ statistically, which implies that at this point there is no influence of the SiC size on flexural strength. However, there is a difference when comparing the samples SiC4.5-A30-600 °C and SiC6.5-A30-600 °C, which indicates the positive influence of SiC size at 600 °C.

3.4 Discussion

The use of a liquid shaping process as tape casting was feasible with polysiloxanes acting as a binder, which after heating under controlled atmosphere resulted in a hybrid polymer/ceramic matrix. The incorporation of macroporosity in the structure was achieved by using ADA as pore former agent. The 3D representation in Figure 3.7a shows that the main parameter responsible for creating open macroporous is the addition of ADA, especially for amounts larger than 10 wt.%. Within the 20 to 30 wt.% range, the macroporosity and open pore size are greatly amplified. On the other hand, the shape of the surface in Figure 3.7b indicates the additional influence of the inert filler size on the average pore size. The increase in the pore size is more noticeable using 6.5 µm SiC particles pyrolyzed at 1000 °C. This response is presumably due to larger vacancies between particle-to-particle contacts. Thus, after burning at 1000 °C small pores completely collapsed into bigger ones, which was not the case for SiC4.5.

In contrast, microporosity is negatively affected by the insertion of macroporosity and high pyrolysis temperature. Figure 3.7c demonstrate that at 1000 °C inert filler size plays a major role in sustaining larger SSA. Probably the use of microsized inert filler combined with the slow heating rate can hinder the complete collapse of micro/mesopores in the material [34]. This assumption may be sustained by the occurrence of isotherms type IV with hysteresis loop H4 in all the samples pyrolyzed at 1000 °C (see Figure 3.10, section 3.9), particularly

when using smaller inert filler (4.5 μm). Thus, some of the micropores formed due to the thermal decomposition of the cross-linked polymer collapsed into mesopores, which maintained a substantial value of SSA even after pyrolysis at 1000 $^{\circ}\text{C}$ [24].

Considering that the inert fillers are embedded in the polysiloxane matrix, the hydrophobic/hydrophilic behavior is tailored by the preceramic polymer and its thermal treatment. The tendency toward a hydrophobic behavior can be observed at temperatures below 600 $^{\circ}\text{C}$ since the organic groups, such as methyl and phenyl, are not completely decomposed. Furthermore, the hydrophobicity may also be increased by using a higher amount of MK [18] because the decomposition of methyl groups requires more energy as compared to phenyl groups [35]. Nonetheless, hydrophilicity is achieved by applying high temperatures (\geq 1000 $^{\circ}\text{C}$) where ceramization takes place [36], modifying polysiloxanes with hydrophilic cross-linking agents (e.g. APTES) [24], or increasing the relative amount of a specific polymer (e.g. H44) [18].

Mechanical stability of porous ceramics is directly related to their microstructure, porosity, type and size of particles (inert filler in this case), bonding, etc. Figure 3.7d shows the major influence of temperature and porosity (azodicarbonamide content) on the maximum flexural strength of the tape. Increment in porosity means enlarging macrodefects in the structure, which drastically reduced the σ_{max} in both studied temperatures (600 and 1000 $^{\circ}\text{C}$). Regarding temperature, at 1000 $^{\circ}\text{C}$ high mechanical strength is expected due to ceramization process. Another factor that may enhance the σ_{max} at high pyrolysis temperature is the presence of free carbon between the Si-O-C bonds [37,38]. Moreover, the use of smaller inert filler also contributed to improving σ_{max} (see Figure 3.6), which is probably connected to the higher number of particle-to-particle contacts. The lower mechanical performance of porous SiC6.5 samples can also be correlated to the internal cracks identified in the SEM pictures (Figure 3.2c-d).

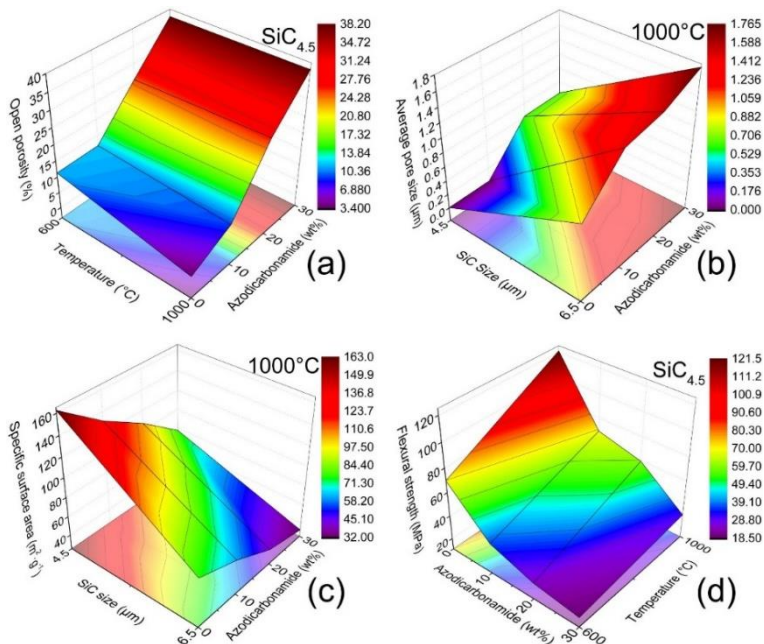


Figure 3.7: 3D representation of the influence of azodicarbonamide amount, pyrolysis temperatures, and inert particle size on: open porosity (a); average pore size (b); specific surface area (c); and maximum flexural strength (d).

3.5 Conclusions

Polysiloxane-based ceramics with hierarchical pore structure were produced by tape casting. Open macroporosity was controlled by using azodicarbonamide as a sacrificial pore former. Since ADA was entrapped in the cross-linked polysiloxanes matrix, its foaming behavior was suppressed. Pyrolysis at 600 °C generated microporosity in the structure, consequently, a higher SSA was obtained. Furthermore, a hydrophobic behavior is more pronounced at 600 °C whereas at 1000 °C hydrophilicity is increased as observed by vapor adsorption analysis. At 1000 °C, micropores collapsed into meso-macropores mostly. Although mechanical stability could be increased by using smaller inert filler and higher pyrolysis temperature, the introduction of macroporosity drasti-

cally diminished the flexural strength. The average pore size can be controlled mainly by the inert filler size and pyrolysis temperature. The range of values combined with the tailored surface characteristics indicated a potential application of this material for membrane separation processes such as microfiltration systems (0.1 – 10 μm).

3.6 Acknowledgements

The Deutsche Forschungsgemeinschaft (DFG) as well as the Brazilian funding agencies National Council for Scientific and Technological Development (CNPq) and Coordination for the Improvement of Higher Education Personnel (CAPES) through the Brazilian-German Collaborative Research Initiative on Manufacturing (BRAGECRIM) are gratefully acknowledged. The authors would like also to thank the support of the Erasmus+ programme of the European Union for the academic exchange between the University of Bremen and the Federal University of Santa Catarina.

3.7 Authors contributions

The article is mainly based on the work of the first author and author of this thesis Rafael Kenji Nishihora. The precise contributions of each author are listed below.

Table 3.1: Authors contributions for Chapter 3.

Author	Contribution
Nishihora, R. K.	Conceptualized the work, performed and analyzed the experiments, wrote the manuscript
Quadri, M. G. N.	Gave conceptual and scientific advices, helped in the scientific evaluation and editing of the manuscript
Hotza, D.	Gave conceptual and scientific advices, helped in the scientific evaluation and editing of the manuscript
Rezwan, K.	Gave conceptual and scientific advices, helped in the scientific evaluation and editing of the manuscript
Wilhelm, M.	Gave conceptual and scientific advices, helped in the scientific evaluation and editing of the manuscript

3.8 References

- [1] R.E. Mistler, The principles of tape casting and tape casting applications, in: R.A. Terpstra, P.P.A.C. Pex, A.H. de Vries (Eds.), *Ceram. Process.*, Springer Netherlands, Dordrecht, 1995: pp. 147–173. doi:10.1007/978-94-011-0531-6_5.
- [2] D. Hotza, P. Greil, Review: aqueous tape casting of ceramic powders, *Mater. Sci. Eng. A*. 202 (1995) 206–217. doi:http://dx.doi.org/10.1016/0921-5093(95)09785-6.
- [3] R.E. Mistler, E.R. Twiname, *Tape Casting: Theory and Practice*, Wiley, 2000.
- [4] M. Boaro, J.M. Vohs, R.J. Gorte, Synthesis of Highly Porous Ytria-Stabilized Zirconia by Tape-Casting Methods, *J. Am. Ceram. Soc.* 86 (2003) 395–400. doi:10.1111/j.1151-2916.2003.tb03311.x.
- [5] S. Ramanathan, K.P. Krishnakumar, P.K. De, S. Banerjee, Powder dispersion and aqueous tape casting of YSZ-NiO composite, *J. Mater. Sci.* 39 (2004) 3339–3344. doi:10.1023/b:jmsc.0000026934.88520.67.
- [6] H. Moon, S.D. Kim, S.H. Hyun, H.S. Kim, Development of IT-SOFC unit cells with anode-supported thin electrolytes via tape casting and co-firing, *Int. J. Hydrogen Energy*. 33 (2008) 1758–1768. doi:http://dx.doi.org/10.1016/j.ijhydene.2007.12.062.
- [7] L. Ren, Y.-P. Zeng, D. Jiang, The improved photocatalytic properties of P-type NiO loaded porous TiO₂ sheets prepared via freeze tape-casting, *Solid State Sci.* 12 (2010) 138–143. doi:http://dx.doi.org/10.1016/j.solidstatesciences.2009.09.021.
- [8] W.A. Meulenber, J. Mertens, M. Bram, H.-P. Buchkremer, D. Stöver, Graded porous TiO₂ membranes for microfiltration, *J. Eur. Ceram. Soc.* 26 (2006) 449–454. doi:http://dx.doi.org/10.1016/j.jeurceramsoc.2005.06.035.
- [9] A. Sanson, P. Pinasco, E. Roncari, Influence of pore formers on slurry composition and microstructure of tape cast supporting an-

- odes for SOFCs, *J. Eur. Ceram. Soc.* 28 (2008) 1221–1226.
doi:<http://dx.doi.org/10.1016/j.jeurceramsoc.2007.10.001>.
- [10] F. Scheffler, M. Scheffler, Polymer derived ceramic tapes as substrate and support for zeolites, *Adv. Appl. Ceram.* 108 (2009) 468–475. doi:10.1179/174367609X459540.
- [11] N. Das, S. Bandyopadhyay, D. Chattopadhyay, H.S. Maiti, Tape-cast ceramic membranes for microfiltration application, *J. Mater. Sci.* 31 (1996) 5221–5225. doi:10.1007/bf00355928.
- [12] N. Das, H.S. Maiti, Formation of pore structure in tape-cast alumina membranes – effects of binder content and firing temperature, *J. Memb. Sci.* 140 (1998) 205–212.
doi:[http://dx.doi.org/10.1016/S0376-7388\(97\)00282-2](http://dx.doi.org/10.1016/S0376-7388(97)00282-2).
- [13] R.K. Nishihora, P.L. Rachadel, M.G.N. Quadri, D. Hotza, Manufacturing porous ceramic materials by tape casting-A review, *J. Eur. Ceram. Soc.* 38 (2018) 988–1001.
doi:10.1016/j.jeurceramsoc.2017.11.047.
- [14] P. Colombo, C. Vakifahmetoglu, S. Costacurta, Fabrication of ceramic components with hierarchical porosity, *J. Mater. Sci.* 45 (2010) 5425–5455. doi:10.1007/s10853-010-4708-9.
- [15] P. Greil, Polymer Derived Engineering Ceramics, *Adv. Eng. Mater.* 2 (2000) 339–348. doi:10.1002/1527-2648(200006)2:6<339::AID-ADEM339>3.0.CO;2-K.
- [16] G. Mera, E. Ionescu, Silicon-Containing Pre-ceramic Polymers, in: *Encycl. Polym. Sci. Technol.*, John Wiley & Sons, Inc., 2002. doi:10.1002/0471440264.pst591.
- [17] E. Ionescu, Polymer-Derived Ceramics, in: *Ceram. Sci. Technol.*, Wiley-VCH Verlag GmbH & Co. KGaA, 2012: pp. 457–500. doi:10.1002/9783527631957.ch18.
- [18] T. Prenzel, M. Wilhelm, K. Rezwan, Pyrolyzed polysiloxane membranes with tailorable hydrophobicity, porosity and high specific surface area, *Microporous Mesoporous Mater.* 169 (2013) 160–167.
doi:<http://dx.doi.org/10.1016/j.micromeso.2012.10.014>.

- [19] P. Colombo, G. Mera, R. Riedel, G.D. Sorarù, Polymer-Derived Ceramics: 40 Years of Research and Innovation in Advanced Ceramics, *J. Am. Ceram. Soc.* 93 (2010) 1805–1837. doi:10.1111/j.1551-2916.2010.03876.x.
- [20] B. V Manoj Kumar, Y.-W. Kim, Processing of polysiloxane-derived porous ceramics: a review, *Sci. Technol. Adv. Mater.* 11 (2010) 44303. doi:10.1088/1468-6996/11/4/044303.
- [21] C. Vakifahmetoglu, D. Zeydanli, P. Colombo, Porous polymer derived ceramics, *Mater. Sci. Eng. R Reports.* 106 (2016) 1–30. doi:10.1016/j.mser.2016.05.001.
- [22] P. Cromme, M. Scheffler, P. Greil, Ceramic Tapes from Pre-ceramic Polymers, *Adv. Eng. Mater.* 4 (2002) 873–877. doi:10.1002/1527-2648(20021105)4:11<873::AID-ADEM873>3.0.CO;2-G.
- [23] J.-F. Drillet, M. Adam, S. Barg, A. Herter, D. Koch, V. Schmidt, M. Wilhelm, Development of a Novel Zinc/Air Fuel Cell with a Zn Foam Anode, a PVA/KOH Membrane and a MnO₂/SiOC-Based Air Cathode, *ECS Trans.* 28 (2010) 13–24. doi:10.1149/1.3507923.
- [24] H. Zhang, C.L. Fidelis, A.L.T. Serva, M. Wilhelm, K. Rezwan, Water-based freeze casting: Adjusting hydrophobic poly-methylsiloxane for obtaining hierarchically ordered porous SiOC, *J. Am. Ceram. Soc.* 100 (2017) 1907–1918. doi:10.1111/jace.14782.
- [25] A. Idesaki, P. Colombo, Synthesis of a Ni-containing porous SiOC material from polyphenylmethylsiloxane by a direct foaming technique, *Adv. Eng. Mater.* 14 (2012) 1116–1122. doi:10.1002/adem.201100354.
- [26] M. Adam, C. Vakifahmetoglu, P. Colombo, M. Wilhelm, G. Grathwohl, Polysiloxane-derived ceramics containing nanowires with catalytically active tips, *J. Am. Ceram. Soc.* 97 (2014) 959–966. doi:10.1111/jace.12708.

- [27] DIN EN 843-1, Advanced technical ceramics - Mechanical properties of monolithic ceramics at room temperature - Part 1: Determination of flexural strength, Beuth. (2006).
- [28] M. Naviroj, S.M. Miller, P. Colombo, K.T. Faber, Directionally aligned macroporous SiOC via freeze casting of preceramic polymers, *J. Eur. Ceram. Soc.* 35 (2015) 2225–2232. doi:10.1016/j.jeurceramsoc.2015.02.013.
- [29] M. Fukushima, P. Colombo, Silicon carbide-based foams from direct blowing of polycarbosilane, *J. Eur. Ceram. Soc.* 32 (2012) 503–510. doi:10.1016/j.jeurceramsoc.2011.09.009.
- [30] H. Zhang, P. D'Angelo Nunes, M. Wilhelm, K. Rezwan, Hierarchically ordered micro/meso/macroporous polymer-derived ceramic monoliths fabricated by freeze-casting, *J. Eur. Ceram. Soc.* 36 (2016) 51–58. doi:http://dx.doi.org/10.1016/j.jeurceramsoc.2015.09.018.
- [31] K.S.W. Sing, D.H. Everett, R.A.W. Haul, L. Moscou, R.A. Pierotti, J. Rouquerol, T. Siemieniowska, Reporting physisorption data for gas/solid systems with special reference to the determination of surface area and porosity (Recommendations 1984), *Pure Appl. Chem.* 57 (1985) 603–619. doi:10.1351/pac19857040603.
- [32] T. Prenzel, K. Döge, R.P.O. Motta, M. Wilhelm, K. Rezwan, Controlled hierarchical porosity of hybrid ceramics by leaching water soluble templates and pyrolysis, *J. Eur. Ceram. Soc.* 34 (2014) 1501–1509. doi:10.1016/j.jeurceramsoc.2013.11.033.
- [33] J.B. Wachtman, W.R. Cannon, M.J. Matthewson, *Mechanical Properties of Ceramics*, John Wiley & Sons, Ltd., 2009.
- [34] H. Schmidt, D. Koch, G. Grathwohl, P. Colombo, Micro- / Macroporous Ceramics from Preceramic Precursors, *J. Am. Ceram. Soc.* 55 (2001) 2252–2255. doi:10.1111/j.1151-2916.2001.tb00997.x.
- [35] P. Olier, L. Delchet, S. Breunig, Tailoring New Silicone Oil for Aluminum Demolding, in: *Organosilicon Chem. I From Mol. to Mater.*, WILEY-VCH Verlag GmbH, 2008: pp. 687–769. doi:10.1002/9783527620777.ch5be.

- [36] M. Scheffler, T. Gambaryan-Roisman, T. Takahashi, J. Kaschta, H. Muenstedt, P. Buhler, P. Greil, Pyrolytic decomposition of preceramic organo polysiloxanes, *Ceram. Trans.* 115 (2000) 239–250.
doi:https://www.tib.eu/de/suchen/id/BLCP%3ACN042344424/Pyrolytic-Decomposition-of-Preceramic-Organo-Polysiloxanes/.
- [37] H.J. Kleebe, Y.D. Blum, SiOC ceramic with high excess free carbon, *J. Eur. Ceram. Soc.* 28 (2008) 1037–1042.
doi:10.1016/j.jeurceramsoc.2007.09.024.
- [38] G. Puyoo, G. Chollon, R. Pailler, F. Teyssandier, Microstructure and Thermodynamic Descriptions of SiC-Based Ceramic Fibers, in: *Mech. Prop. Perform. Eng. Ceram. Compos. V*, John Wiley & Sons, Inc., 2010: pp. 159–172.
doi:10.1002/9780470944127.ch17.

3.9 Supplementary material

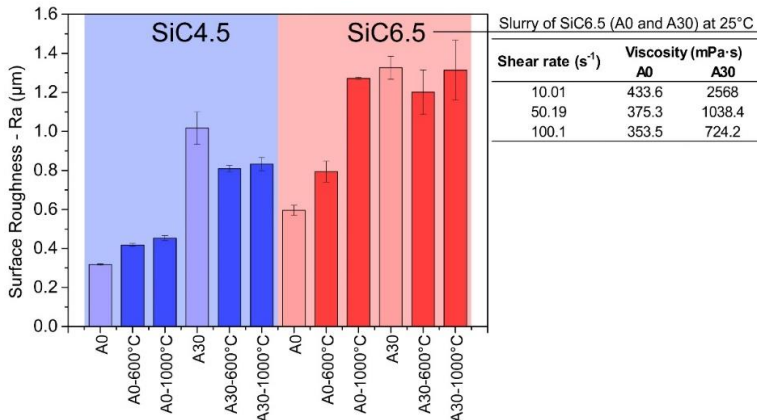


Figure 3.8: Surface roughness (Ra) for samples with different SiC particle sizes (4.5 or 6.5 µm), varying azodicarbonamide content (0 or 30 wt.%), and non-pyrolyzed samples (light blue and pink bars) and pyrolyzed at 600 °C or 1000 °C.

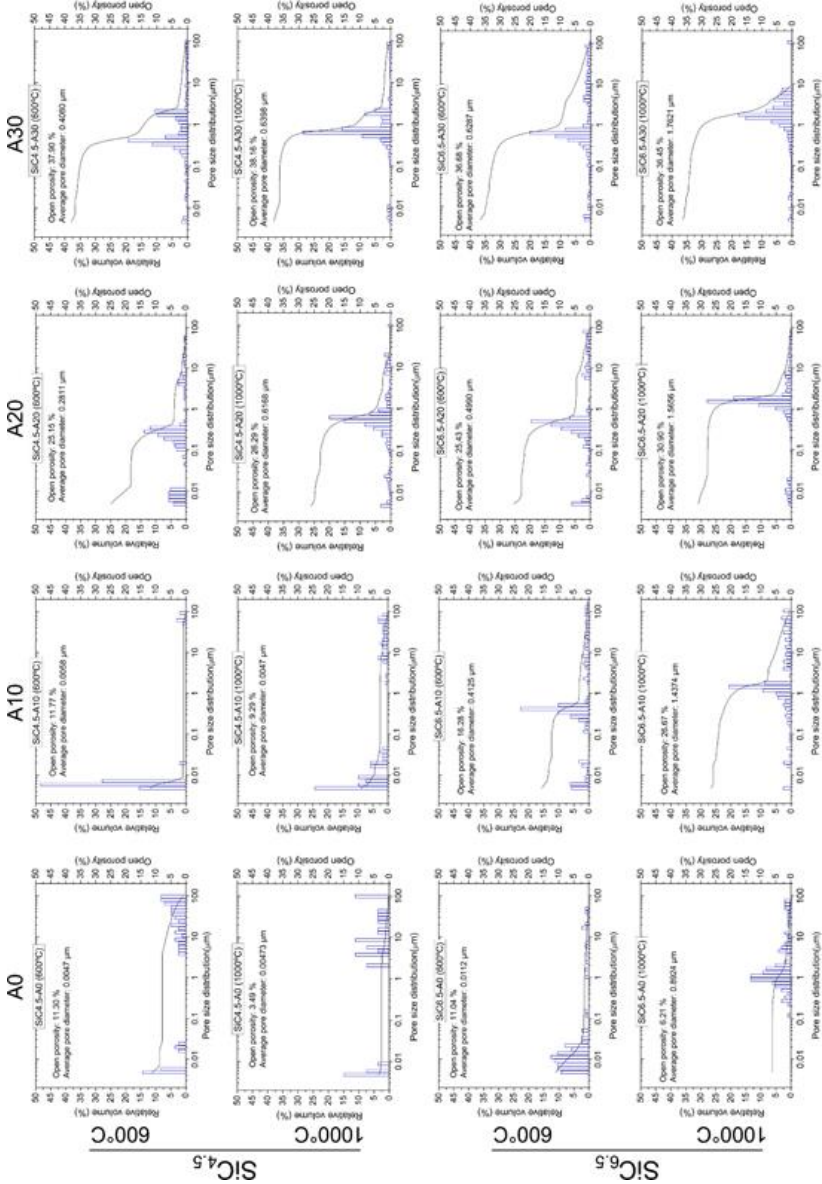


Figure 3.9: Pore size distribution versus relative pore volume and open porosity curves obtained from mercury intrusion porosimetry of pyrolyzed sample.

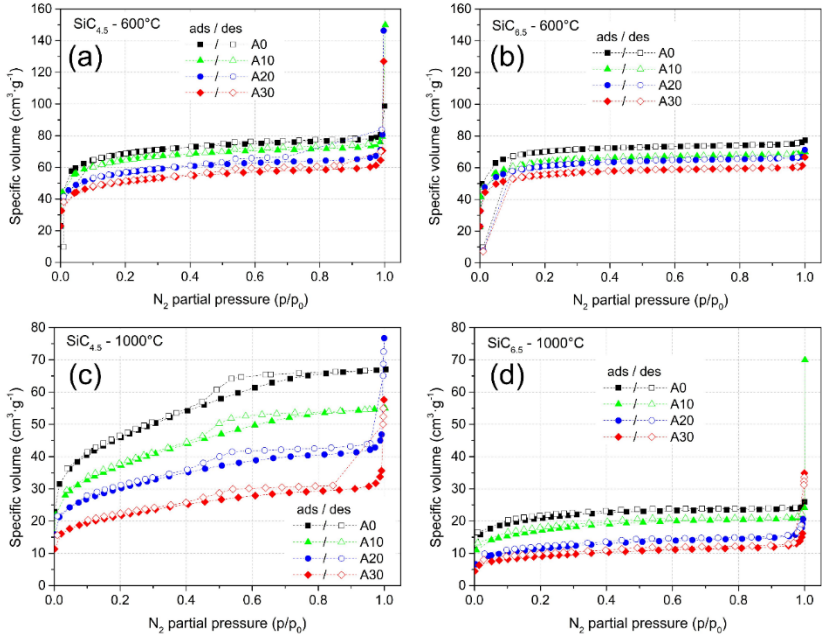


Figure 3.10: Nitrogen adsorption-desorption isotherms for samples with different SiC particle sizes, varying azodicarbonamide content and pyrolyzed at 600 °C/1000 °C.

4 Asymmetric mullite membranes manufactured by phase-inversion tape casting from polymethylsiloxane and aluminum diacetate³

Polymethylsiloxane (MK) and aluminum diacetate have been stoichiometrically combined to synthesize a mullite-based powder ($3\text{Al}_2\text{O}_3 \cdot 2\text{SiO}_2$) at 850 °C (5 h) or 1200 °C (3 h). High-purity crystalline mullite (>99%) was obtained by heating the mixture in the air (thermal oxidation) at 1200 °C for 3 h, mainly due to the formation of highly reactive silica and alumina precursors. Afterward, the mullite-based powders were used to prepare planar asymmetric microfiltration membranes by phase-inversion tape casting. The green membranes were sintered at 1600, 1650 or 1700 °C during 2 h. The asymmetric morphology identified in the membranes by scanning electron microscopy analysis reveals a thin skin-layer (microfiltration layer, <10 μm) followed by a porous support, in which two different structures were observed: finger- and/or sponge-like layer. Water permeation performance in a dead-end configuration was investigated at different pressures (3, 4, and 5 bar). The obtained results clearly indicated an improved water permeation flux compared to a symmetric commercial membrane (133.6 $\text{m}^3/\text{m}^2 \cdot \text{h}$ compared to 14.7 $\text{m}^3/\text{m}^2 \cdot \text{h}$, respectively, at 5 bar). This observation could be ascribed to the asymmetric morphology resultant from the phase-inversion process.

4.1 Introduction

A rising interest in ceramic membranes has been observed by the industry and research fields. The development of advanced processing techniques made possible the preparation of high-performance ceramic membranes. In comparison to traditional polymeric membranes, ceramic presents higher chemical and thermal stability, structural resistance, and long working life [1,2]. There are plenty of techniques to prepare ceramic membranes, such as structural leaching, extrusion, pressing, chemical

³ Based on a paper published in the Journal of Membrane Science:
<https://doi.org/10.1016/j.memsci.2019.03.047>

vapor deposition, sol-gel, slip casting, and tape casting [3]. Recently, an increasing number of works have reported the use of phase-inversion (pore forming strategy) coupled with tape casting (shaping method) for the preparation of asymmetric flat ceramic membranes [4–10].

Phase-inversion has been widely used to produce polymeric membranes [11]. However, this process has been adapted to prepare ceramic membranes by simply adding ceramic particles into the polymeric solution and later burning out the organic components and consolidating the structure through sintering [4,12–14]. This method is based on thermodynamic and kinetic principles, such as the relationship between the chemical potentials and diffusivities of the individual components and Gibb's free energy of mixing of the entire system [15]. The most common phase-inversion strategy is the non-solvent induced process. In this approach, the polymer is converted from the liquid phase into a solid by the phase separation or "demixing" what is induced by a non-solvent (normally water) [16]. The membrane formation is dictated by many parameters, such as slurry composition, particle size, rheological properties, and non-solvent characteristics [13,17]. The main advantage of this technique relies on the flexibility to tailor the morphology in order to produce an asymmetric structure composed by a thick sub-layer (porous support) and a thin layer (membrane). Therefore, this one-step approach is possible by adjusting one of the aforementioned parameters, which can result in different morphologies in the sub-layer (e.g. finger or sponge-like structures) [18].

The predominant materials used to prepare ceramic membranes include α -alumina, silica, zirconia, titania, perovskites, and aluminum silicates (e.g. mullite). Mullite is the only stable crystalline phase in the alumina-silica ($\text{Al}_2\text{O}_3\text{-SiO}_2$) system under normal atmospheric pressure and its composition varies in the range of $3\text{Al}_2\text{O}_3\cdot 2\text{SiO}_2$ to $2\text{Al}_2\text{O}_3\cdot \text{SiO}_2$ [19]. This material presents a great importance in both traditional and advanced ceramics, which is directly related to its particular properties: high thermal stability, low thermal expansion, high resistance to creep, corrosion stability, low density (compared to pure α -alumina), good mechanical strength and fracture toughness [20,21]. The traditional

method to produce mullite requires high temperature ($> 1587\text{ }^{\circ}\text{C}$) and holding times. Exploring reactive silica and/or alumina precursors has been one strategy to produce pure mullite under mild conditions. For instance, highly reactive amorphous silica has been prepared by thermal-oxidation of polysiloxanes [22]. Even though high-purity mullite ($>99\%$) has been produced by combining polysiloxanes and microsized ($0.8\text{ }\mu\text{m}$) $\alpha\text{-Al}_2\text{O}_3$ [22] and nanosized (15 nm) $\gamma\text{-Al}_2\text{O}_3$ [23], the temperatures applied were in the range of $1700\text{ }^{\circ}\text{C}$ and $1350\text{ }^{\circ}\text{C}$, respectively. Alternatively, recent studies have reported the preparation of mullite membranes using materials like natural bauxite [24] with fly ash [25,26], and kaolin-based powders [27]. In particular, kaolin can form mullite at temperatures up to $1200\text{ }^{\circ}\text{C}$ [28]. However, the resultant mullite phase is accompanied by cristobalite (SiO_2) [27]. Hence, some works include extra alumina content and a crystallization catalyst (e.g. AlF_3) to enhance mullitization, yet impurities such as corundum and cristobalite phases are still commonly found [29,30].

With the purpose of exploring an alternative alumina source to prepare high-purity mullite powder in conjunction with silica originated from a polysiloxane, the present work reports the use of aluminum diacetate [31] and polymethylsiloxane. The prepared mullite-based powder was characterized with regard to particle size distribution and crystallinity. Afterward, phase-inversion tape casting was employed to prepare planar asymmetric microfiltration mullite membranes using the synthesized powder. The sintering temperature was varied and the prepared membranes were evaluated in terms of morphology, crystallinity, macroporosity, mechanical strength, and water permeation flux.

4.2 Experimental

4.2.1 Materials

A commercially available methyl-polysiloxane (PMS Silres MK®, Wacker) was used as the starting preceramic polymer and silica source. Aluminum diacetate ($\text{C}_4\text{H}_7\text{AlO}_5$, purum p.a., Sigma-Aldrich)

was used as alumina source. For comparison purposes, α -alumina (Al-matis, CT3000, $d_{50} \sim 0.5 \mu\text{m}$) was also used as alumina source for the preparation of mullite. For the production of the asymmetric membranes, a polyethersulfone (PES, 58,000 g/mol, GoodFellow Cambridge Limited) was selected as the polymer source and polyvinylpyrrolidone (PVP – K40, Sigma-Aldrich) as an additive. The solvent for the polymer and liquid medium for the ceramic particles was N-methyl-2-pyrrolidone (NMP, Sigma-Aldrich).

4.2.2 Mullite-based powder preparation

The MK powder was dissolved in acetone (1 g of MK per 50 mL of acetone) [23] and stirred for 15 min. Then the alumina or aluminum diacetate [31] was added based on a stoichiometric proportion to produce pure mullite phase ($3\text{Al}_2\text{O}_3 \cdot 2\text{SiO}_2$). The mixture was ultrasonicated for 10 min and stirred in a closed beaker during 3 h and further 4 h with the beaker open. To ensure further solvent removal and pre-crosslink of the polysiloxane, an additional thermal treatment step was employed for 12 h at 70 °C. In order to get a fine powder, the obtained solid material was ground in a ball mill for 6 h at 350 rpm. Afterward, the fine powder was calcined at 850 °C (5 h) or 1200 °C (3 h) with a heating/cooling rate of 5 °C/min [31]. The final powder was characterized and applied to produce the ceramic membranes. The preparation steps of the mullite-based powder are shown in Figure 4.1a.

4.2.3 Membrane preparation

The slurries compositions are given in Table 4.1. The polyethersulfone and polyvinylpyrrolidone were dissolved in N-methyl-2-pyrrolidone. After the polymer solution was formed, the mullite-based powder was added and stirred for 24 h at room temperature. The as-prepared slurry was degassed for 30 min using a vacuum pump (20 mbar). Then, the slurry was cast over a polyethylene terephthalate carrier film (Mylar, G10JRM, Richard E. Mistler, Inc.) with a doctor

blade using a gap height of 1.2 mm. The cast slurry was solidified by immersion precipitation in deionized water (non-solvent) for 24 h at room temperature. Afterward, the green tape was dried in the fume hood at room temperature for 3 days. The dried green tape was cut into desired shape and size, heated at a rate of 3 °C/min to 850 °C in air, and kept at that temperature for 3 h to remove the organic moieties. Then the samples were heated at a rate of 2 °C/min to final temperature (1600 – 1650 – 1700 °C) and kept at that temperature for 2 h in air, and cooled down at a rate of 2 °C/min to room temperature. The preparation steps of the membranes are illustrated in Figure 4.1b.

Table 4.1: Slurry compositions (vol.%) for the preparation of the mullite-based membranes.

Material	Slurry 1, 2 (vol.%)	Slurry 3 (vol.%)
N-methyl-2-pyrrolidone (NMP)	67.14	65.21
Polyethersulfone (PES)	6.22	8.15
Polyvinylpyrrolidone (PVP-40)	0.79	0.79
Ceramic powder (mullite-based powders)	25.85	25.85

Slurry 1, 2: Ceramic powder – Diac-850 (2.591 g/cm³) or Diac-1200 (3.045 g/cm³)

Slurry 3: Ceramic powder – Alu-850 (3.134 g/cm³). Note: in order to improve the processability of the Slurry 3 and produce a homogenous and stable green membrane, the PES amount was increased accompanied by the decreasing of NMP content.

Density of the ceramic powders was measured using Helium Pycnometer device (Pycnomatic, Porotec).

4.2.4 Specimen denotation

The mullite-based powders were prepared with MK (silica source) and either α -alumina or aluminum diacetate as alumina source. The ceramic powder denotation is given by the alumina source accompanied by the calcination temperature. For instance, Diac-850 means that the aluminum diacetate is the alumina source plus MK calcined at 850 °C, and Alu-850 means that the aluminum diacetate is the alumina

source plus MK calcined at 850 °C. In addition, in the case of membranes denotation, the sintering temperature is added as follows: Diac-850-1700 indicates the mullite-based powder used (as aforementioned) followed by the sintering temperature of the membrane produced (1700 °C).

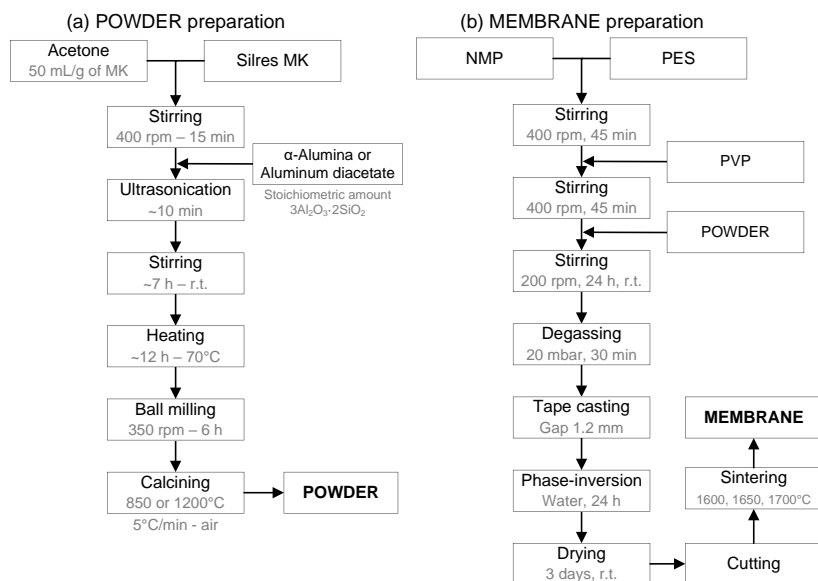


Figure 4.1: Process scheme of the preparation of mullite-based (a) powder and (b) membrane.

4.2.5 Characterization

The macrostructure of the powder and membranes was analyzed by Scanning Electron Microscopy (SEM, 20 kV; Series 2, Obducat CamScan; Supra 40-Carl Zeiss). For this purpose, the samples were sputtered with gold (K550, Emitech, Judges Scientific). In order to evaluate the skin-layer thickness and the pore sizes presented on the bottom and top surface of the sintered membranes, the SEM images were processed and analyzed by an image processing software (ImageJ) [32]. The number of pores detected from the SEM images varied from around

400 up to 1200 data points accounted. The particle size distribution of the mullite-based powder was measured by a laser diffraction device (Malvern Mastersizer 2000). The density of these powders was acquired by Helium Pycnometer (Pycnometer, Porotec). Porosity and pore size distributions of the tapes were determined using mercury intrusion porosimetry (Pascal 140/440, Porotec). X-ray diffraction analysis (powder XRD, Seifert 3003) was conducted to identify the obtained crystal phases from both calcined powders and sintered membranes. In order to quantify the composition in terms of crystal phases, Rietveld refinement was performed with the diffractograms by a software (MAUD – Material Analysis Using Diffraction, version 2.84, December 7, 2018) [33]. The MAUD software was developed to analyze diffraction spectra and determine crystal structures, quantify the relative contribution of crystalline phases, and microstructure of phases along with the texture and residual stresses. A detailed documentation about the software usage is available online [34]. The reference diffractograms can be obtained from the Crystallography Open Database (COD), which is an open-access collection of crystal structures of organic, inorganic, metal-organic compounds and minerals (excluding biopolymers) [35,36].

The mechanical behavior of the sintered tapes was studied by three-point bending tests (Roell Z005, Zwick – [37]). These measurements were performed using a 5 kN load cell (piezoelectric force sensor). The samples were cut into a rectangular shape (16 mm length, ~2 mm width, and 0.7–1.0 mm thickness) and placed in the center of a sample holder with 10 mm distance between the support rollers (diameter of 1.5 mm). The crosshead speed and pre-load were fixed at 0.1 mm·min⁻¹ and 0.25 N, respectively. Twenty samples for each composition and temperature were tested and statistically evaluated by Weibull analysis. Water permeation tests were performed using a homemade setup in a dead-end configuration (see Figure 4.8, section 4.9). The membranes were cut into a circular shape (10 mm diameter) and tested in triplicate at various pressures. For comparison, a commercially available borosilicate glass membrane (Por5, Robugas) was also

tested. The permeation flux was calculated according to the following equation:

$$J = \frac{l}{A} \cdot \frac{dV}{dt} \quad \text{Equation 4.1}$$

where J is the membrane permeation flux ($\text{m}^3 \cdot \text{m}^{-2} \cdot \text{h}^{-1}$); A is the effective cross-sectional surface area of the ceramic membrane (m^2); dV and dt represent the variation in volume (m^3) and time (h), respectively.

4.3 Results

Preparation of mullite-based powder was performed by using a commercially available polysiloxane (MK) as silica precursor, and either commercially available α -alumina powder or aluminum diacetate as alumina sources. From the prepared mullite-based powders, microfiltration ceramic membranes were successfully produced by phase-inversion tape casting method. The green bodies were stable and easy to handle. The produced tapes presented an average thickness of ~ 1.0 mm and a cut area of 10×20 cm, as obtained prior to sintering. The samples for the mechanical test were cut into rectangular shapes (5×3 cm), whose dimensions were adjusted after sintering to the required specifications for the test. The samples for permeation tests were cut into circles (diameter: 2.5 cm) and/or squares (2.5×2.5 cm). It is noteworthy that the warping during sintering constitutes one of the major technological challenges to produce large sizes of ceramic membrane plates. However, there are some strategies frequently used even in industrial scales such as applying the vertical or overhanging sintering [38], supported and vertically inclined sintering, and overstacking samples or using ceramic weights (e.g. inert inorganic powder, ceramic pieces, etc) [39]. The particle size and sintering temperature were varied to investigate their influence on pore structure, mechanical properties, and water permeation flux.

4.3.1 Powder size and composition

Figure 4.2 shows SEM images (left) of the prepared powders alongside with the particle size distributions measured by laser diffraction (right). The SEM images evidence the tendency to form agglomerates, especially due to increases in temperature and by using α -alumina as alumina source. The particle size distribution analysis corroborates the SEM findings by exhibiting narrower size distribution for Diac-850 sample (mean particle size of 5.3 μm), which is slightly enlarged by increasing the calcination temperature up to 1200 $^{\circ}\text{C}$ (Diac-1200, mean particle size: 6.4 μm). However, the substitution of aluminum diacetate by α -alumina has a great impact on particle size, even at the lower calcination temperature (850 $^{\circ}\text{C}$). As a result, the specimen Alu-850 shows the widest range of particle size distribution (span = 4.3), where the mean value was further raised up to 13.2 μm . Since the sample Alu-1200 resulted in a single agglomerated block after calcination, this composition was not suitable to be measured and, hence impracticable to prepare stable microfiltration membranes. Therefore, the membranes were prepared using the Diac-850, Diac-1200, and Alu-850 powders.

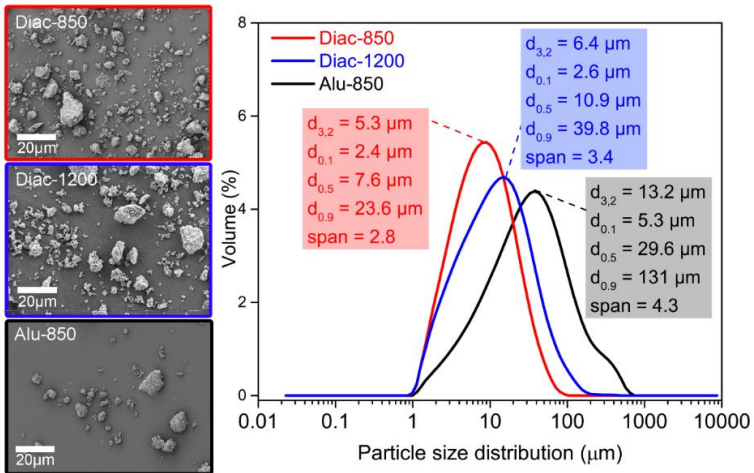


Figure 4.2: SEM images (left) of the prepared mullite-based powders and particle size distribution analysis by laser diffraction (right).

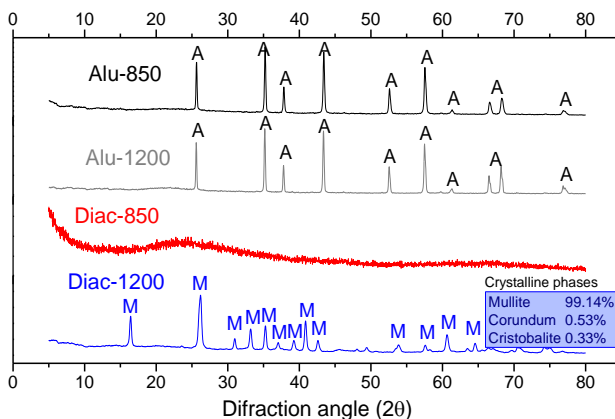


Figure 4.3: X-ray diffraction (XRD) analysis of the obtained mullite-based powders. A – α -Alumina or Corundum (ref.: PDF#04-071-1123); M – Mullite ($3\text{Al}_2\text{O}_3 \cdot 2\text{SiO}_2$) (ref.: PDF#01-079-1454). (The values in the blue box represent the crystalline phases of Diac-1200 sample quantified by Rietveld Refinement; Goodness of fit: sig = 1.5; Rwp = 13.96%; Mullite-COD ID 2310785; Corundum-COD ID 2300448; Cristobalite-COD ID 9001579.).

The investigation of the mullitization process of the calcined powders is shown in Figure 4.3. The Alu-850 specimen does not exhibit any peak characteristic of mullite, expressing only the α -alumina phase. The same is true for the Alu-1200, shown here for comparison purposes since it was not studied for membrane preparation as justified before. The Diac-850 is completely composed by amorphous phase at this temperature, which explains the lower density value obtained for this powder (2.591 g/cm^3) in comparison to the literature value for mullite ($\sim 3.2 \text{ g/cm}^3$) [20]. On the other hand, the Diac-1200 sample features mainly mullite peaks that corroborate with the higher density observed (3.045 g/cm^3). This observation is confirmed by the Rietveld refinement analysis in which 99.14% of the crystalline phase is composed by mullite (COD ID 2310785). As expected, the mullitization is facilitated by bringing together two reactive precursors, MK and aluminum diacetate. Nonetheless, considering that the Rietveld refinement is only capable of quantifying crystalline portions of the samples, the assumption of the

presence of some amorphous contribution may not be excluded at this temperature.

4.3.2 Membrane composition

Table 4.2: Crystalline phases content (wt.%) and goodness of fit determined by Rietveld refinement method of the X-ray powder diffractograms from the sintered membranes.

Sample	Crystalline phases content (wt.%)			Goodness of fit	
	Mullite	Corundum	Cristobalite	sig	R _{wp} (%)
Alu-850-1600	99.96	0.02	0.02	1.85	17.13
Alu-850-1650	99.94	0.00	0.06	2.06	18.61
Alu-850-1700	99.39	0.60	0.01	1.73	17.03
Diac-850-1600	99.97	0.03	0.00	1.86	16.56
Diac-850-1650	99.86	0.00	0.14	2.02	16.86
Diac-850-1700	99.97	0.00	0.03	1.93	16.03
Diac-1200-1600	99.96	0.31	0.00	1.84	17.15
Diac-1200-1650	99.69	0.30	0.01	2.17	18.95
Diac-1200-1700	99.77	0.23	0.00	1.92	16.12

Mullite-COD ID 2310785; Corundum-COD ID 2300448; Cristobalite-COD ID 9001579.

R_{wp} = weighted profile R-factor

sig = R_{wp}/R_{expected}

As presumed, since the lower sintering temperature is above the minimum mullitization temperature, all sintered membranes disclose peaks characteristic of mullite crystalline phase, as shown in Figure 4.9 (section 4.9). Although relatively short holding time has been employed (2 h), the analyzed crystalline phase contains a high degree of mullite given the reactive nature of the amorphous silica formed due the thermooxidation of MK. Table 4.2 summarizes the crystalline phases content for all sintered membranes using the Rietveld refinement method. There is no perceptible difference among the produced samples, in which mullite content is above 99 wt.%. The goodness of fit values are in general in an acceptable range (sig ≤ 2 and R_{wp} ≤ 20%). Notwithstanding corundum represents the most noticeable impurity in the mul-

lite system, its value is not significant in the total crystalline phase (< 0.6 wt.%). Even though the Rietveld method is insensitive to amorphous phases (as stated before), given the applied sintering temperatures (above the eutectic temperature, ~ 1590 °C), amorphous contributions are not expected in this case [40,41].

4.3.3 Membrane morphology and macroporosity

Figure 4.4a-b-c shows the cross-section of the sintered mullite-based membranes (1700 °C) along the thickness direction. These images reveal an asymmetric structure for all the analyzed samples. The upper part is composed by a thin layer (skin layer), in which the thickness varies inversely proportional to the mullite based powder size ~ 6 μm (Alu-850-1700), ~ 8 μm (Diac-1200-1700), and ~ 10 μm (Diac-850-1700). Below the skin layer it is possible to identify a more pronounced porous structure for the samples Alu-850-1700 and Diac-1200-1700. They present the typical finger-like pores (yellow highlighted zone) that were initiated from the top surface of the membrane and penetrated into less than half of the bulk structure. The blue highlighted zone is composed by sponge-like structures, which extends until the bottom surface. Contrastingly, the specimen Diac-850-1700 does not display a three-layered configuration as the other two compositions. Instead, it only exhibits the skin layer followed by a sponge-like structure with a denser aspect.

The top and bottom surface morphologies supplemented by the pore diameter range are shown in Figure 4.4d-e-f and Figure 4.4g-h-i, respectively. In respect of surface morphology, there is no apparent difference in pore shape, being the main distinction with regard to pore diameter size. The pore diameter range increases according to the ceramic particle size, as to be expected. Alu-850-1700 presents the wider pore size distribution for both top (Figure 4.4d, pore diameter < 4 μm) and bottom (Figure 4.4g, pore diameter < 20 μm) surface among the displayed samples. Hence, Diac-850-1700 is positioned in the smaller pore diameter range since it was produced using the smaller mullite-

based powder. The pore sizes on the top surface are inferior to $2\ \mu\text{m}$ (Figure 4.4f), while the bottom surface presents values smaller than $4\ \mu\text{m}$ with a consistent peak in the $2\ \mu\text{m}$ region (Figure 4.4i). The intermediate sample, Diac-1200-1700, exhibits values closely related to the sample Diac-850-1700 rather than Alu-850-1700. This response is quite predictable, reflecting the ceramic powder size of the studied samples.

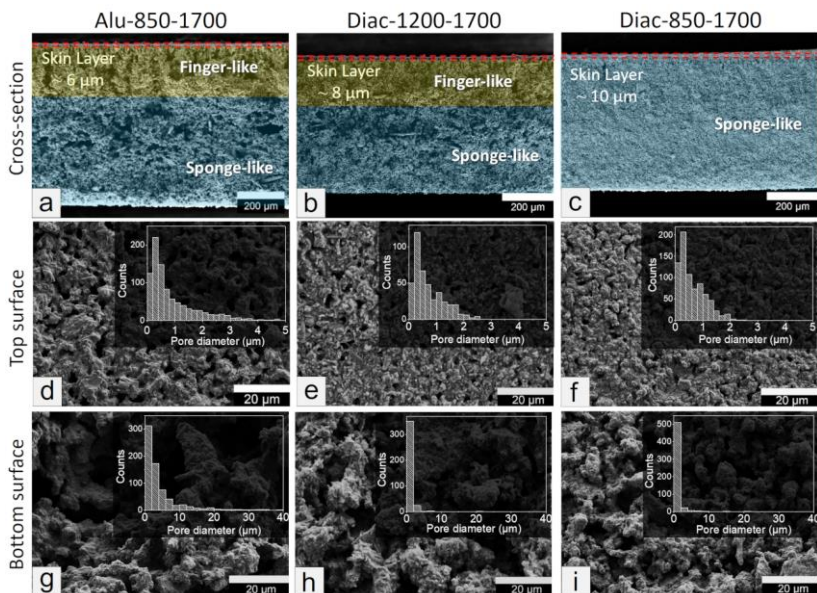


Figure 4.4: SEM images of the cross-sections (a, b, c), top surface (d, e, f), and bottom surface (g, h, i) of the membranes sintered at $1700\ ^\circ\text{C}$. Pore diameter distribution graphs are displayed for the top and bottom surface based on image analysis using ImageJ.

Taking into account the limitation of the image analysis as an exploratory method for determining the pore size, the use of another technique in conjunction is highly advisable. The mercury intrusion analysis is a well-established method for determining pore size distribution and open porosity. Figure 4.5a-b-c shows the results of the Hg-intrusion porosimetry of the prepared membranes sintered at different temperatures ($1600\ ^\circ\text{C}$, $1650\ ^\circ\text{C}$ and $1700\ ^\circ\text{C}$).

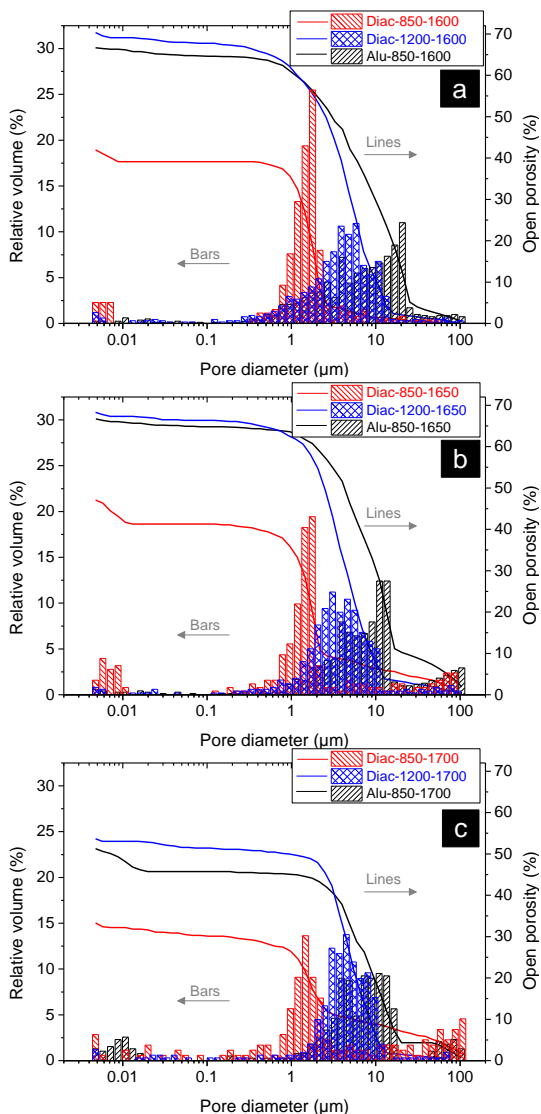


Figure 4.5: Pore size distribution (μm) versus relative pore volume (%) and open porosity (%) curves obtained from Hg-intrusion porosimetry of the sintered mullite membranes at different temperatures: (a) 1600 °C, (b) 1650 °C and (c) 1700 °C.

The detected macropore sizes displayed a quite wide pore size distribution for the samples Diac-1200 (1 to 10 μm) and Alu-850 (~2 to 20 μm), for all the sintering temperatures. On the other hand, the samples prepared with Diac-850 exhibit a very narrow distribution in the range of 1 μm , especially at 1600 °C and 1650 °C. Regarding the effect of sintering temperature on the pore size distribution, it is basically negligible. Notwithstanding, the open porosity is highly affected by increasing the temperature from 1650 °C to 1700 °C, in which densification is favored. For instance, Diac-1200-1650 decreases from 68.27% to 53.68% at 1700 °C (Diac-1200-1700); Alu-850-1650 from 66.68% to 51.28% at 1700 °C (Alu-850-1700); and Diac-850-1650 reduces from 47.08% to 33.33% at 1700 °C (Diac-850-1700). In terms of percentage reduction, all the samples show a similar range of open porosity diminution (14–15%).

4.3.4 Mechanical behavior of sintered membranes

Figure 4.6a shows the Weibull failure distribution of the flexural strength of selected sintered membranes, exhibiting their respective characteristic flexural strength (σ_0) and Weibull modulus (m). The Alu-850-1XXX specimens and all samples sintered at 1600 °C could not be tested due to their high brittle response, which made the preparation (cutting) of these samples impossible. The samples sintered at 1700 °C display higher flexural strength, 134 MPa for Diac-850-1700 and 74.37 MPa for Diac-1200-1700. Meanwhile, Diac-850-1650 and Diac-1200-1650 present σ_0 values equal to 49.46 MPa and 34.66 MPa, respectively. However, the m value is in the range of 4 for all studied membranes except for Diac-850-1700 ($m = 6$). This distinct value can be correlated to the inferior open porosity compared to the other specimens, as shown in Figure 4.6b. Furthermore, Figure 4.6b also shows that the obtained flexural strength–porosity pairs in this work are comparable to values reported in the literature (taking into consideration 3 point bending tests of porous mullite).

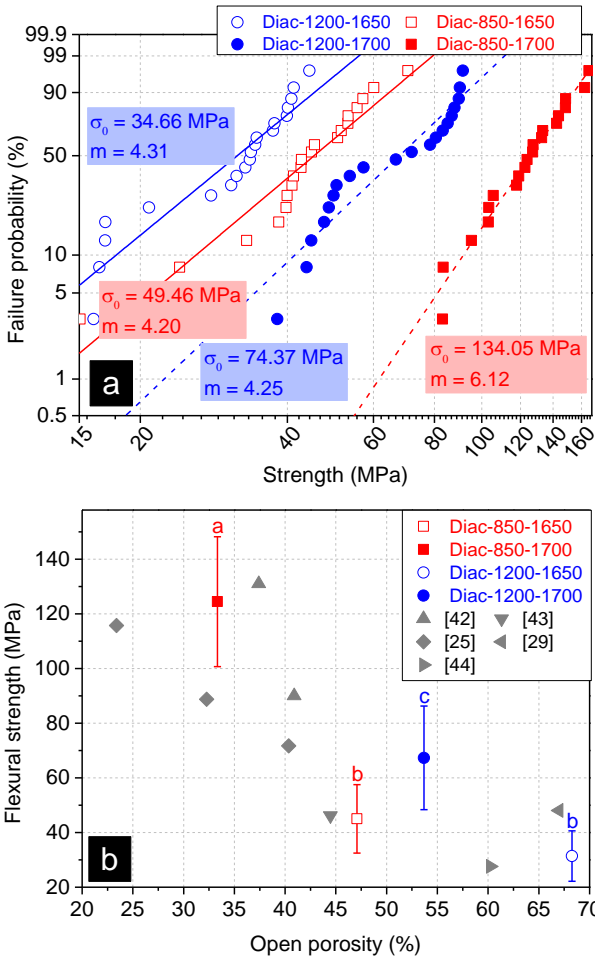


Figure 4.6: (a) Weibull failure distribution of flexural strength of selected sintered membranes measured by three-point bending test; (b) flexural strength as a function of open porosity for tested membranes and literature comparison (She and Ohji “▲” [42], Dong et al. “▼” [43], Cao et al. “◆” [25], Hou et al. “◀” [29], and Hua et al. “▶” [44]). (Diac-X-X samples in Fig.6b followed by different letters were significantly different at $p < 0.05$ according to Tukey's test).

Tukey's test ($p < 0.05$) shows that the samples sintered at 1700 °C are statistically different (in terms of flexural strength) from each other and from the samples sintered at 1650 °C. However, Diac-850-1650 and Diac-1200-1650 samples do not display any significant difference according to Tukey's multiple comparison test despite the expressive difference with regard to the open porosity. All the presented data denote a negative linear relationship between flexural strength and porosity, as expected.

4.3.5 Membrane performance and transport properties

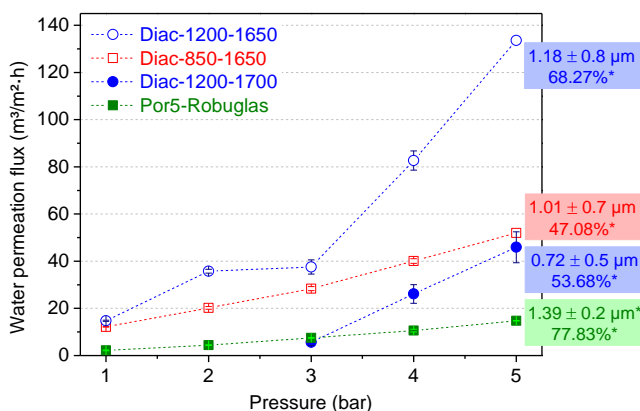


Figure 4.7: Water permeation flux ($\text{m}^3/\text{m}^2\cdot\text{h}$) as a function of the applied pressure (bar) for selected membranes in a dead-end configuration (the values inside the colored boxes represent the average pore size (top) and the open porosity (bottom). Values signed with “*” were obtained from Hg-porosimetry; values without markers were determined by image analysis from SEM pictures of the top surface).

The water permeation flux according to the applied pressure for some selected membranes is shown in Figure 4.7. The composition Diac-850-1700 is not displayed here due to the poor permeability observed during the tests. For comparison purposes, a commercial borosilicate glass membrane (Por5 from Robuglas) with a symmetric pore structure was also studied. This membrane has an average pore diameter of 1.39

μm and open porosity about 78% as determined by Hg-porosimetry (Figure 4.11, section 4.9). Despite the larger average pore size and its elevated open porosity, the commercial membrane presents the lowest water permeation flux among the tested membranes. Nevertheless, it is noticed a 6.7 times increase in flux when raising the pressure from 1 to 5 bar for Por5, resulting on fluxes of $2.2 \text{ m}^3/\text{m}^2\cdot\text{h}$ and $14.7 \text{ m}^3/\text{m}^2\cdot\text{h}$, respectively. The prepared asymmetric mullite membranes show a superior flux increase with the applied pressures. Diac-1200-1650 exhibits the best outcome, in which the water flux increases from $14.7 \text{ m}^3/\text{m}^2\cdot\text{h}$ up to $133.6 \text{ m}^3/\text{m}^2\cdot\text{h}$ (~ 9.1 times increment), just by changing the pressure from 1 bar to 5 bar. Samples Diac-850-1650 and Diac-1200-1700 differ in terms of water flux at pressures below 5 bar but show quite similar values at 5 bar, $52.0 \text{ m}^3/\text{m}^2\cdot\text{h}$ and $45.9 \text{ m}^3/\text{m}^2\cdot\text{h}$, respectively.

Table 4.3 summarizes the transport properties of the studied membranes based on the pure water permeation test (Figure 4.12 with the linear fittings and the considered equations are detailed in the supplementary material – section 4.9). The asymmetric membranes exhibited a similar thickness (δ_m) in the range of 6 to 8 μm , while the symmetric commercial membrane presents the thickness in the millimeter range ($\sim 1 \text{ mm}$). Despite the slight inferior water flux output and permeance presented by Diac-1200-1700 compared to Diac-850-1650, the membrane resistance and the intrinsic permeability of Diac-1200-1700 are superior due to the slight thinner skin-layer (δ_m). However, due to the impossibility of acquiring more data points regarding the water flux of Diac-1200-1700, the calculated transport properties should be carefully considered. As one may expect, the symmetric thick Por5 membrane shows lowest permeance ($2.72 \pm 0.12 \text{ m}^3/\text{m}^2\cdot\text{h}\cdot\text{bar}$) and inferior permeability ($6.72 \times 10^{-15} \text{ m}^2$). Diac-1200-1650 displays the highest permeance ($k_w = 21.78 \pm 2.62 \text{ m}^3/\text{m}^2\cdot\text{h}\cdot\text{bar}$) and intrinsic permeability ($k_{v,intr} = 3.29 \times 10^{-16} \text{ m}^2$), hence the lowest membrane resistance ($R_m = 1.86 \times 10^{10} \text{ m}^{-1}$).

Table 4.3: Membrane thickness (δ_m) and transport properties in terms of permeance (k_w), clean membrane resistance (R_m), and intrinsic permeability ($k_{v,intr}$) of the tested asymmetric and symmetric ceramic membranes.

Sample	δ_m (m)	k_w (m ³ /m ² ·h·bar)	R_m (m ⁻¹)	$k_{v,intr}$ (m ²)
Diac-1200-1650	6.11×10^{-6}	21.78 ± 2.62	1.86×10^{10}	3.29×10^{-16}
Diac-1200-1700	7.66×10^{-6}	7.02 ± 1.89	5.76×10^{10}	1.33×10^{-16}
Diac-850-1650	6.86×10^{-6}	10.14 ± 0.21	3.99×10^{10}	1.72×10^{-16}
Por5-Robuglas	1.00×10^{-3}	2.72 ± 0.12	1.49×10^{11}	6.72×10^{-15}

4.4 Discussion

This work revealed that the stoichiometric combination of polysiloxane and aluminum diacetate is feasible to synthesize high-purity mullite ($3\text{Al}_2\text{O}_3 \cdot 2\text{SiO}_2$) crystal phase at relatively low temperature (1200 °C) and short holding time (3 h). Even though the SEM images from the powder (Figure 4.2) show some extent of agglomeration according to the alumina precursor and calcining temperature, the mullitization is not hindered for the sample Diac-1200. This is possible due to the high reactivity of the precursors during thermooxidative treatment. The thermo-oxidational degradation of polysiloxane in oxygen-containing atmospheres leads to the development of highly reactive amorphous SiO_2 [22,23,45]. Regarding the aluminum diacetate, the literature reports that its thermal oxidation results in reactive amorphous alumina at low temperature (~ 450 °C), which is converted into $\gamma\text{-Al}_2\text{O}_3$ at around 860 °C, followed by a phase transformation to $\alpha\text{-Al}_2\text{O}_3$ at 1150 °C [31]. Despite the fact that only Diac-1200 resulted in mullite phase during the calcination of the powders, all the prepared membranes originate mullite phase above 99% after sintering (Table 4.2). This is quite expected given the applied temperatures; however, it is important to stress that high-purity mullite was produced under reasonably shorter holding time (2 h) compared to traditional methods [46,47].

The membrane morphology in the phase-inversion process is dictated primarily by the composition of both the slurry and the precipitation bath. Since this study did not focus on evaluating different non-solvents, the morphology has to be explained in terms of slurry compo-

sition. In this regard, the main difference among the samples is the particle size of the mullite-based powder. It is well known that the particle has a direct influence on the rheology of the system [13,17]. Generally, when comparing similar ceramic slurries compositions, the particle size is found to be inversely proportional to slurry viscosity (see Figure 4.2 and Figure 4.10). However, the formation of finger-like voids (observed in the Alu-850 and Diac-1200 samples) is favored by reducing the viscosity of the system, intensifying the viscous fingering phenomena [48,49]. Diac-850 specimen only shows the skin-layer followed by the sponge-layer. This indicates that the viscosity threshold at which the finger-like structure can be completely suppressed was reached for the referred composition.

The average pore size distribution and open porosity displayed in Figure 4.5 clearly reflect the particle size and distribution of their respective precursor powders (Figure 4.2). As evident from these figures, the narrower the particle size distribution the narrower is the resultant pore size distribution. The same interpretation can be transferred to the average values of the particle and pore size [50]. With respect to the open porosity, the same trend can be inferred. Moreover, the Diac-850-1XXX samples possibly have an additional feature that led to a more pronounced reduction of open porosity, which is the implied higher reactivity compared to the other mullite-based powders. This hypothesis may be sustained by the XRD data in Figure 4.3, which can indicate a latent potential of the amorphous Diac-850 powder for reacting and/or sintering.

The evaluation of the mechanical properties of brittle materials normally requires plenty of caution, especially when dealing with porous ceramics. Therefore, Weibull analysis consists of a suitable method to analyze the mechanical performance of such components [51]. The degradation of the mechanical strength due to the presence of pores/porosity is well defined in the literature. Hence, pores are characterized as macrodefects in the ceramic structure. Nevertheless, it is worth mentioning that porosity has little effect on the bending strength if porosity is over 30% [52]. This is probably the main reason for the

higher flexural strength exhibited by Diac-850-1700 (σ_0 : 134 MPa; Open porosity: 33%). Another factor that perhaps impacted on this result could be related to Diac-850 morphology, in which the exclusive presence of sponge-layer configuration results in a more concise macrostructure than the finger-like layer [48,53].

As previously mentioned, Figure 4.7 illustrates the water permeation performance for selected asymmetric mullite membranes and a commercial symmetric borosilicate membrane (Por5). Taking into account the pore size and porosity displayed, it is possible to infer that both parameters have a direct influence on permeation flux. Nonetheless, this assumption is mostly valid if Por5 is not considered. When Por5 is compared to the prepared membranes, the aforementioned assumption does not sustain itself. Therefore, the asymmetric morphology is playing a major role in membrane performance, in which the porous support minimizes mass transport limitations [54–56]. Furthermore, the determined transport properties corroborates the superior performance of the asymmetric membranes, especially Diac-1200-1650, in which the clean membrane resistance (R_m) is almost one order of magnitude below the usual range given in literature for microfiltration membranes ($1 \times 10^{11} - 1 \times 10^{12} \text{ m}^{-1}$) [57,58].

4.5 Conclusions

Asymmetric mullite membranes in the microfiltration range were successfully prepared by phase-inversion tape casting. The mullite powder was produced by using polymethylsiloxane as silica precursor and aluminum diacetate as alumina source. Almost complete mullitization could be achieved after 3 h at 1200 °C from these precursors. There is a great potential in preparing high-purity mullite using polysiloxanes in combination with aluminum diacetate. The membrane morphology varied due to slurry viscosity, which depends on the ceramic particle size in this case. The increase in viscosity by using smaller mullite-based powder (Diac-850) suppressed the formation of finger-like layer. Nevertheless, samples prepared with Diac-1200 and Alu-850 exhibited a skin-

layer followed by a porous support composed by a mix of finger-like and sponge-like structures. Moreover, all membranes presented a pore size range on the skin-layer in the microfiltration range (0.4 – 2 μm). However, due to mechanical constraints and porosity some membranes were not suitable to be further characterized. Among the tested samples the Diac-1200-1650 specimen seems to be prospective to be applied in membrane technology, given its outstanding water flux and transport properties.

4.6 Acknowledgements

This study was financed in part by the Brazilian Coordination for the Improvement of Higher Education Personnel (CAPES) through the Brazilian-German Collaborative Research Initiative on Manufacturing (BRAGECRIM) Program. The German Research Foundation (DFG) as well as the Brazilian National Council for Scientific and Technological Development (CNPq) are also gratefully acknowledged. The authors thank Laura Luhede and Alexander Schulz at the Leibniz-Institut für Werkstofforientierte Technologien for helping with the measurement of the particle size and slurry viscosity, respectively. Wenhui Zhong is also acknowledged by performing water permeation tests.

4.7 Authors contributions

The article is mainly based on the work of the first author and author of this thesis Rafael Kenji Nishihora. The precise contributions of each author are listed below.

Table 4.4: Authors contributions for Chapter 4.

Author	Contribution
Nishihora, R. K.	Conceptualized the work, performed and analyzed the experiments, wrote the manuscript
Rudolph, E.	Performed and analyzed the experiments, helped in the scientific evaluation and editing of the manuscript
Quadri, M. G. N.	Gave conceptual and scientific advices, helped in the scientific

	evaluation and editing of the manuscript
Hotza, D.	Gave conceptual and scientific advices, helped in the scientific evaluation and editing of the manuscript
Rezwan, K.	Gave conceptual and scientific advices, helped in the scientific evaluation and editing of the manuscript
Wilhelm, M.	Gave conceptual and scientific advices, helped in the scientific evaluation and editing of the manuscript

4.8 References

- [1] S. Benfer, P. Árki, G. Tomandl, Ceramic membranes for filtration applications — preparation and characterization, *Adv. Eng. Mater.* 6 (2004) 495–500. doi:10.1002/adem.200400577.
- [2] S. Luque, D. Gómez, J.R. Álvarez, Industrial applications of porous ceramic membranes (pressure-driven processes), *Membr. Sci. Technol.* 13 (2008) 177–216. doi:10.1016/S0927-5193(07)13006-0.
- [3] D. da Silva Biron, V. dos Santos, M. Zeni, *Ceramic Membranes Applied in Separation Processes*, 2018. doi:10.1007/978-3-319-58604-5.
- [4] H. Fang, C. Ren, Y. Liu, D. Lu, L. Winnubst, C. Chen, Phase-inversion tape casting and synchrotron-radiation computed tomography analysis of porous alumina, *J. Eur. Ceram. Soc.* 33 (2013) 2049–2051. doi:http://dx.doi.org/10.1016/j.jeurceramsoc.2013.02.032.
- [5] W. He, H. Huang, J. fen Gao, L. Winnubst, C. sheng Chen, Phase-inversion tape casting and oxygen permeation properties of supported ceramic membranes, *J. Memb. Sci.* 452 (2014) 294–299. doi:10.1016/j.memsci.2013.09.063.
- [6] R.H. Yuan, W. He, Y. Zhang, J.F. Gao, C.S. Chen, Preparation and characterization of supported planar Zr_{0.84}Y_{0.16}O_{1.92}-La_{0.8}Sr_{0.2}Cr_{0.5}Fe_{0.5}O_{3-δ} composite membrane, *J. Memb. Sci.* 499 (2016) 335–342. doi:10.1016/j.memsci.2015.10.066.
- [7] J. Gu, C. Ren, X. Zong, C. Chen, L. Winnubst, Preparation of alumina membranes comprising a thin separation layer and a

- support with straight open pores for water desalination, *Ceram. Int.* 42 (2016) 12427–12434.
doi:<http://dx.doi.org/10.1016/j.ceramint.2016.04.183>.
- [8] J. Gao, X. Meng, T. Luo, H. Wu, Z. Zhan, Symmetrical solid oxide fuel cells fabricated by phase inversion tape casting with impregnated SrFe 0.75 Mo 0.25 O 3- δ (SFMO) electrodes, *Int. J. Hydrogen Energy.* (2017) 3–7.
doi:10.1016/j.ijhydene.2017.03.205.
- [9] Y. Meng, W. He, X. Li, J. Gao, Z. Zhan, J. Yi, C. Chen, H.J.M. Bouwmeester, Asymmetric La 0.6 Sr 0.4 Co 0.2 Fe 0.8 O 3- δ membrane with reduced concentration polarization prepared by phase-inversion tape casting and warm pressing, *J. Memb. Sci.* 533 (2017) 11–18. doi:10.1016/j.memsci.2017.03.025.
- [10] R.K. Nishihora, P.L. Rachadel, M.G.N. Quadri, D. Hotza, Manufacturing porous ceramic materials by tape casting-A review, *J. Eur. Ceram. Soc.* 38 (2018) 988–1001.
doi:10.1016/j.jeurceramsoc.2017.11.047.
- [11] E. Drioli, L. Giorno, *Comprehensive Membrane Science and Engineering*, Elsevier, 2010.
- [12] N. Yang, X. Tan, Z. Ma, A phase inversion/sintering process to fabricate nickel/yttria-stabilized zirconia hollow fibers as the anode support for micro-tubular solid oxide fuel cells, *J. Power Sources.* 183 (2008) 14–19.
doi:<http://dx.doi.org/10.1016/j.jpowsour.2008.05.006>.
- [13] S.K. Hubadillah, Z. Harun, M.H.D. Othman, A.F. Ismail, W.N.W. Salleh, H. Basri, M.Z. Yunus, P. Gani, Preparation and characterization of low cost porous ceramic membrane support from kaolin using phase inversion/sintering technique for gas separation: Effect of kaolin content and non-solvent coagulant bath, *Chem. Eng. Res. Des.* 112 (2016) 24–35.
doi:10.1016/j.cherd.2016.06.007.
- [14] D.D. Athayde, D.F. Souza, A.M.A. Silva, D. Vasconcelos, E.H.M. Nunes, J.C. Diniz da Costa, W.L. Vasconcelos, Review of perovskite ceramic synthesis and membrane preparation meth-

- ods, *Ceram. Int.* 42 (2016) 6555–6571.
doi:<http://dx.doi.org/10.1016/j.ceramint.2016.01.130>.
- [15] N. Hilal, A.F. Ismail, C. Wright, *Membrane Fabrication*, CRC Press, 2015.
- [16] H.P. Hsieh, *Inorganic Membranes for Separation and Reaction*, Elsevier Science, 1996.
- [17] S.K. Hubadillah, Z. Harun, M.H.D. Othman, A.F. Ismail, P. Gani, Effect of kaolin particle size and loading on the characteristics of kaolin ceramic support prepared via phase inversion technique, *J. Asian Ceram. Soc.* 4 (2016) 164–177.
doi:[10.1016/j.jascer.2016.02.002](https://doi.org/10.1016/j.jascer.2016.02.002).
- [18] G.R. Guillen, Y. Pan, M. Li, E.M. V Hoek, Preparation and characterization of membranes formed by nonsolvent induced phase separation: A review, *Ind. Eng. Chem. Res.* 50 (2011) 3798–3817. doi:[10.1021/ie101928r](https://doi.org/10.1021/ie101928r).
- [19] R.F. Davis, J.A. Pask, Mullite, in: *Refract. Glas. Glas. Ceram. - High Temp. Oxides, Part IV*, 1971: pp. 37–76. doi:[10.1016/B978-0-12-053304-6.50011-4](https://doi.org/10.1016/B978-0-12-053304-6.50011-4).
- [20] H. Schneider, J. Schreuer, B. Hildmann, Structure and properties of mullite-A review, *J. Eur. Ceram. Soc.* 28 (2008) 329–344.
doi:[10.1016/j.jeurceramsoc.2007.03.017](https://doi.org/10.1016/j.jeurceramsoc.2007.03.017).
- [21] M.F. Serra, M.S. Conconi, M.R. Gauna, G. Suárez, E.F. Aglietti, N.M. Rendtorff, Mullite ($3\text{Al}_2\text{O}_3 \cdot 2\text{SiO}_2$) ceramics obtained by reaction sintering of rice husk ash and alumina, phase evolution, sintering and microstructure, *J. Asian Ceram. Soc.* 4 (2016) 61–67. doi:[10.1016/j.jascer.2015.11.003](https://doi.org/10.1016/j.jascer.2015.11.003).
- [22] D. Suttor, H.-J. Kleebe, G. Ziegler, Formation of Mullite from Filled Siloxanes, *J. Am. Ceram. Soc.* 80 (1997) 2541–2548.
doi:[10.1111/j.1151-2916.1997.tb03156.x](https://doi.org/10.1111/j.1151-2916.1997.tb03156.x).
- [23] E. Bernardo, P. Colombo, E. Pippel, J. Woltersdorf, Novel mullite synthesis based on alumina nanoparticles and a preceramic polymer, *J. Am. Ceram. Soc.* 89 (2006) 1577–1583.
doi:[10.1111/j.1551-2916.2006.00963.x](https://doi.org/10.1111/j.1551-2916.2006.00963.x).

- [24] L. Li, M. Chen, Y. Dong, X. Dong, S. Cerneaux, S. Hampshire, J. Cao, L. Zhu, Z. Zhu, J. Liu, A low-cost alumina-mullite composite hollow fiber ceramic membrane fabricated via phase-inversion and sintering method, *J. Eur. Ceram. Soc.* 36 (2015) 2057–2066. doi:10.1016/j.jeurceramsoc.2016.02.020.
- [25] J. Cao, X. Dong, L. Li, Y. Dong, S. Hampshire, Recycling of waste fly ash for production of porous mullite ceramic membrane supports with increased porosity, *J. Eur. Ceram. Soc.* 34 (2014) 3181–3194. doi:10.1016/j.jeurceramsoc.2014.04.011.
- [26] M. Chen, L. Zhu, Y. Dong, L. Li, J. Liu, Waste-to-Resource Strategy to Fabricate Highly Porous Whisker-Structured Mullite Ceramic Membrane for Simulated Oil-in-Water Emulsion Wastewater Treatment, *ACS Sustain. Chem. Eng.* 4 (2016) 2098–2106. doi:10.1021/acssuschemeng.5b01519.
- [27] Z. Cuo, H. Liu, F. Zhao, W. Li, S. Peng, Y. Chen, Highly porous fibrous mullite ceramic membrane with interconnected pores for high performance dust removal, *Ceram. Int.* 44 (2018) 11778–11782. doi:10.1016/j.ceramint.2018.03.259.
- [28] S.K. Hubadillah, M.H.D. Othman, T. Matsuura, A.F. Ismail, M.A. Rahman, Z. Harun, J. Jaafar, M. Nomura, Fabrications and applications of low cost ceramic membrane from kaolin: A comprehensive review, *Ceram. Int.* 44 (2018) 4538–4560. doi:10.1016/j.ceramint.2017.12.215.
- [29] Z. Hou, B. Cui, L. Liu, Q. Liu, Effect of the different additives on the fabrication of porous kaolin-based mullite ceramics, *Ceram. Int.* 42 (2016) 17254–17258. doi:10.1016/j.ceramint.2016.08.020.
- [30] J. Ma, F. Ye, B. Zhang, Y. Jin, C. Yang, J. Ding, H. Zhang, Q. Liu, Low-temperature synthesis of highly porous whisker-structured mullite ceramic from kaolin, *Ceram. Int.* 44 (2018) 13320–13327. doi:10.1016/j.ceramint.2018.04.163.
- [31] R.R. Menezes, E. Fagury-Neto, M.C. Fernandes, P.M. Souto, R.H.G. a. Kiminami, Obtenção de mullita porosa a partir da sílica da casca de arroz e do acetato de alumínio, *Cerâmica*. 54 (2008) 245–252. doi:10.1590/S0366-69132008000200015.

- [32] C.A. Schneider, W.S. Rasband, K.W. Eliceiri, NIH Image to ImageJ: 25 years of image analysis, *Nat. Methods.* 9 (2012) 671–675. doi:10.1038/nmeth.2089.
- [33] L. Lutterotti, M. Bortolotti, G. Ischia, I. Lonardelli, H.R. Wenk, Rietveld texture analysis from diffraction images, *Zeitschrift Für Krist. Suppl.* 2007 (2007) 125–130. doi:10.1524/zksu.2007.2007.suppl_26.125.
- [34] L. Lutterotti, MAUD - Materials Analysis Using Diffraction, (2019). <http://maud.radiographema.eu/>.
- [35] S. Gražulis, A. Daškevič, A. Merkys, D. Chateigner, L. Lutterotti, M. Quirós, N.R. Serebryanaya, P. Moeck, R.T. Downs, A. LeBail, Crystallography Open Database (COD): an open-access collection of crystal structures and platform for world-wide collaboration, *Nucleic Acids Res.* 40 (2012) D420–D427. doi:10.1093/nar/gkr900.
- [36] COD - Crystallography Open Database, (2019). <http://www.crystallography.net/cod/index.php>.
- [37] D.E. 843-1, Advanced technical ceramics - Mechanical properties of monolithic ceramics at room temperature - Part 1: Determination of flexural strength, Beuth. (2006).
- [38] F.H. Liu, Y.S. Liao, Fabrication of inner complex ceramic parts by selective laser gelling, *J. Eur. Ceram. Soc.* 30 (2010) 3283–3289. doi:10.1016/j.jeurceramsoc.2010.08.001.
- [39] F. Dogan, J. Feng, L.G. Ferguson, Method for sintering ceramic tapes, 6447712, 2002. <http://www.freepatentsonline.com/6447712.html>.
- [40] Z. Nakagawa, T. Aosaki, N. Enomoto, Crystallization process of amorphous aluminas to α -alumina, *Mater. Sci. Eng. Serv. Soc.* (1998) 52–55. doi:10.1016/B978-044482793-7/50015-1.
- [41] I.G. Polyakova, 4. The Main Silica Phases and Some of Their Properties, in: J.W.P. Schmelzer (Ed.), *Glas. Sel. Prop. Cryst.*, De Gruyter, Berlin, Boston, 2014: pp. 197–268. doi:10.1515/9783110298581.197.

- [42] J.H. She, T. Ohji, Porous mullite ceramics with high strength, *J. Mater. Sci. Lett.* 21 (2002) 1833–1834.
doi:10.1023/A:1021576104859.
- [43] Y. Dong, J. er Zhou, B. Lin, Y. Wang, S. Wang, L. Miao, Y. Lang, X. Liu, G. Meng, Reaction-sintered porous mineral-based mullite ceramic membrane supports made from recycled materials, *J. Hazard. Mater.* 172 (2009) 180–186.
doi:10.1016/j.jhazmat.2009.06.148.
- [44] K. Hua, A. Shui, L. Xu, K. Zhao, Q. Zhou, X. Xi, Fabrication and characterization of anorthite-mullite-corundum porous ceramics from construction waste, *Ceram. Int.* 42 (2016) 6080–6087.
doi:10.1016/j.ceramint.2015.12.165.
- [45] B. V Manoj Kumar, Y.-W. Kim, Processing of polysiloxane-derived porous ceramics: a review, *Sci. Technol. Adv. Mater.* 11 (2010) 44303. doi:10.1088/1468-6996/11/4/044303.
- [46] M.D. Sacks, J.A. Pask, Sintering of Mullite-Containing Materials: II, Effect of Agglomeration, *J. Am. Ceram. Soc.* 65 (1982) 70–77. doi:10.1111/j.1151-2916.1982.tb10360.x.
- [47] L. Montanaro, J.M. Tulliani, C. Perrot, A. Negro, Sintering of industrial mullites, *J. Eur. Ceram. Soc.* 17 (1997) 1715–1723.
doi:10.1016/S0955-2219(97)00043-5.
- [48] B.F.K. Kingsbury, K. Li, A morphological study of ceramic hollow fibre membranes, *J. Memb. Sci.* 328 (2009) 134–140.
doi:10.1016/j.memsci.2008.11.050.
- [49] B. Wang, Z. Lai, Finger-like voids induced by viscous fingering during phase inversion of alumina/PES/NMP suspensions, *J. Memb. Sci.* 405–406 (2012) 275–283.
doi:10.1016/j.memsci.2012.03.020.
- [50] N. Das, H.S. Maiti, Effect of Size Distribution of the Starting Powder on the Pore Size and its Distribution of Tape Cast Alumina Microporous Membranes, *J. Eur. Ceram. Soc.* 19 (1999) 341–345. doi:http://dx.doi.org/10.1016/S0955-2219(98)00205-2.
- [51] R. Danzer, P. Supancic, J. Pascual, T. Lube, Fracture statistics of ceramics - Weibull statistics and deviations from Weibull statis-

- tics, *Eng. Fract. Mech.* 74 (2007) 2919–2932.
doi:10.1016/j.engfracmech.2006.05.028.
- [52] Q. Chang, Y. Yang, X. Zhang, Y. Wang, J. Zhou, X. Wang, S. Cerneaux, L. Zhu, Y. Dong, Effect of particle size distribution of raw powders on pore size distribution and bending strength of Al₂O₃ microfiltration membrane supports, *J. Eur. Ceram. Soc.* 34 (2014) 3819–3825.
doi:<http://dx.doi.org/10.1016/j.jeurceramsoc.2014.06.001>.
- [53] Z. Wu, B. Wang, K. Li, A novel dual-layer ceramic hollow fibre membrane reactor for methane conversion, *J. Memb. Sci.* 352 (2010) 63–70. doi:10.1016/j.memsci.2010.01.062.
- [54] M. Kukizaki, M. Goto, Preparation and characterization of a new asymmetric type of Shirasu porous glass (SPG) membrane used for membrane emulsification, *J. Memb. Sci.* 299 (2007) 190–199. doi:10.1016/j.memsci.2007.04.040.
- [55] X. Chang, C. Zhang, Y. He, X. Dong, W. Jing, N. Xu, A Comparative Study of the Performance of Symmetric and Asymmetric Mixed-conducting Membranes, *Chinese J. Chem. Eng.* 17 (2009) 562–570. doi:10.1016/S1004-9541(08)60245-1.
- [56] L. Chen, L. Liu, J. Xue, L. Zhuang, H. Wang, Asymmetric membrane structure: An efficient approach to enhance hydrogen separation performance, *Sep. Purif. Technol.* 207 (2018) 363–369. doi:10.1016/j.seppur.2018.06.066.
- [57] M. Li, Y. Zhao, S. Zhou, W. Xing, F.S. Wong, Resistance analysis for ceramic membrane microfiltration of raw soy sauce, *J. Memb. Sci.* 299 (2007) 122–129. doi:10.1016/j.memsci.2007.04.033.
- [58] M.M. Benjamin, D.F. Lawler, *Water Quality Engineering: Physical / Chemical Treatment Processes*, Wiley, 2013.

4.9 Supplementary material

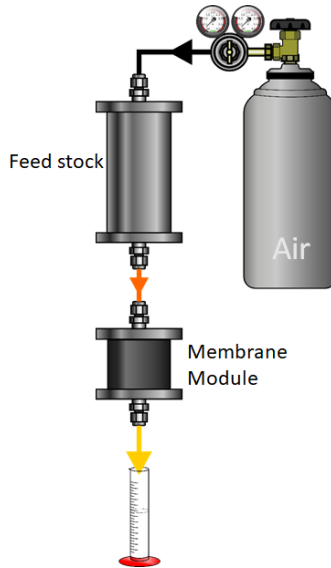


Figure 4.8: Scheme of the water permeability and membrane emulsification setup.

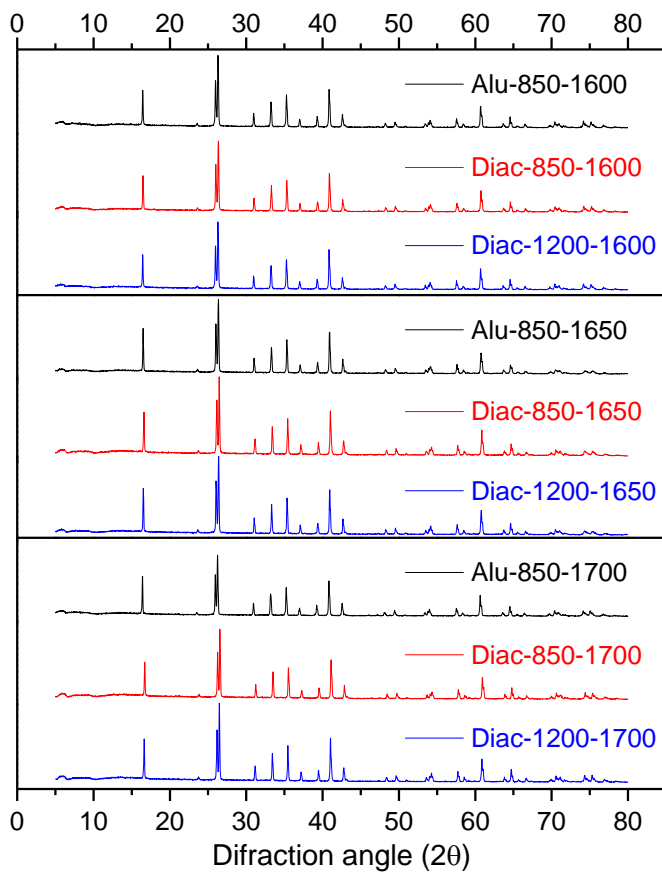


Figure 4.9: XRD and Rietveld Refinement of the sintered membranes (Mullite-COD ID 2310785; Corundum-COD ID 2300448; Cristobalite-COD ID 9001579.).

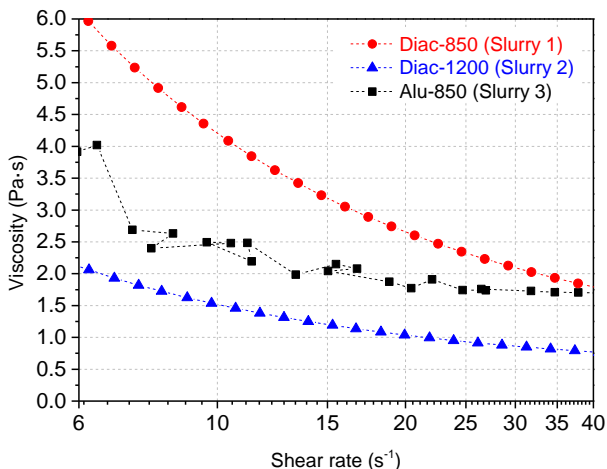


Figure 4.10: Viscosity curves of the prepared slurries.

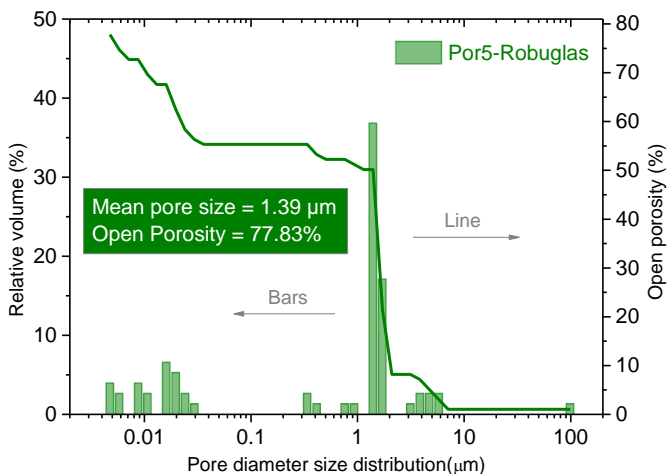


Figure 4.11: Pore size distribution and open porosity obtained from Hg-porosimetry of a commercial borosilicate membrane – Por5 from Robuglas (Company information: 1 – 1.6 μm by ISO 4793-80, and 0.9 – 1.4 μm by ASTM E128-99/ Available on: <https://www.robuglas.com/en/service/poresizes.html>).

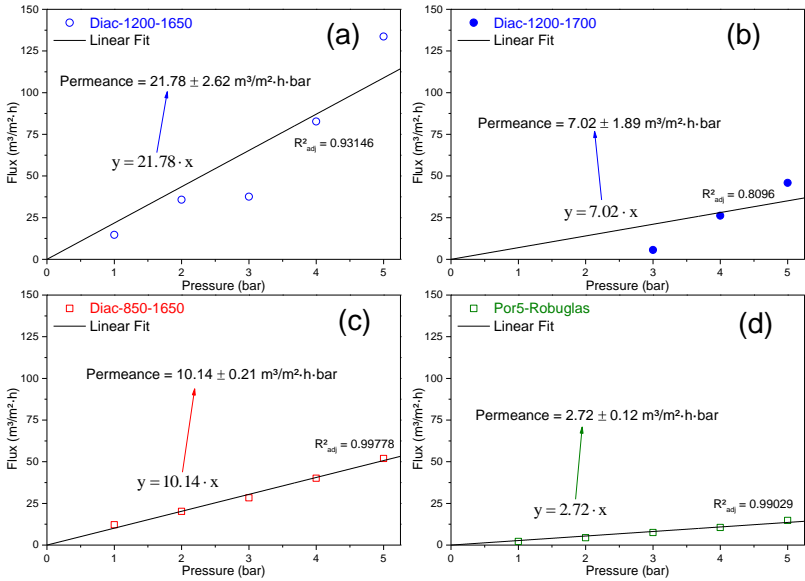


Figure 4.12: Determination of the permeance ($\text{m}^3/\text{m}^2 \cdot \text{h} \cdot \text{bar}$) of selected sintered membranes based on the pure water flux measurements as a function of the applied transmembrane pressure.

Assuming that Darcy's Law is valid and considering that the permeance (k_w) in pressure-driven membrane processes is given by the flux (J) per unit pressure (P), we can define k_w as follows [1]:

$$k_w = \frac{J}{\Delta P}$$

Additionally, the clean membrane resistance (R_m) can be written as

$$R_m = \frac{\Delta P}{\mu \cdot J}$$

where μ is the dynamic viscosity of the clean water at the testing temperature (25 °C in our studies; 0.00089 Pa·s). Taking into account k_w expression, the membrane resistance can be re-written as

$$R_m = \frac{l}{\mu \cdot k_w}$$

Furthermore, the membrane permeability in terms of the intrinsic permeability ($k_{v,intr}$) can be approximated according to the following equation:

$$k_{v,intr} = \frac{\mu \cdot J}{\Delta P / \delta_m} \equiv \left(\frac{R_m}{\delta_m} \right)^{-1}$$

Reference:

- [1] M.M. Benjamin, D.F. Lawler, Water Quality Engineering: Physical / Chemical Treatment Processes, Wiley, 2013.

5 Premix membrane emulsification using flat ceramic membranes with tailored structure and composition⁴

Uniform oil-in-water emulsions were prepared using MCT (medium-chain fatty acid triglyceride, 10 wt.%) as the oily dispersed phase and polysorbate 80 as the surfactant (1 wt.%). The emulsification process was performed via premix membrane emulsification (PME) using 3 flat microfiltration ceramic membranes with different mean pore sizes (d_m): Por5 (symmetric, commercial, d_m : 1.39 μm); SiOC (symmetric manufactured, d_m : 1.76 μm); and mullite (asymmetric, manufactured, $d_{m\text{-top-layer}}$: 1.18 μm). The droplets size and their distribution varied according to the membrane type and number of permeation cycles (up to a limit of 2 passes). All prepared emulsions presented a tendency to monomodal droplet distribution with span values in the range of 0.82–0.97. The coarse emulsion (premix) droplets were reduced from 6.30 to 4.57–2.22 μm . The asymmetric membrane (mullite) exhibited the highest permeation fluxes for both water ($43.1 \times 10^{-3} \text{ m}^3/\text{m}^2 \cdot \text{s}$) and premix (Pass-1: $4.6 \times 10^{-3} \text{ m}^3/\text{m}^2 \cdot \text{s}$; Pass-2: $5.3 \times 10^{-3} \text{ m}^3/\text{m}^2 \cdot \text{s}$), still maintaining satisfactory emulsification results.

5.1 Introduction

A simple emulsion system consists of a mixture of two immiscible liquid phases. The major component of such a mixture is called the continuous phase, and the minor one is the dispersed phase [1]. Emulsions have an important role in cosmetics, pharmaceuticals, paints, as well as in chemical, petrochemical, and food products [2,3]. Even though there are plenty of techniques already established in the lab and industrial scale to prepare emulsified systems, they still present some technological issues. For instance, conventional emulsification devices, such as colloid mills and dispersing machines, consume low energy but produce polydispersed emulsions. On the other hand, high-pressure homogenizers generate monodispersed emulsions at the expense of high-energy consumption [3–5]. To overcome the operational limita-

⁴ Based on a paper to be submitted for publication.

tions from the aforementioned devices, the technology of membrane emulsification (ME) has been attracting great attention as a sustainable and efficient alternative [6,7].

The primary features of membrane emulsification include: (i) production of uniform particles with a narrow size distribution, (ii) low shear stress, (iii) low energy requirement, (iv) tailoring of droplet size by the proper selection of the membrane, and (v) operational flexibility and simplicity [8].

There are two main ME processes: direct or cross-flow, and premix membrane emulsification (PME). In the direct membrane emulsification (DME), an applied pressure forces the to-be-dispersed phase through the porous structure of a membrane into the cross-flowing continuous phase, which can contain stabilizers (e.g. surfactants) [9,10]. The PME method starts with a coarse emulsion, which is pushed through a membrane to produce a finer emulsion [11]. The premix process may be preferred over cross-flow given its main advantages, such as smaller mean droplet sizes, simpler experimental set-up, and easier process control [12]. One of the major disadvantages in PME is the polydispersity compared to DME, which normally can be overcome by increasing the number of cycles or passes through the membrane [13].

Several parameters are involved in PME process; however, the literature emphasizes especially the transmembrane pressure, disperse phase fraction, stabilizers, continuous phase viscosity, number of homogenizing cycles, and membrane properties [11]. Among membrane properties, we can highlight pore size (and distribution), porosity, interconnectivity, and material class (polymeric, metallic, or ceramic) [6].

There is an increasing interest in applying ceramic membranes as an alternative to the conventional metallic sieves and polymeric membranes. This is mainly due to the chemical and structural stability intrinsic from ceramic materials [14]. Most of the efforts regarding the use ceramic membranes in ME processes involve the so-called Shirasu Porous Glass (SPG) membranes, due to their narrow pore size range [15,16]. Later in this work, Table 5.2 provides an overview of the main

studies concerning PME of oil-in-water emulsions using ceramic membranes in a dead-end configuration.

Therefore, this work aims to address the still current lack of studies with respect to the application of a larger variety of ceramic membranes in the ME process. With this in mind, we present a systematic investigation evaluating the feasibility of producing oil-in-water emulsions by PME, using three distinct microfiltration flat ceramic membranes. The influence of process parameters on the mean droplet size, size distribution, and permeation flux are evaluated.

5.2 Experimental

5.2.1 Chemicals and membranes

The emulsions were prepared with a medium-chain triglycerides oil (MCT, viscosity = 290 mPa·s at 200 s⁻¹ and 20 °C, density = 952 kg/m³, refractive index = 1.450) as dispersed phase. A non-ionic surfactant was added to the continuous aqueous phase (polysorbate 80, Tween[®] 80, Sigma-Aldrich). The membranes used in the experiments are summarized in Table 5.1.

Table 5.1: Main characteristics and additional remarks of the membranes used in the premix emulsification experiments.

Membrane	Main characteristics and additional remarks	Ref
Por2	Commercial support structure for the other membranes; Pore size range: 40 – 100 μm; symmetrical structure	[17,18]
Por4	Commercial membrane applied in the coarse premix preparation; Pore size range: 10 – 16 μm; symmetrical structure	[17,18]
Por5	Commercial membrane applied in the premix emulsification; Pore size range: 1 – 1.6 μm; symmetrical structure	[17,18]
SiOC	Synthesized membrane applied in the premix emulsification; Mean pore size: 1.76 μm ; symmetrical structure	[19]
Mullite	Synthesized membrane applied in the premix emulsification; Pore size _{skin-layer} : 1.18 ± 0.8 μm; asymmetrical structure	[20]

In order to prepare a more stable premix, a commercially available glass membrane was used (Por4, Robu Glasfilter-Geräte) with pore size of 10 – 16 μm , according to ISO 4793-80 (Figure 5.10, section 5.8) [17,18]. For the premix emulsification tests, three flat ceramic membranes with 10 mm of diameter and ~ 1.0 mm of thickness were studied. However, the effective selective layer (top/skin-layer) of the asymmetric mullite membrane has a thickness of 6.11 μm [20]. The commercially available membranes (Por2, Por4, and Por5, Robu Glasfilter-Geräte) consist of a symmetric structure made of sintered non-spherical fragmented borosilicate glass (80.6% SiO_2 , 12.6% B_2O_3 , 4.2% Na_2O , 2.2% Al_2O_3 , 0.29% others, by weight). According to the supplier, Por5 presents a pore size in the range of 1 – 1.6 μm (ISO 4793-80) [17, 18]. The other two membranes were prepared in previous studies in our group. The symmetric SiOC membrane and the asymmetric mullite membrane have been further described and characterized in previous studies [19, 20], in which they are referred to as “SiC_{6.5}-A30-1000” and “Diac-1200-1650”, respectively. The support structure (Por2, Robus Glasfilter-Geräte GmbH, as indicated in the Figure 5.1) presents a coarse pore size distribution (40 – 100 μm , ISO 4793-80; Figure 5.10, section 5.8) [17] and has the same composition as Por4 and Por5. Preliminary tests showed that the support (Por2) has no influence on the permeation and emulsification experiments (see Figure 5.11, section 5.8).

5.2.2 Premix preparation

The premix was prepared by mixing 1 wt.% polysorbate 80 in 89 wt.% of bidistilled water for 2 min in a magnetic stirrer (200 rpm, ~ 25 °C). Then, 10 wt.% of MCT oil was added and dispersed by a rotor-stator device (IKAs T18 basic Ultraturrax), applying a constant rotation speed of 3600 min^{-1} for 30 s. Subsequently, the obtained mixture was passed once through the Por4 glass membrane at 6 bar using the setup displayed in Figure 5.1 (see APPENDIX A.2 for a 3D representation of the membrane module) to produce a less unstable coarse premix.

5.2.3 Membrane permeation flux and premix emulsification tests

For the water permeation and premix emulsification experiments, a testing dead-end device was used as schematically shown in Figure 5.1. The silicone displayed in Figure 5.1 was prepared using a commercial silicone elastomer (Sylgard® 184, Dow Corning), which successfully provided the side sealing of the membrane. Due to mechanical and flux constraints observed during experimental tests, all the experiments comparing the three membranes were performed at a fixed pressure of 5 bar. The permeation flux was calculated according to Darcy's Law:

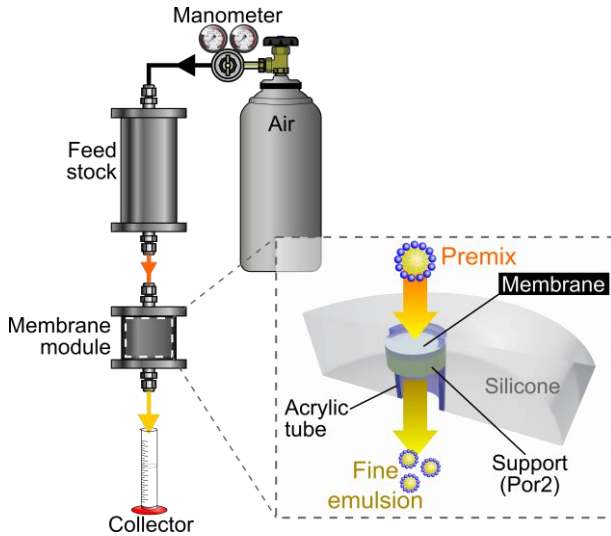


Figure 5.1: Schematic representation of the membrane permeation flux and emulsification setup (adapted from [20]).

$$J = \frac{1}{A} \cdot \frac{dV}{dt} \quad \text{Equation 5.1}$$

where J is the membrane permeation flux ($\text{m}^3/\text{m}^2 \cdot \text{s}$), A is the effective transverse area of the ceramic membrane (m^2), dV and dt represent the variation in permeated volume (m^3) and time (s), respectively.

For the emulsification tests, the collected permeated premix went through the membranes for two times (without cleaning in between), which represents the number of passes necessary to have no changes on droplet size.

5.2.4 Membrane and emulsion characterization

The morphology of the membranes was analyzed by scanning electron microscopy (SEM, 20 kV; Series 2, Obducat CamScan). For this purpose, the samples were sputtered with gold (K550, Emitech, Judges Scientific). Porosity and pore size distribution of the membranes were determined using mercury intrusion porosimetry (Pascal 140/440, Porotec). Due to the asymmetric morphology of the mullite membrane, the SEM surface micrograph of the top layer was examined by image analysis (ImageJ software). Hydrophobicity and hydrophilicity were investigated by measuring water and n-heptane vapor adsorption. For this purpose, vessels with ~0.4 g of sample powder (particle sizes $\leq 300 \mu\text{m}$) were placed inside closed Erlenmeyer flasks filled with the solvent at equilibrium with its vapor phase at room temperature (~22 °C). Samples were weighted at the start and end of a 24 h measurement period to determine the vapor uptake of the material. Afterwards, the uptake was recalculated into mmol of solvent per square meter using the specific surface area of the materials.

The droplet size and distribution of the emulsions and premix were measured by a laser particle size analyzer (Horiba LA-960). The continuous phase was distilled water with a refractive index of 1.333. The width of the droplet size distribution is given by the span value defined as:

$$\text{span} = \frac{d_{90} - d_{10}}{d_{50}} \quad \text{Equation 5.2}$$

where d_x is the diameter corresponding to x vol.% on a relative cumulative droplet size distribution curve. All measurements were done in triplicate; the values reported are the average of three measurements.

5.3 Results and discussion

5.3.1 Membrane characteristics

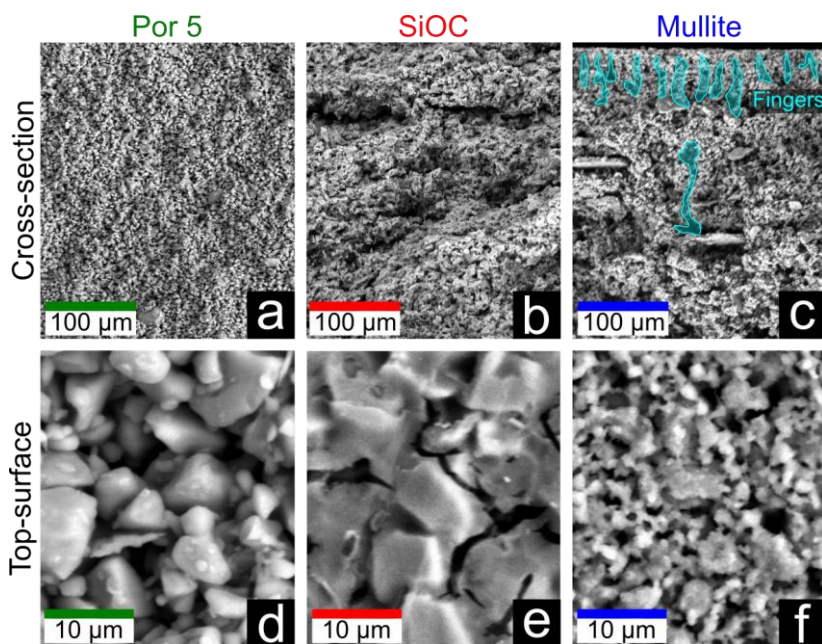


Figure 5.2: Cross-section and top surface SEM images of the symmetric membranes (a,d) Por5 and (b,e) SiOC (the image presented in “b” was adapted from [19]), and the asymmetric Mullite membrane (c,f).

The morphology of the cross-section and top surface of the ceramic membranes are depicted in Figure 5.2. The commercial membrane Por5 exhibits a very homogenous inner arrangement (Figure 5.2a) with irregular pore shapes due to the non-spherical fragmented borosilicate glass (Figure 5.2d) that composes its structure. SiOC membrane seems to present a uniform distribution of spherical pores accompanied by some cracks in the cross-section (Figure 5.2b). On the other hand, the top surface displays irregular pores mostly in a crack-like shape, probably as a result of the gas release during pyrolysis [20]. The asymmetric mullite membrane (see Figure 5.2c) consists of a top-layer with a thick-

ness around 6 μm followed by support layer that is composed of a small portion of a finger-like structure (highlighted in light blue) and majorly a sponge-like layer. The top surface (Figure 5.2f) shows a quite homogeneous pore distribution, where the pores mostly exhibit a spherical shape, inherent of rounded sintered particles.

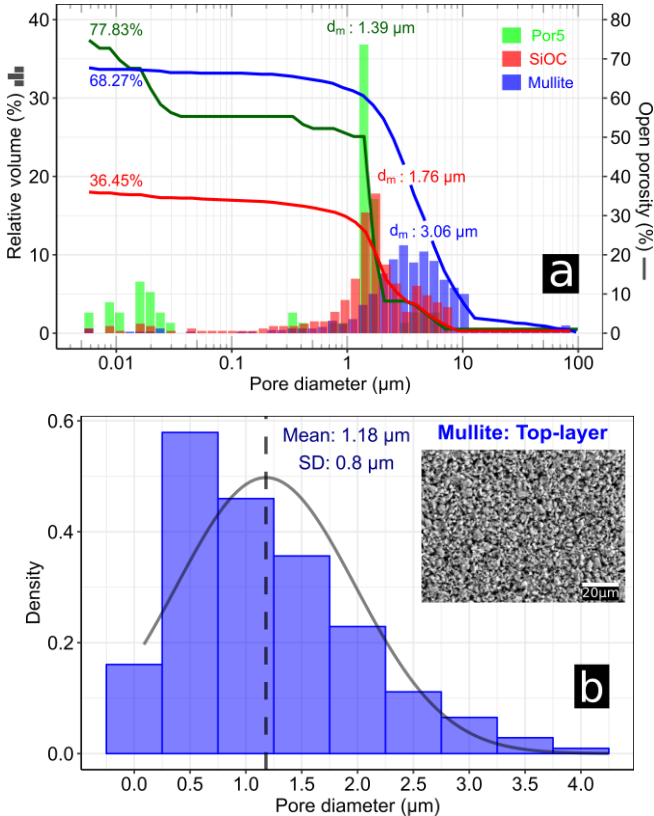


Figure 5.3: (a) Pore size distribution versus relative pore volume (bars) and open porosity curves (lines) measured by Hg-porosimetry (the data referred to SiOC and mullite were adapted from [19] and [20], respectively). (b) Pore size distribution of the skin-layer of the mullite asymmetric membrane obtained from an SEM image analyzed by ImageJ software.

Figure 5.3a displays the pore diameter distribution (μm) and open porosity (%) of the studied membranes. All analyzed samples show a pore diameter on the microfiltration range ($0.1 - 5 \mu\text{m}$). The Hg-intrusion analysis of the symmetric membranes reveals a similar mean pore size (d_m), in which Por5 exhibits the smallest value of $1.39 \mu\text{m}$ while SiOC has $1.76 \mu\text{m}$. Despite the mentioned similarity, Por5 presents the narrowest distribution and more than the double of open porosity (77.83%) when compared to the SiOC membrane (36.45%). The mullite asymmetric membrane presents the highest mean pore size ($3.06 \mu\text{m}$), the widest distribution, and a considerable open porosity (68.27%). These results reflect the great variation in the pore structure visualized in the support layer of the mullite membrane (Figure 5.2c). Nevertheless, when analyzing the top surface (skin-layer) of this asymmetric membrane (Figure 5.3b), the pore size range ($1.2 \pm 0.8 \mu\text{m}$) is comparable to the main peaks exhibited by the other two membranes.

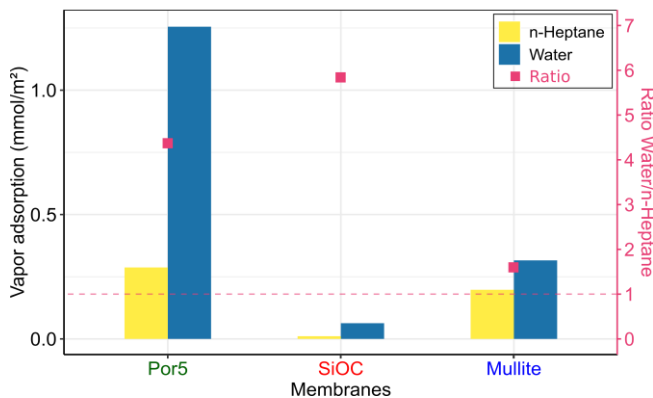


Figure 5.4: Surface hydrophilicity-hydrophobicity measured by water and n-heptane vapor adsorption analysis of the ceramic membranes at $25 \text{ }^\circ\text{C}$ (the data correspondent to SiOC sample was extracted from [19]).

The surface characteristics (hydrophilicity-hydrophobicity) of the membranes were accessed by the vapor adsorption of a non-polar (n-heptane) and a polar (water) solvent (Figure 5.4). Despite the differences in the magnitude of water and n-heptane uptake (mmol/m^2), all mem-

branes are hydrophilic (ratio > 1). The hydrophilic nature is inherent to the oxide ceramic materials [22]. Unexpectedly, the SiOC membranes present the most elevated water by n-heptane ratio (5.84) among the tested membranes (Por5 = 4.37; Mullite = 1.60). Notwithstanding the presence of carbon and SiC domains in their structure, the hydrophilicity is presumed to be due to the hydrophilic amorphous SiO₂-rich nanodomains that are accessed by the water vapor molecules [23,24].

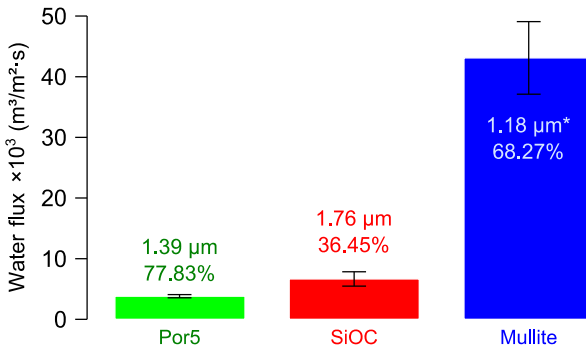


Figure 5.5: Water permeation flux of the ceramic membranes at a fixed pressure of 5 bar in a dead-end configuration (the data correspondent to Por5 was extracted from [20]; values showed inside the graph correspond to average pore size (μm) and open porosity (%); value signed with “*” was determined by image analysis from SEM pictures of the top surface, and values without marker were obtained from Hg-porosimetry).

The water permeation flux through the ceramic membranes at a fixed transmembrane pressure of 5 bar is depicted in Figure 5.5. As one may expect, the asymmetric membrane (mullite) shows the most expressive water permeation performance ($43.1 \times 10^{-3} \pm 6.0 \times 10^{-3} \text{ m}^3/\text{m}^2 \cdot \text{s}$). The asymmetric morphology minimizes the hydraulic resistance, hence resulting in higher flux against symmetric structures [25]. Concerning the symmetric membranes, the SiOC sample ($6.7 \times 10^{-3} \pm 1.2 \times 10^{-3} \text{ m}^3/\text{m}^2 \cdot \text{s}$) presents almost two times the performance of Por5 ($3.8 \times 10^{-3} \pm 0.3 \times 10^{-3} \text{ m}^3/\text{m}^2 \cdot \text{s}$). These values corroborate that the pore diameter, pore size distribution, and morphology (asymmetry or symmetry) are the major parameters that affect the water flow through the

membrane. However, the open porosity in the symmetric membranes appears to have no major effect on the permeation properties. The higher hydrophilic behavior of SiOC (ratio = 5.84) compared to Por5 (ratio = 4.37) may have a contribution to its slight superior water flux. Nonetheless, it is not possible to clearly quantify its effect on the water permeation flux.

5.3.2 Premix emulsification using different ceramic membranes

Figure 5.6a shows the droplet size distribution curves and the cumulative curves of the prepared premix and the fine emulsions after one and two passes through the ceramic membranes at 5 bar. The mean droplet sizes (d_{32} – surface mean or Sauter diameter) are also given within the signaled boxes. The fluctuation in the characteristic sizes (d_{10} , d_{50} , d_{90}) and span values based on each sample and pass are displayed in Figure 5.6b. All the studied ceramic membranes display a tendency to generate a monomodal distribution (span < 1.0 μm). Por5 seems to be insensitive to the number of passes, producing similar outputs in terms of d_{32} and span values after Pass-1 (2.22 μm ; 0.82) and Pass-2 (2.26 μm ; 0.82). SiOC and mullite membranes demonstrate a major advantage in terms of practical application over the commercial Por5 concerning tailoring of the droplet size. Both membranes show an expected tendency of droplet size reduction due to the number of passes. The mean droplet sizes obtained from SiOC membrane varied from 4.57 μm (Pass-1) to 3.48 μm (Pass-2), with span values decreasing from 0.97 to 0.91, respectively. Mullite membrane produced d_{32} -span values in the range of 3.09 μm -0.86 (Pass-1) and 2.34 μm -0.91. The results from the mullite membrane after Pass-2 are comparable to the ones from Por5. Generally, in premix membrane emulsification, thicker membranes generate more uniform emulsions due to multiple break-up points inside the membrane [11]. Nevertheless, in our work, the asymmetric structure produces a monomodal tendency analogous to the studied symmetric commercial membrane (Por5).

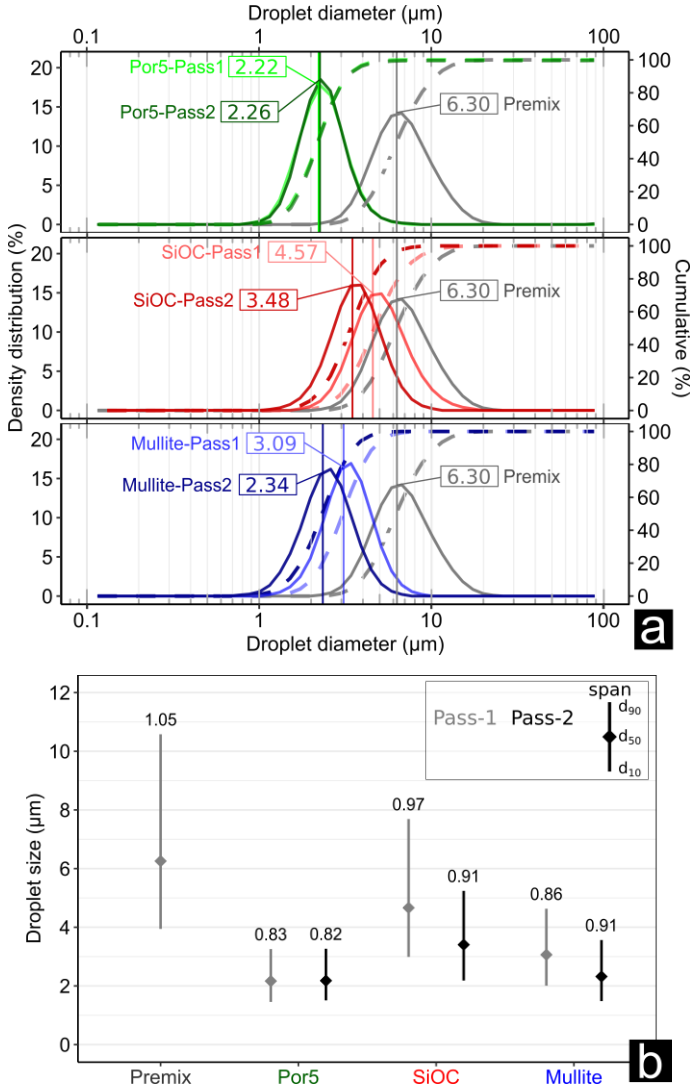


Figure 5.6: (a) Droplet size distribution obtained from premix emulsification of oil-in-water emulsion (Premix = MCT 10 wt.% + 1 wt.% Tween[®] 80) at 5 bar for the studied ceramic membranes (vertical lines and values within the boxes indicate the mean droplet size given by the Sauter mean diameter in $\mu\text{m} - d_{32}$). (b) Span values and characteristics sizes in terms of d_{10} , d_{50} , and d_{90} according to the membrane and number of passes at 5 bar.

Comparatively, a study reported the preparation of stable oil-in-water emulsions (10 vol% sunflower oil fraction, and 2 wt% polysorbate 20) using flat commercial nitrocellulose mixed ester (MCE) membranes (0.8 μm pore size) [5]. Although the authors show a reduction of the mean droplet diameter (d_{32}) from $\sim 5 \mu\text{m}$ (premix) up to $\sim 2 \mu\text{m}$ after one pass at 5 bar (emulsion flux $\sim 6.9 \times 10^{-3} \text{ m}^3/\text{m}^2 \cdot \text{s}$), the droplet size distribution exhibited two main peaks at 1 and 10 μm . A monomodal tendency was obtained only after the third pass (emulsion flux $\sim 9.2 \times 10^{-3} \text{ m}^3/\text{m}^2 \cdot \text{s}$) where the mean droplet size was around 1.24 μm with a span value of 0.82. Despite some similarities in trend and results with our work, there is a fundamental point that differentiates our membrane from this mentioned study, which is structural stability inherent from ceramic materials. Since the mentioned work deals with organic microfiltration membranes, changes in the membrane surface structure and thickness were observed, which can drastically reduce reproducibility, efficiency, and lifespan.

The relationship between mean droplet size and permeation flux at 5 bar according to the number of passes is given in Figure 5.7. Although mullite and Por5 have similar emulsification performance regarding droplet size and span values; Figure 5.7 reveals that mullite is much more suitable for upscaling given their permeation fluxes ($4.6 \times 10^{-3} - 5.3 \times 10^{-3} \text{ m}^3/\text{m}^2 \cdot \text{s}$, Pass-1 and Pass-2, respectively). The symmetric membranes show inferior premix permeation fluxes, falling in a range below $1 \times 10^{-3} \text{ m}^3/\text{m}^2 \cdot \text{s}$. Another interesting observation concerns the diminishment of the flux during the second pass (Pass-2) for the symmetric membranes suggesting problems related to fouling. Even though the SiOC membrane displays a reduction in flux, it also results in a steep decrease in mean droplet size. Conversely, Por5 results suggest that this membrane is already operating in a threshold zone, in which there is a small negative oscillation in flux and mean droplet size. On the other hand, the asymmetric mullite membrane depicts a reduction in droplet size from Pass-1 to Pass-2 as well as an increment in premix permeation flux.

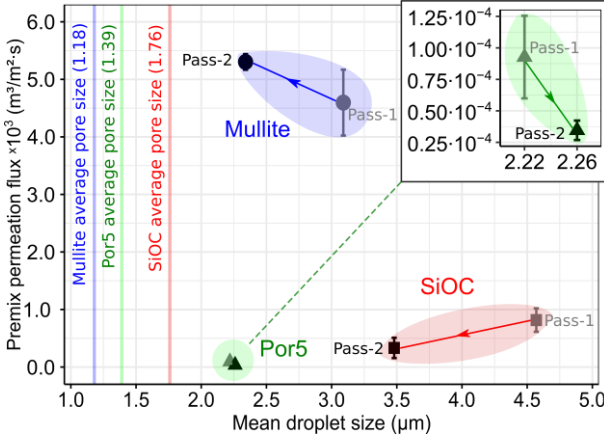


Figure 5.7: Premix permeation flux ($\text{m}^3/\text{m}^2\cdot\text{s}$) at 5 bar as a function of the mean droplet size ($d_{32}/\mu\text{m}$) and the number of passes for the studied membranes in a dead-end configuration.

5.3.3 Premix emulsification using mullite membrane at lower pressures

Considering its outstanding premix permeation flux and the resultant droplet size, the Mullite membrane was further studied under lower transmembrane pressures (2 to 4 bar). Figure 5.8a and Figure 5.8b portray, respectively, the droplet diameter distribution (μm) and the premix permeation flux ($\text{m}^3/\text{m}^2\cdot\text{s}$) of the prepared emulsions as a function of the number of passes and the applied pressure. From Figure 5.8a, it is possible to observe that the droplet diameter is inversely proportional to the applied pressure and number of passes. Nevertheless, the reduction of the droplet size does not appear to follow a linear relationship. For instance, taking into consideration the Pass-1, the premix was reduced from $6.30 \mu\text{m}$ to $4.06 \mu\text{m}$ (2 bar), $3.33 \mu\text{m}$ (3 bar), and $3.09 \mu\text{m}$ (4 bar). Moreover, the span values of the produced emulsions are quite similar, however, it seems to have a trend of slight broadening of the size distribution after the second pass through the membrane (span: Pass-1 < Pass-2). With respect to the premix permeation flux (Figure 5.8b), an increment with the transmembrane pressure is observed. None-

theless, as one may expect, compared to pure water flux there is a clear decrease in the premix flux due to the presence of a viscous dispersed component (oil phase) [26,27]. In addition, as observed in Figure 5.7 at 5 bar, during the Pass-2 the permeation flux presented a substantial increase at 2 and 4 bar. Even though, at 3 bar the mean flux value of Pass-2 ($2.04 \times 10^{-3} \pm 0.4 \times 10^{-3} \text{ m}^3/\text{m}^2 \cdot \text{s}$) is marginally inferior to Pass-1 ($2.19 \times 10^{-3} \pm 0.1 \times 10^{-3} \text{ m}^3/\text{m}^2 \cdot \text{s}$), the superior limit of the error bar in Pass-2 overpasses the one in Pass-1.

The observed reduction in droplet size due to the applied pressure (Figure 5.8a) may be described as an effect of the direct relationship between pressure and permeating flux (as stated in Darcy's law) [28]. Another possible phenomenon is the coalescence of the droplets at the exit of pores, once the flux is lower at lower pressures. On the other hand, the enhancement in permeation flux (Figure 5.8b) during the second pass (Pass-2) is a result of the decreased viscosity related to droplet size reduction. Since the primary droplet disruption and size reduction occur during the first pass, an intensification in flux may be expected in the second pass [11]. This assumption can be delineated by analyzing the slope of the premix permeation flux as a function of the transmembrane pressure (Figure 5.9). Considering that the pores of the membrane result from the voids between sintered particles, we can assume that the membrane transport is characterized by the Carman-Kozeny equation:

$$J = \frac{\varepsilon^3}{K \cdot \mu \cdot S^2 \cdot (1 - \varepsilon)^2} \cdot \frac{\Delta P}{\Delta z} = L_p \cdot \Delta P \quad \text{Equation 5.3}$$

where J is the flux of the permeate; ε is the membrane porosity; ΔP the transmembrane pressure; Δz the membrane thickness; K is the Carman-Kozeny constant that depends upon the pore shape and tortuosity; S is the specific surface area of the membrane; and, μ is the permeate viscosity. In Figure 5.9 the tangent of α_i corresponds to L_p [29], which takes into account membrane properties and the viscosity (μ) of the permeate fluid. Given that the membrane properties (ε , K , Δz , S) remain the same during Pass-1 and Pass-2, then the increase in flux must be due to a local

decrease in the fluid viscosity in Pass-2 in order to satisfy the Equation (3) ($\alpha_{\text{Pass-1}} < \alpha_{\text{Pass-2}} \therefore \mu_{\text{Pass-1}} > \mu_{\text{Pass-2}}$).

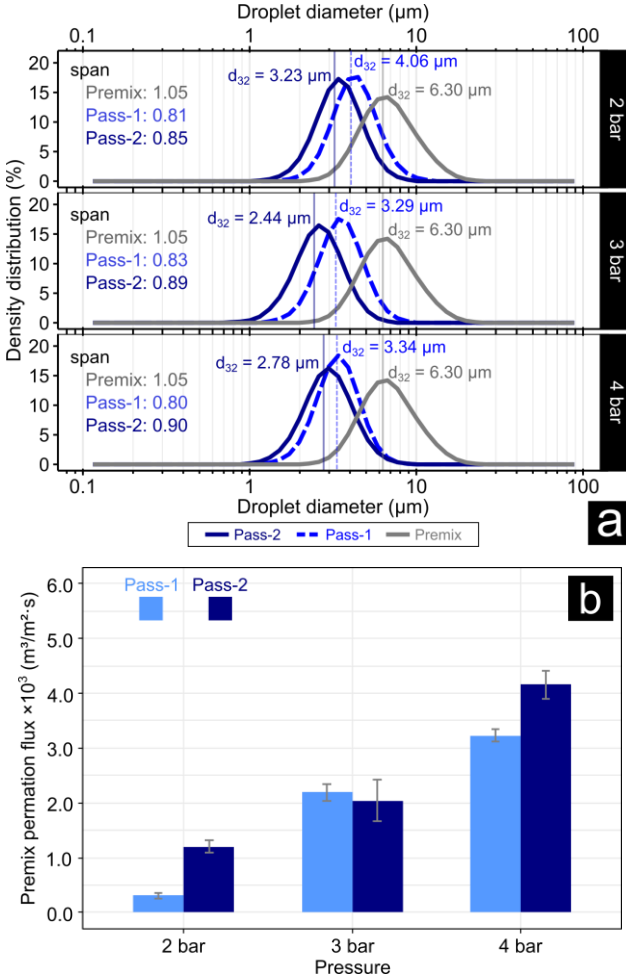


Figure 5.8: (a) Droplet size distribution (μm) and span values obtained from the premix membrane emulsification experiment of oil-in-water emulsion (MCT 10 wt.%) at different pressures (2, 3, and 4 bar) and 2 passes through the mullite asymmetric membrane. (b) Premix permeation flux ($\text{m}^3/\text{m}^2 \cdot \text{s}$) as a function of the applied pressure and number of passes for the mullite membrane.

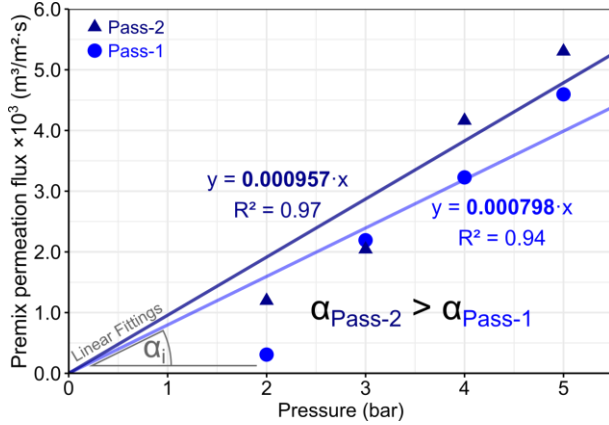


Figure 5.9: Linear fittings of the studied premix permeation fluxes as a function of the transmembrane pressure for the asymmetric mullite membrane.

Table 5.2 summarizes the main parameters and outcomes concerning the premix emulsification process in a dead-end configuration using ceramic membranes. The results of our work are compared to the main studies from the literature. It is noteworthy that our membranes are quite competitive, particularly the asymmetric mullite membrane due to its flux performance. For instance, the flat mullite membrane from this work presents characteristics similar to the work described by Jing et al. [30]. Nevertheless, the flux output from asymmetric mullite at Pass-2 ($1.2 \times 10^{-3} \text{ m}^3/\text{m}^2 \cdot \text{s}$) is 10 times higher ($1.26 \times 10^{-4} \text{ m}^3/\text{m}^2 \cdot \text{s}$) at the same applied pressure (2 bar) [30]. However, such comparison should be treated with caution given the differences in membrane characteristics and premix composition. Moreover, most of the studies presented in Table 5.2 are related to tubular membranes, which are still the most usual in the current market of inorganic membranes. This fact is probably related to the more uniform pressure distribution in cylindrical shapes when compared to flat ones, which may reduce membrane breakage due to differential stress spots in the structure.

Table 5.2: Premix emulsification studies of oil-in-water emulsions using different ceramic membranes in a dead-end configuration.

Membrane characteristics	Premix (OW)		Droplet characteristics after PME		PME parameters		Ref.
	Composition	Characteristics	Size (μm)	span	P (bar)	J ($\text{m}^3/\text{m}^2 \cdot \text{s}$)	
Por5 (Robugas) borosilicate glass; flat disc, symmetric structure; $d_m = 1.39 \mu\text{m}$; $\epsilon = 71.83\%$	MCT oil [10 wt.%] Poly sorbate 80 [1 wt.%] ($\sim 25^\circ\text{C}$)	$d_{32} = 6.30 \mu\text{m}$ span = 1.05 $\sim 25^\circ\text{C}$	$d_{32(\text{pass}1)} = 2.22$ $d_{32(\text{pass}2)} = 2.26$	Pass1 = 0.83 Pass2 = 0.82	5	Pass1 = 9.3×10^{-5} Pass2 = 3.5×10^{-5}	This work
SiOC flat disc membrane, symmetric structure; $d_m = 1.76 \mu\text{m}$; $\epsilon = 36.45\%$	MCT oil [10 wt.%] Poly sorbate 80 [1 wt.%] ($\sim 25^\circ\text{C}$)	$d_{32} = 6.30 \mu\text{m}$ span = 1.05 $\sim 25^\circ\text{C}$	$d_{32(\text{pass}1)} = 4.57$ $d_{32(\text{pass}2)} = 3.48$	Pass1 = 0.97 Pass2 = 0.91	5	Pass1 = 8.2×10^{-4} Pass2 = 3.3×10^{-4}	This work
Mullite flat disc membrane; asymmetric structure; $d_m = 3.06 \mu\text{m}$; $\epsilon = 68.27\%$ $d_{m(\text{top})} = 1.18 \pm 0.8 \mu\text{m}$	MCT oil [10 wt.%] Poly sorbate 80 [1 wt.%]	$d_{32} = 6.30 \mu\text{m}$ span = 1.05 $\sim 25^\circ\text{C}$	$d_{32(\text{pass}1)} = 4.06 - 3.09$ $d_{32(\text{pass}2)} = 3.23 - 2.34$	Pass1 = 0.81 - 0.86 Pass2 = 0.85 - 0.91	2 - 5	Pass1 = $(0.3 - 4.6) \times 10^{-3}$ Pass2 = $(1.2 - 5.3) \times 10^{-3}$	This work
Glass membrane; Tubular shape; $d_m = 2.70 \mu\text{m}$ $d_{m(\text{top})} = 4.20 \mu\text{m}$	Com oil [25 wt.%] PGPR [0.5 wt.%] and PGFE [0.75 - 3.0 wt.%]	$d_{50} = \sim 10 \mu\text{m}$ 25 $^\circ\text{C}$	$d_{32(A)} = 4.70 - 5.72$ $d_{32(B)} = 6.07 - 8.72$	A = 0.4 - 1.0 B = 0.62 - 0.66	A = 0.4 - 1.0 B = 0.1 - 0.6	A = $(8.1 - 197) \times 10^{-6}$ B = $(20 - 986) \times 10^{-6}$	[31]
$\alpha\text{-Al}_2\text{O}_3$; Tubular shape; $d_m = 1.5 \mu\text{m}$	Toluene SDS [2 wt.%]	$d_{50} = 54.69 \mu\text{m}$ 20 $^\circ\text{C}$	$d_{50} = 2.29$	1.2	2	1.26×10^{-4}	[30]
Shirasu Porous Glass; Tubular shape; $d_m = 8.0 \mu\text{m}$	Com oil [40 wt.%] SDS [0.06 - 2 wt.%] or Poly sorbate 20 [0.1 - 2 wt.%]	$d_m = 119 \mu\text{m}$ range = 10 - 204 μm 25 $^\circ\text{C}$	$d_{m(\text{Tween}+\text{pass})} = 6.4 - 8.7$ $d_{m(\text{SDS}+\text{pass})} = 4.1 - 6.8$	n.a.	1	Tween = $(1.4 - 1.3) \times 10^{-3}$ SDS = $(8.1 - 17) \times 10^{-3}$	[32]
Shirasu Porous Glass; Tubular shape; $d_m = 8.0 \mu\text{m}$	Com oil [10 or 20 wt.%] Lecithin [2 wt.%]	$d_{m10} = \sim 90 \mu\text{m}$ $d_{m20} = \sim 300 \mu\text{m}$ 20 $^\circ\text{C}$	$50 \mu\text{m} < d_m < d_{m(\text{premix})}$	n.a.	1 or 1.5	$(2.8 - 83) \times 10^{-4}$	[13]
Por2/3/4 (Robugas) borosilicate glass; $d_{50} = 13/28/70 \mu\text{m}$; $\epsilon = 42/41/36\%$; alumina/silica membranes; $d_m = 130 - 314 \mu\text{m}$; $\epsilon = 34 - 40\%$; Flat discs	Repesced oil [0.5 v/v] Tween20 or Tween80	$d_{32} = \sim 80 - 170 \mu\text{m}$ span = 0.99 - 1.23	$d_{32} = 9 - 29 \mu\text{m}$	1.471 - 1.807	0.5 - 5	~ 120 (highest disperse phase flux rate)	[33]
Shirasu Porous Glass; Tubular shape; $d_m = 0.2 - 0.8 \mu\text{m}$	Ethylhexyl palmitate (EHP) [5-40 wt.%] poly sorbate 20 or 80 [2.5 - 20 wt.%]	$d_{50} = \sim 15 \mu\text{m}$	$d_{50} = 0.26 - 1.0$	0.41 - 0.48	10 - 60	$5 - 200 \text{ mL} \cdot \text{min}^{-1}$	[34]

ϵ - Porosity (%); PGPR - Polyglycerol polyricinoleate (CR-500); PGFE - Polyglycerol fatty acid esters (Decaglycerol monolaurate; HLB: 10-15); SDS - Sodium dodecyl sulfate; n.a. - not available.

5.4 Conclusions

The preparation of a stable food grade oil-in-water emulsion is investigated by using the PME process with three distinct microfiltration ceramic membranes. The effect of the number of passes on the mean droplet size and the dispersity (span) is demonstrated. The commercial symmetric Por5 is the only membrane insensitive to the number of passes. The symmetric SiOC and the asymmetric mullite membranes exhibit a decrease in droplet size after a second pass through the membrane, as expected. The droplet size and the span values obtained for the manufactured mullite membrane is comparable to the commercial Por5. However, the asymmetric structure from the mullite membrane shows a superior flux performance against the symmetric membranes. Further investigations with mullite clarified the premix flux increment at the second pass, which is presumably to be due to the local viscosity reduction according to Carman-Kozeny equation. Therefore, the results obtained in this work corroborate the potential application of ceramic membranes in the ME process, particularly the one with asymmetric structure.

5.5 Acknowledgements

We thank the German Research Foundation (DFG) within the Research Training Group GRK 1860 “Micro-, meso- and macroporous nonmetallic Materials: Fundamentals and Applications” (MIMENIMA). We are grateful to the Brazilian funding agencies Coordination for the Improvement of Higher Education Personnel (CAPES) through the Brazilian-German Collaborative Research Initiative on Manufacturing (BRAGECRIM) and National Council for Scientific and Technological Development (CNPq) for supporting this study. Natália Cristina Fontão and Bernardo Araldi da Silva are also acknowledged for the vapor adsorption analysis and BET specific surface area measurement of the Por5 membrane, respectively.

5.6 Authors contributions

The article is mainly based on the work of the first author and author of this thesis Rafael Kenji Nishihora. The precise contributions of each author are listed below.

Table 5.3: Authors contributions for Chapter 5.

Author	Contribution
Nishihora, R. K.	Conceptualized the work, performed and analyzed the experiments, wrote the manuscript
Luhede, L.	Helped to perform initial sets of experiments, helped in the scientific evaluation and editing of the manuscript
Fritsching, U.	Gave conceptual and scientific advices, helped in the scientific evaluation and editing of the manuscript
Quadri, M. G. N.	Gave conceptual and scientific advices, helped in the scientific evaluation and editing of the manuscript
Hotza, D.	Gave conceptual and scientific advices, helped in the scientific evaluation and editing of the manuscript
Rezwan, K.	Gave conceptual and scientific advices, helped in the scientific evaluation and editing of the manuscript
Wilhelm, M.	Gave conceptual and scientific advices, helped in the scientific evaluation and editing of the manuscript

5.7 References

- [1] D.J. Shaw, Introduction to colloid and surface chemistry, Butterworth-Heinemann, 1992.
- [2] S.M. Joscelyne, G. Trägårdh, Membrane emulsification — a literature review, *J. Memb. Sci.* 169 (2000) 107–117.
- [3] C. Charcosset, I. Limayem, H. Fessi, The membrane emulsification process - A review, *J. Chem. Technol. Biotechnol.* 79 (2004) 209–218. doi:10.1002/jctb.969.
- [4] A. Trentin, M. Ferrando, F. López, C. Güell, Premix membrane O/W emulsification: Effect of fouling when using BSA as emulsifier, *Desalination*. 245 (2009) 388–395. doi:10.1016/j.desal.2009.02.002.

- [5] A. Trentin, C. Güell, F. López, M. Ferrando, Microfiltration membranes to produce BSA-stabilized O/W emulsions by premix membrane emulsification, *J. Memb. Sci.* 356 (2010) 22–32. doi:10.1016/j.memsci.2010.03.022.
- [6] L. Giorno, G. De Luca, A. Figoli, E. Piacentini, E. Drioli, Membrane Emulsification: Principles and Applications, in: E. Drioli, L. Giorno (Eds.), *Membr. Oper. Innov. Sep. Transform.*, Wiley-VCH Verlag GmbH & Co. KGaA, 2009: pp. 463–497. doi:10.1002/9783527626779.ch21.
- [7] A. Nazir, R.M. Boom, K. Schroën, Droplet break-up mechanism in premix emulsification using packed beds, *Chem. Eng. Sci.* 92 (2013) 190–197. doi:10.1016/j.ces.2013.01.021.
- [8] E. Piacentini, E. Drioli, L. Giorno, Membrane emulsification technology: Twenty-five years of inventions and research through patent survey, in: *J. Memb. Sci.*, 2014: pp. 410–422. doi:10.1016/j.memsci.2014.05.059.
- [9] H.S. Ribeiro, J.J.M. Janssen, I. Kobayashi, M. Nakajima, Membrane Emulsification for Food Applications, in: Klaus-Viktor Peinemann, S.P. Nunes, L. Giorno (Eds.), *Membr. Technol. 3 Membr. Food Appl.*, Wiley-VCH Verlag GmbH & Co. KGaA, 2010: pp. 129–166. doi:10.1002/9783527631384.ch7.
- [10] V. Zanatta, K. Rezzadori, F. Marques, G. Zin, C. Cunha, M. Di Luccio, E. Lemos-Senna, Stability of oil-in-water emulsions produced by membrane emulsification with microporous ceramic membranes, *J. Food Eng.* 195 (2017) 73–84. doi:10.1016/j.jfoodeng.2016.09.025.
- [11] A. Nazir, K. Schroën, R. Boom, Premix emulsification: A review, *J. Memb. Sci.* 362 (2010) 1–11. doi:10.1016/j.memsci.2010.06.044.
- [12] G.T. Vladisavljević, M. Shimizu, T. Nakashima, Preparation of monodisperse multiple emulsions at high production rates by multi-stage premix membrane emulsification, *J. Memb. Sci.* 244 (2004) 97–106. doi:10.1016/j.memsci.2004.07.008.

- [13] J. Surh, Y.G. Jeong, G.T. Vladislavljević, On the preparation of lecithin-stabilized oil-in-water emulsions by multi-stage premix membrane emulsification, *J. Food Eng.* 89 (2008) 164–170. doi:10.1016/j.jfoodeng.2008.04.023.
- [14] D. da Silva Biron, V. dos Santos, M. Zeni, *Ceramic Membranes Applied in Separation Processes*, 2018. doi:10.1007/978-3-319-58604-5.
- [15] M. Matos, M.A. Suárez, G. Gutiérrez, J. Coca, C. Pazos, Emulsification with microfiltration ceramic membranes: A different approach to droplet formation mechanism, in: *J. Memb. Sci.*, 2013: pp. 345–358. doi:10.1016/j.memsci.2013.05.033.
- [16] F. Spyropoulos, D.M. Lloyd, R.D. Hancocks, A.K. Pawlik, Advances in membrane emulsification. Part A: Recent developments in processing aspects and microstructural design approaches, *J. Sci. Food Agric.* 94 (2014) 613–627. doi:10.1002/jsfa.6444.
- [17] Robu® Glasfilter-Geräte GmbH, Porengrößen, (n.d.). <https://www.robuglas.com/index.php?id=51&L=1> (accessed December 20, 2018).
- [18] ISO4793:1980, Laboratory sintered (fritted) filters - Porosity grading, classification and designation, *Int. Organ. Stand.* (1980). <https://www.iso.org/standard/10772.html>.
- [19] R.K. Nishihora, M.G.N. Quadri, D. Hotza, K. Rezwan, M. Wilhelm, Tape casting of polysiloxane-derived ceramic with controlled porosity and surface properties, *J. Eur. Ceram. Soc.* 38 (2018) 4899–4905. doi:10.1016/j.jeurceramsoc.2018.07.016.
- [20] R.K. Nishihora, E. Rudolph, M.G.N. Quadri, D. Hotza, K. Rezwan, M. Wilhelm, Asymmetric mullite membranes manufactured by phase-inversion tape casting from polymethylsiloxane and aluminum diacetate, *J. Memb. Sci.* 581 (2019) 421–429. doi:10.1016/j.memsci.2019.03.047.
- [21] V. Kozák, Z. Sucharda, M. Havelcová, I. Dlouhý, P. Glogar, Z. Chlup, M. Černý, A. Strachota, Preparation of Silicon Oxycarbide composites toughened by inorganic fibers via pyrolysis of

- precursor siloxane composites, *Acta Phys. Pol. A.* 120 (2016) 326–330. doi:10.12693/aphyspola.120.326.
- [22] J. Kujawa, W. Kujawski, Functionalization of ceramic metal oxide powders and ceramic membranes by perfluoroalkylsilanes and alkylsilanes possessing different reactive groups: physico-chemical and tribological properties, *ACS Appl. Mater. Interfac.* 8 (2016) 7509–7521. doi:10.1021/acsami.5b11975.
- [23] J. Li, K. Lu, Highly porous SiOC bulk ceramics with water vapor assisted pyrolysis, *J. Am. Ceram. Soc.* 98 (2015) 2357–2365. doi:10.1111/jace.13634.
- [24] J. Li, K. Lu, T. Lin, F. Shen, Preparation of micro-/mesoporous SiOC bulk ceramics, *J. Am. Ceram. Soc.* 98 (2015) 1753–1761. doi:10.1111/jace.13541.
- [25] A.J. Burggraaf, Chapter 2 Important characteristics of inorganic membranes, *Membr. Sci. Technol.* 4 (1996) 21–34. doi:10.1016/S0927-5193(96)80005-2.
- [26] G.T. Vladislavljević, U. Lambrich, M. Nakajima, H. Schubert, Production of O/W emulsions using SPG membranes, ceramic α -aluminium oxide membranes, microfluidizer and a silicon micro-channel plate - A comparative study, *Colloids Surfaces A Physicochem. Eng. Asp.* 232 (2004) 199–207. doi:10.1016/j.colsurfa.2003.10.026.
- [27] O. Alliod, L. Messenger, H. Fessi, D. Dupin, C. Charcosset, Influence of viscosity for oil-in-water and water-in-oil nanoemulsions production by SPG premix membrane emulsification, *Chem. Eng. Res. Des.* 142 (2018) 87–99. doi:10.1016/j.cherd.2018.11.027.
- [28] N. Li, K. Sakaki, Performance of an emulsion enzyme membrane reactor combined with premix membrane emulsification for lipase-catalyzed resolution of enantiomers, *J. Memb. Sci.* 314 (2008) 183–192. doi:10.1016/j.memsci.2008.01.052.
- [29] A.C. Habert, *Processos de Separação por Membranas*, E-papers, 2006.

- [30] W. Jing, J. Wu, W. Xing, W. Jin, N. Xu, Emulsions prepared by two-stage ceramic membrane jet-flow emulsification, Part. Technol. Fluid. 51 (2005) 1339–1345. doi:10.1002/aic.10405.
- [31] I.S. and Y.H. Kanichi SUZUKI, Characteristics of the membrane emulsification method combined with preliminary emulsification for preparing corn oil-in-water emulsions, Food Sci. Technol. 2 (1996) 43–47. doi:10.3136/fsti9596t9798.2.43.
- [32] G.T. Vladisavljevic, J. Surh, J.D. McClements, Effect of emulsifier type on droplet disruption in repeated Shirasu Porous Glass membrane homogenization, Langmuir. 22 (2006) 4526–4533. doi:10.1021/la053410f.
- [33] N. Hornig, U. Fritsching, Liquid dispersion in premix emulsification within porous membrane structures, J. Memb. Sci. 514 (2016) 574–585. doi:10.1016/j.memsci.2016.04.051.
- [34] O. Alliod, J. Valour, S. Urbaniak, H. Fessi, D. Dupin, C. Charcosset, Preparation of oil-in-water nanoemulsions at large-scale using premix membrane emulsification and Shirasu Porous Glass (SPG) membranes, Colloids Surfaces A. 557 (2018) 76–84. doi:10.1016/j.colsurfa.2018.04.045.

5.8 Supplementary material

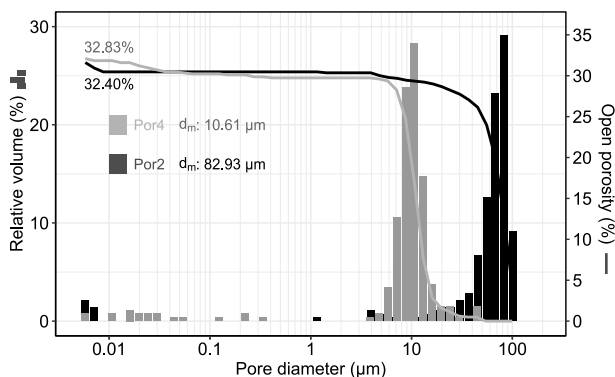


Figure 5.10: Pore size distribution versus relative pore volume (bars) and open porosity curves (lines) measured by Hg-porosimetry of commercial borosilicate glass membranes (Por 2 and Por4 from Robuglas).

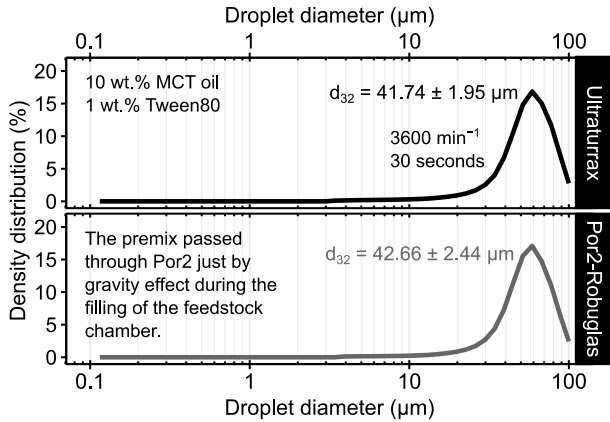


Figure 5.11: Evaluation of the isolated effect of the porous support (Por2-Robuglas) on the premix membrane emulsification process.

6 Conclusion

At this point, it is necessary to highlight the main contributions of this doctoral thesis to the scientific community. Hereby, it is intended to emphasize not only the novelty but rather why this work should be considered valuable.

Even though the published review paper (section 2.1) is not considered an experimental work with original results, its relevance is undeniable to the core topic of this thesis. Thus, compiling and critically discussing in a single document the efforts in the literature showed to be a substantial contribution, particularly to the readers of the Journal of the European Ceramic Society. In fact, this review paper is among the 10 most downloaded articles from this journal since February 2018⁵. This fact corroborates the emerging need and interest of the scientific community in discussing the strategies involved in the preparation of advanced porous ceramics.

Concerning the experimental results, first, it would be important to recall the aim of this thesis: “to prepare planar microfiltration ceramic membranes applied in PME process, exploring different pore forming strategies while using polysiloxanes as one of the main precursors and tape casting as shaping technique”.

In view of the Chapter 3, the aim was addressed by producing a symmetric microfiltration membrane using polysiloxanes as the matrix components. However, inert fillers (SiC particles) were needed to provide mechanical stability and improve the processability via tape casting. A sacrificial filler (ADA) was employed to generate the macroporosity in the material. Although ADA is mainly applied as a foaming agent, in this work the foaming event could be hindered due to the crosslinking of the precursors. The pyrolysis temperature played an important role in tailoring the surface properties. Therefore, here the flexibility of polysiloxanes is demonstrated, in which samples pyrolyzed

⁵<https://www.journals.elsevier.com/journal-of-the-european-ceramic-society/most-downloaded-articles>

under inert atmosphere (N_2) at 600 °C resulted in more hydrophobic behavior, while after treatment at 1000 °C it was shifted to the hydrophilic nature. At 600 °C, still some of the organic moieties cannot be degraded (e.g. CH_3), hence a hybrid polymeric/amorphous ceramic membrane is produced. On the other hand, at 1000 °C the organic part is expected to be completely degraded from the polysiloxane structure, leaving only the amorphous SiOC structure. This feature is particularly interesting in selective permeation and/or separation processes.

In Chapter 4, another key aspect of polysiloxane was considered: its sensitivity to the burning atmosphere. The central idea was taking advantage of the possibility to produce amorphous reactive SiO_2 when calcining polysiloxanes. This reactive powder was combined to another reactive alumina precursor (aluminum diacetate) in stoichiometric proportion, generating mullite-based powder ($3Al_2O_3 \cdot 2SiO_2$) under lower energy input (i.e. time + temperature). Later, the prepared powder was processed via tape casting combined with phase inversion technique. Here, instead of a symmetric membrane an asymmetric microfiltration ceramic membrane was produced. The asymmetric membrane exhibited an enhanced water permeation performance when compared to a commercial symmetric membrane. Once again, the versatility of the polysiloxane precursor and the tape casting method was successfully explored.

Up to now, plenty of PDC-based materials have been prepared and fully characterized in the literature. Even though potential applications are normally proposed, most of the cases remain only as suggestions. In order to address the lack of applied PDC-based materials and expand the use of ceramic membranes, Chapter 5 proposes the application of the prepared materials in an emergent technology, premix membrane emulsification. The symmetric SiOC membrane exhibited better water and premix permeation flux than the commercial Por5. However, the droplet size generated by SiOC during the process was larger than the one obtained by Por5. With regard to the mullite membrane, the asymmetric structure appear to have a crucial role in its outstanding performance compared to the symmetric membranes tested. Mullite

showed exceptional permeation fluxes compared to Por5 and SiOC, whilst maintaining similar droplet size and distribution than the one obtained from Por5.

In summary, this work shows that polysiloxane-based materials can be prepared by conventional processing techniques such as tape casting, using a combination of pore forming strategies that are available to be fully explored in order to tailor the final macrostructure. Furthermore, the versatility of preceramic polymers and the feasibility of manufacturing advanced ceramic materials with practical applications are demonstrated and reinforced in this thesis.

Therefore, I expect that this work would not only fulfill some of the current gaps within this realm but more importantly, expand the universe of possibilities yet to be unraveled.

7 Outlook

Considering that four years were not enough to explore thoroughly all the ideas that still inhabit my mind, here I would like to leave some of these ideas as a legacy and a challenge to future researches colleagues.

Even though in Chapter 3 porous hydrophobic membranes were prepared, they were still quite brittle to be applied. However, it would be interesting to evaluate the use of other fillers (reactive or inert) to improve mechanical stability at low pyrolysis temperature (≤ 600 °C). Additionally, for application in membrane technology, the open porosity and percolation network should be enhanced. An option is to prepare an asymmetric structure instead of the presented symmetric one.

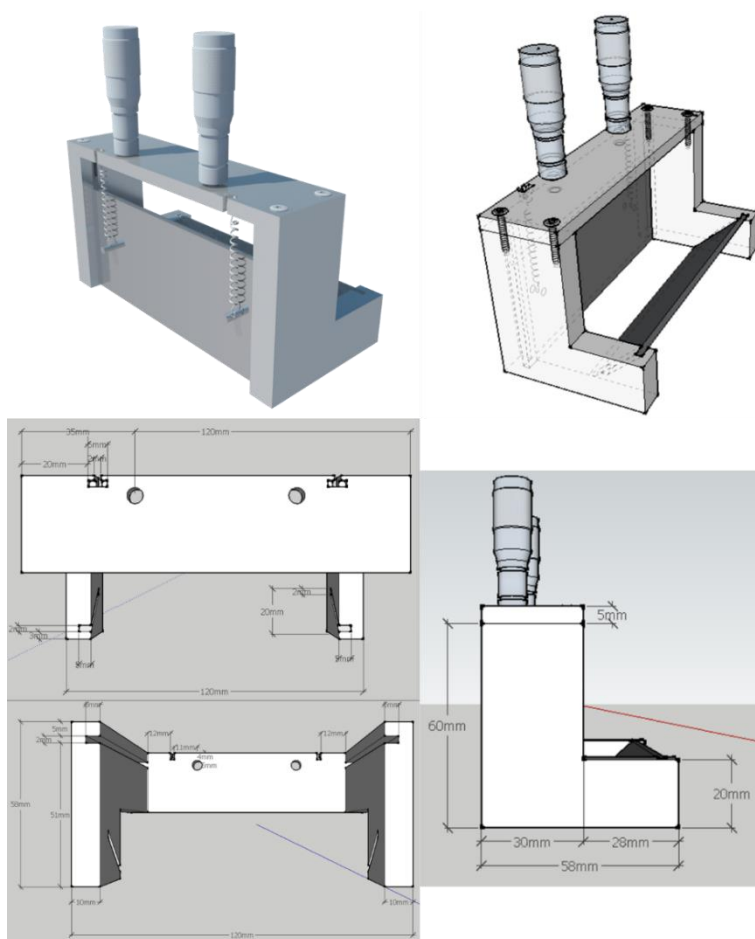
With respect to the symmetry or asymmetry aspect, it is noticeable the lack of phase-inversion strategy applied to PDCs in the current literature. Although Chapter 4 describes the use of polysiloxane as precursor, in the end this material was converted into conventional oxide ceramics. In this sense, it would be a great deal taking advantage of the polymeric nature of PCPs to directly prepare an asymmetric membrane without any carbon-based polymer serving as the matrix generator. Hence, a neat PDC matrix would be prepared in a single or fewer steps. Therefore, macrostructure may be tailored during processing (phase-inversion) and meso/microporosity and surface properties via heat treatment (temperature plus atmosphere). Here the primary challenge is to properly combine preceramic polymer, solvent, and non-solvent.

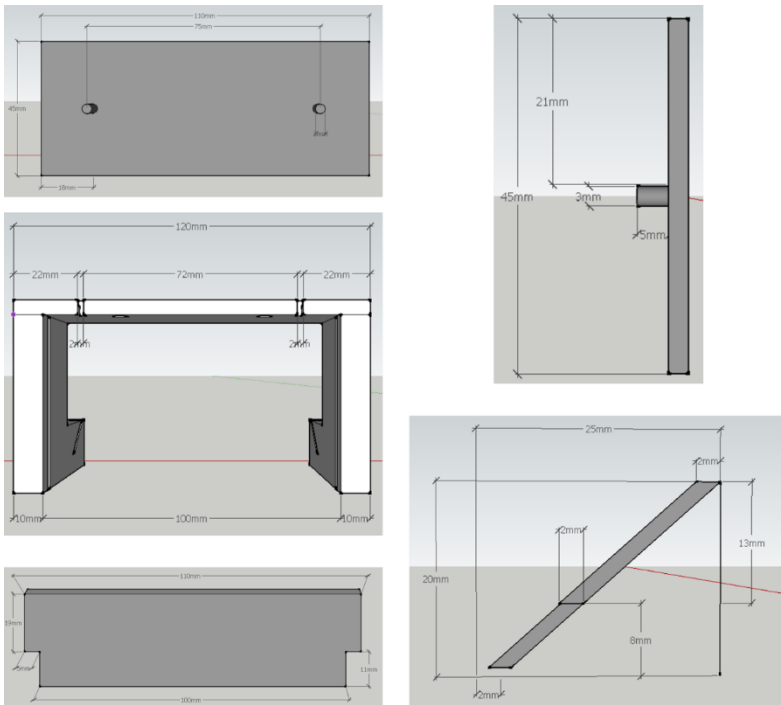
Regarding the application tests in membrane emulsification process, an investigation with different configurations (e.g. DME, see APPENDIX A.3), oil phases, and surfactants, would enrich the discussion raised in Chapter 5. For instance, a study comparing the hydrophobic membranes against functionalized traditional ceramic membranes would be challenging. Furthermore, testing the prepared membranes in separation process is also another attractive possibility.

Appendix

Some of the devices that have been used in this work (A.1 and A.2) were firstly designed in 3D software (Sketchup Free version). Here, the sketches and projects are shown in detail.

A.1 Doctor blade project and 3D design



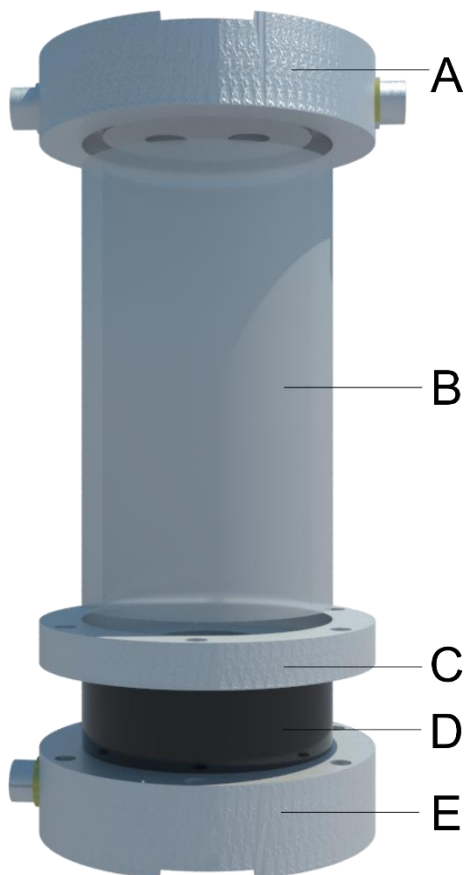


A.2 Simple 3D design of the membrane module setup for permeation and premix experiments

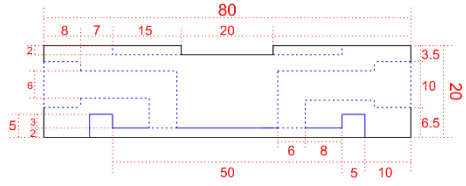


A.3 New design of the membrane module setup for permeation, separation, premix, and direct emulsification experiments

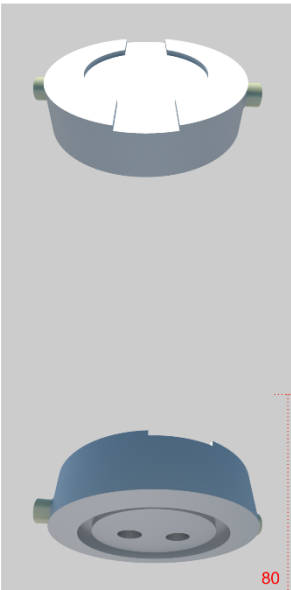
This setup has been designed during this doctorate, however, since it was not concluded on time it remains as a prospective device to future applications.



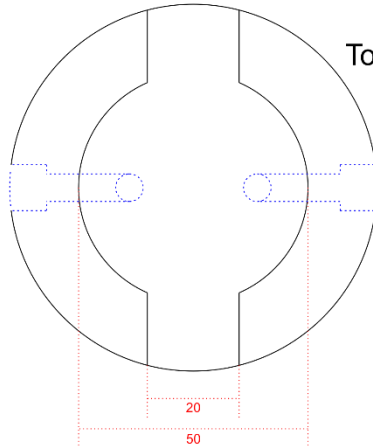
Front



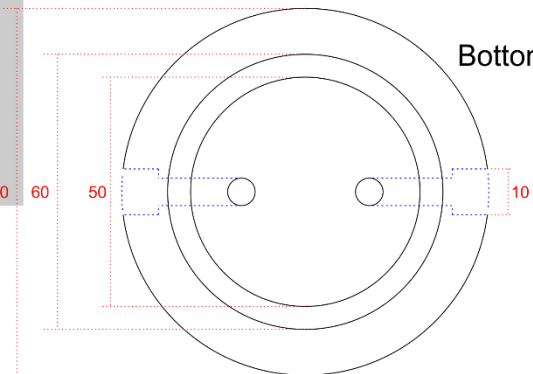
Part: A

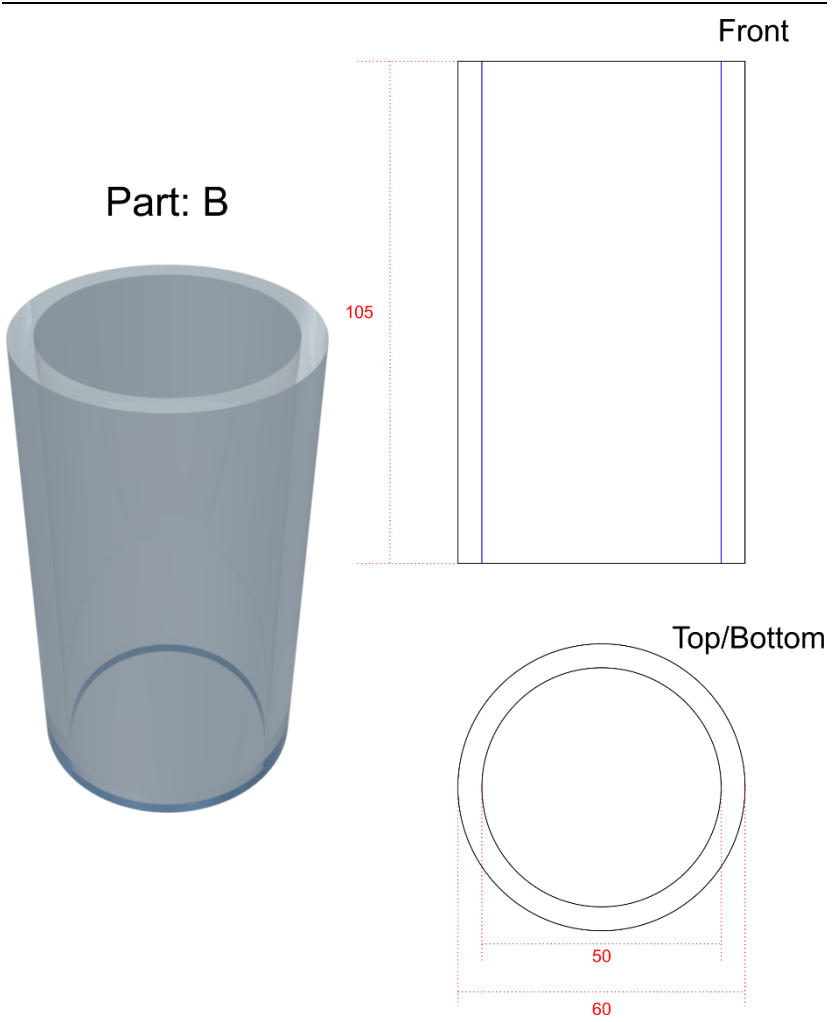


Top

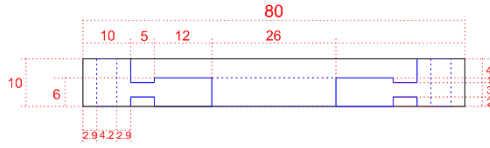


Bottom

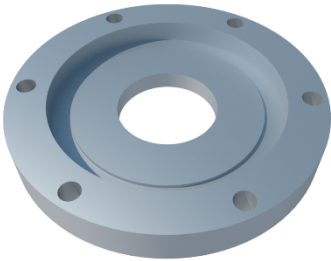




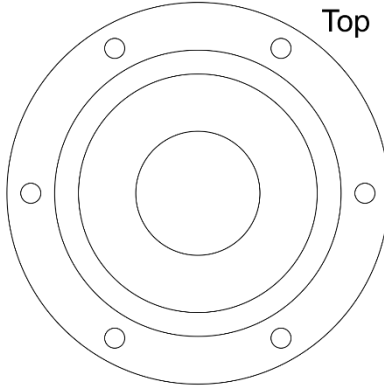
Front



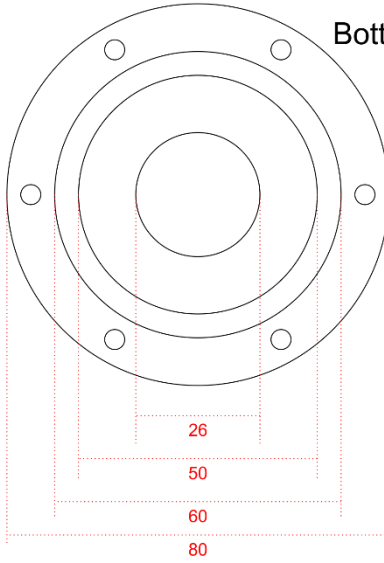
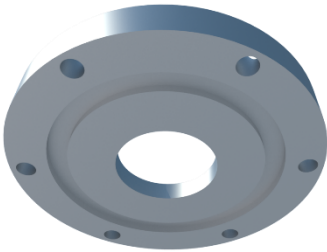
Part: C

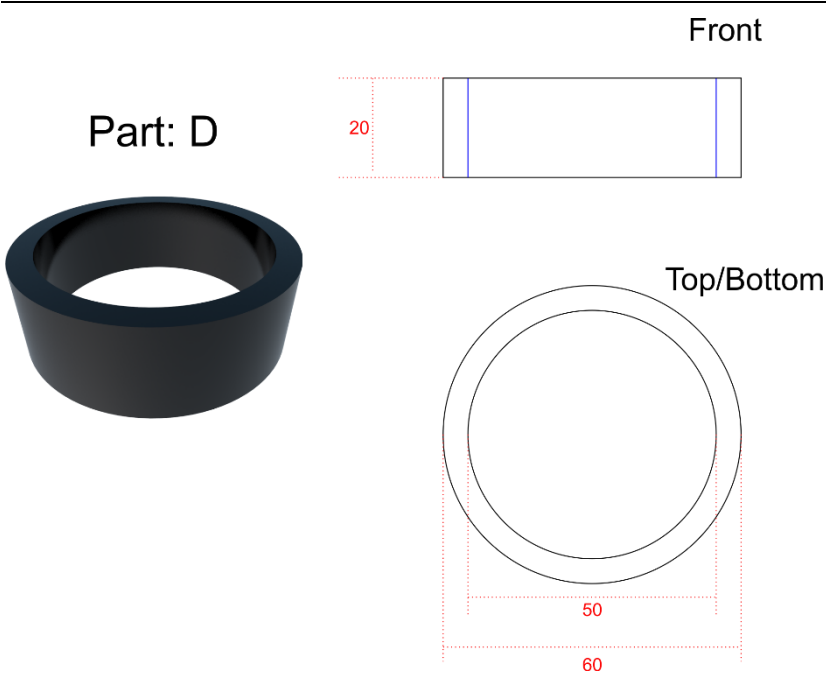


Top

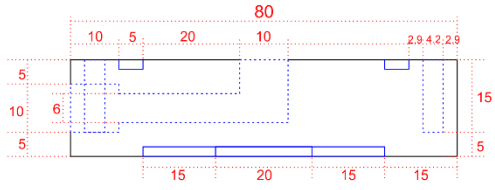


Bottom





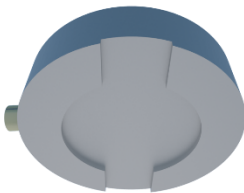
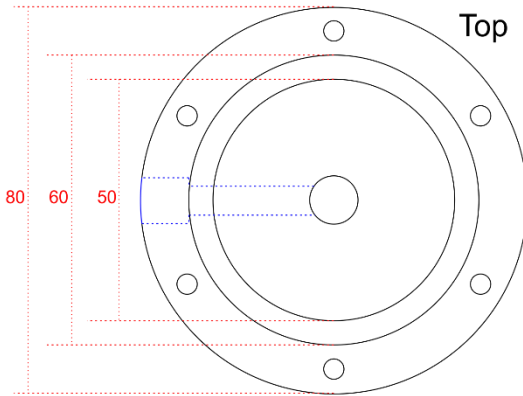
Front



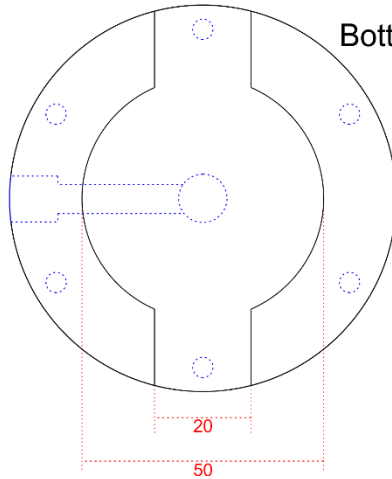
Part: E



Top



Bottom



Curriculum vitae

Surname: Nishihora
First name: Rafael
Middle name: Kenji
Date / Place of birth: 27. May. 1990 / Criciúma, Brazil
Nationality: Brazilian

Education

2013 – 2015 Master in Chemical Engineering
Universidade Federal de Santa Catarina
Florianópolis, Brazil

2008 – 2012 Diploma in Chemical Engineering
Universidade do Sul de Santa Catarina
Tubarão, Brazil

Professional / Research Experience

03.2015 – Today Ph.D. student
Universidade Federal de Santa Catarina
Department of Chemical Engineering
CNPq scholarship
Florianópolis, Brazil

09.2017 – 08.2018 Visiting Ph.D. student
Universität Bremen – Advanced Ceramics
BRAGECRIM, CAPES scholarship
Bremen, Germany

02.2017 – 08.2017 Visiting Ph.D. student
Universität Bremen – Advanced Ceramics
ERASMUS+ programme
Bremen, Germany

-
- 06.2012 – 12.2012** Internship, Monitoring of the wastewater treatment system,
Duarte Pescados Ltda,
Laguna, Brazil
- 03.2012 – 07.2012** Scholarship for Unit Operations Tutoring
Universidade do Sul de Santa Catarina
Tubarão, Brazil
- 2010 – 2012** Research assistant student
Universidade do Sul de Santa Catarina
Topic: Production of biodiesel from animal fatty by transesterification
Scholarship by the frame of “Artigo 170”
Tubarão, Brazil

Awards / Additional qualifications

- 03.2013** Diploma of Merit - Best student of Chemical Engineering (2012-2). Awarded by Universidade do Sul de Santa Catarina, Conselho Regional de Química (CRQ-SC), and Conselho Regional de Engenharia e Agronomia (CREA-SC)
Tubarão, Brazil
- 2013** Best Group Project in Chemical Engineering (2012-2)
Awarded by Universidade do Sul de Santa Catarina
Tubarão, Brazil
- 2013** Best Internship Report in Chemical Engineering (2012-2)
Awarded by Universidade do Sul de Santa

	Catarina Tubarão, Brazil
Portuguese	Mother tongue
English	Fluent
Spanish	Basic
German	Basic
IT knowledge	R Programming Language, LaTeX, Microsoft Office, OriginLab, SciDavis, Statistica, Design Expert 7, ChemSketch, Xpert High Score Plus, MAUD, ImageJ, Octave/Matlab, CorelDraw, Inkscape, Photoshop, Gimp, Skechup, V-Ray

Supervised student project

The work described in Chapter 4 could just be accomplished due to the great performance and help of Ellen Rudolph – “Phase-inversion tape casting of mullite membranes based on alumina/alumina precursor and polymethylsiloxane” (Diploma thesis, Bremen, Germany, 2018 – Supervised by Rafael Kenji Nishihora and Dr. Michaela Wilhelm).

List of publications

Peer-reviewed

From this Thesis:

R. K. Nishihora, P. L. Rachadel, M. G. N. Quadri, D. Hotza. “Manufacturing porous ceramic materials by tape casting—a review”. *Journal of the European Ceramic Society*, vol. 38 (4), pp. 988-1001, 2018.
<https://doi.org/10.1016/j.jeurceramsoc.2017.11.047>

R. K. Nishihora, M. G. N. Quadri, D. Hotza, K. Rezwan, M. Wilhelm. “Tape casting of polysiloxane-derived ceramic with controlled porosity and surface properties”. *Journal of the European Ceramic Society*, vol. 38 (15), pp. 4899-4905, 2018.
<https://doi.org/10.1016/j.jeurceramsoc.2018.07.016>

R. K. Nishihora, E. Rudolph, M. G. N. Quadri, D. Hotza, K. Rezwan, M. Wilhelm. “Asymmetric mullite membranes manufactured by phase-inversion tape casting from polymethylsiloxane and aluminum diacetate”. *Journal of Membrane Science*, vol. 581, pp. 421-429, 2019.
<https://doi.org/10.1016/j.memsci.2019.03.047>

Others:

R. K. Nishihora, E. Niehues, M. G. N. Quadri, Propriedades mecânicas e solubilidade de filmes de gelatina reticulados com transglutaminase, XX Congresso Brasileiro de Engenharia Química, Blucher Chemical Engineering Proceedings, vol. 1, pp. 14067-14074, ISSN 2359-1757, 2015.
[10.5151/chemeng-cobeq2014-1485-19055-178172](https://doi.org/10.5151/chemeng-cobeq2014-1485-19055-178172)

M.S.P. Damas, V.A. Pereira Junior, **R.K. Nishihora**, M.G.N. Quadri, Edible films from mucilage of *Cereus hildmannianus* fruits: develop-

ment and characterization, *Journal of Applied Polymer Science*, vol. 134, 2017.

<https://doi.org/10.1002/app.45223>

J.J. João, T. Emerick, U. de S. Filho, **R.K. Nishihora**, Processo de eletrocoagulação-flotação: investigação dos parâmetros operacionais para o tratamento de águas residuais da indústria de pescados, *Química Nova*, vol. 41, pp 163–168, 2018.

<http://dx.doi.org/10.21577/0100-4042.20170166>

D. Hotza, **R. K. Nishihora**, R. A. F. Machado, P.-M. Geffroy, T. Chartier, S. Bernard, Tape casting of preceramic polymers toward advanced ceramics: a review, *International Journal of Ceramic Engineering and Science*, Vol. 1, 2019.

<https://doi.org/10.1002/ces2.10009>

Conference presentation/proceedings

From this Thesis:

R. K. Nishihora*, E. Rudolph, M. Di Luccio, M. G. N. Quadri, D. Hotza, K. Rezwan, M. Wilhelm. Tape cast porous mullite membranes based on alumina/aluminum precursors and polysiloxane. In *15th International Conference on Inorganic Membranes*, Dresden, Germany, 2018. (*Speaker)

R. K. Nishihora, M. G. N. Quadri, D. Hotza, K. Rezwan, M. Wilhelm*. Polysiloxane-based ceramic tapes applied for membrane emulsification process. In *7th International Congress on Ceramics*, Foz do Iguaçu, Brazil, 2018. (*Speaker)

Others:

R. K. Nishihora*; J. R. B. Damineli*, J. J. João, E. Skoronski. Obtenção de biodiesel através de reações de transesterificação da gordura residual dos abatedouros de suínos. In *XVIII Encontro de Química da Região Sul – Contribuições para o Futuro*, Curitiba, Brazil, 2010. (*Poster presenters)

J. Silva*, J. J. João, **R. K. Nishihora**. Avaliação do efluente gerado no Porto Pesqueiro de Laguna, Santa Catarina: Uma proposta de tratamento. In *XIX Encontro de Química da Região Sul – A Contribuição da Química para o Desenvolvimento Tecnológico e Sustentável*, Tubarão, Brazil, 2012. (*Poster presenter)

J. J. João*, U. S. Filho; **R. K. Nishihora**, J. M. Ribeiro. Aplicação da eletroflotação para tratamento de efluentes gerados na indústria de pescados. In *36ª Reunião Anual da Sociedade Brasileira de Química*, Águas de Lindóia, Brazil, 2013. (*Poster presenter)

R. K. Nishihora*, E. Niehues, M. G. N. Quadri. Propriedades mecânicas e solubilidade de filmes de gelatina reticulados com transglutaminase. In *XX Congresso Brasileiro de Engenharia Química*, Florianópolis, Brazil, 2014. (*Poster presenter)

R. K. Nishihora, M. G. N. Quadri, L. A. H. M*. Transglutaminase effect on the viscosity and solubility of gelatin films. In *4th French Brazilian Meeting on Polymers*, Florianópolis, Brazil, 2014. (*Poster presenter)

R. K. Nishihora, M. G. N. Quadri*. Mechanical, morphological and water interaction characterization of gelatin films crosslinked with UV. In *Brazil MRS Meeting – XIV Symposium Polymers and Hybrid Materials for Nanomedicine*, Rio de Janeiro, Brazil, 2015. (*Poster presenter)

M. S. P. Damas, V. A. Pereira Júnior*, **R. K. Nishihora**, M. G. N. Quadri. Thermal and spectroscopic characterization of mucilage films from *Cereus hildmannianus* plasticized with glycerol. In *Brazil MRS Meeting – XIV Symposium Polymers and Hybrid Materials for Nanomedicine*, Rio de Janeiro, Brazil, 2015. (*Poster presenter)

T. V. Rego, M. Di Luccio*, **R. K. Nishihora**, E. Lemons-Senna, D. Hotza, J. C. C. Petrus. Ceramic membrane emulsification for production of vegetable oil-in-water emulsions with whey protein as surfactant. In *15th International Conference on Inorganic Membranes*, Dresden, Germany, 2018. (*Poster presenter)